General Disclaimer

One or more of the Following Statements may affect this Document

- This document has been reproduced from the best copy furnished by the organizational source. It is being released in the interest of making available as much information as possible.

- This document may contain data, which exceeds the sheet parameters. It was furnished in this condition by the organizational source and is the best copy available.

- This document may contain tone-on-tone or color graphs, charts and/or pictures, which have been reproduced in black and white.

- This document is paginated as submitted by the original source.

- Portions of this document are not fully legible due to the historical nature of some of the material. However, it is the best reproduction available from the original submission.

PREENTRY COMMUNICATIONS STUDY

Outer Planets Atmospheric Entry Probe

By C.A. Hinrichs

JAN 1977
RECEIVED
NASA STI FACILITY
INPUT BRANCH

(NASA-CR-137876)   PREENTRY COMMUNICATIONS   N77-14295
STUDY.   OUTER PLANETS ATMOSPHERIC ENTRY
PROBE (McDonnell-Douglas Astronautics Co.)
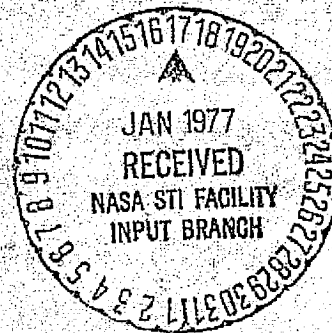97 p HC A05/MF A01   CSCL 17B   Unclas
                                              G3/32 58987

PREENTRY COMMUNICATIONS STUDY

Outer Planets Atmospheric Entry Probe

JAN 1977
RECEIVED
NASA STI FACILITY
INPUT BRANCH

By C.A. Hinrichs

Prepared by

MCDONNELL DOUGLAS ASTRONAUTICS COMPANY — EAST

St. Louis, Missouri 63166 (314) 232-0232

for Ames Research Center
Moffett Field, California 94035

NATIONAL AERONAUTICS AND SPACE ADMINISTRATION

FOREWORD

This pre-entry communications study was conducted under contract NAS 2-9027 and was performed under the auspices of the NASA Ames Research Center. The object of the study is to reduce the uncertainties in a relay communications system for a Jupiter probe. Specifically addressed are the performance characteristics and the hardware impact of probe spacecraft communications prior to atmospheric entry. The study reviews the propagation channel about Jupiter, defines optimal trajectories from a maximal data return sense, defines the various communications links, and the physical impact of the pre-entry communications on the probe and spacecraft, and finally develops a conceptual design of an electronically despun antenna for a roll axis stabilized spacecraft.

The author expresses appreciation provided by Mr. T. L. Grant of Ames Research Center for his direction of this study.

TABLE OF CONTENTS

LIST OF PAGES

Title Page
ii through viii
1 through 90

LIST OF FIGURES

LIST OF TABLES

SUMMARY

A pre-entry communications study is presented for a relay link between a Jupiter entry probe and a spacecraft in hyperbolic orbit. Throughout the study there are two generic communications links of interest: a pre-entry link to a spun spacecraft antenna, and a pre-entry link to a despun spacecraft antenna. The terminology spun spacecraft antenna refers to an antenna with a toroidally shaped radiation pattern. The terminology despun spacecraft antenna refers to an antenna with a quasi-pencil beam shaped radiation pattern.

In the first step of the study the propagation environment of Jupiter is defined. Although this is one of the least well known features of Jupiter, enough information exists to reasonably establish bounds on the performance of a communications link. Within these bounds, optimal carrier frequencies are defined.

The next step of the study is to identify optimal relative geometries between the probe and the spacecraft. The thrust of this portion of the analysis is to maximize the joint data return from both the pre-entry and post entry phases of the mission. Optimal trajectories are established for both spun and despun spacecraft antennas.

Given the optimal carrier frequencies, and the optimal trajectories, the data carrying capacities of the pre-entry links are defined. The relative merit of each link is weighed against a typical instrument load.

The impact of incorporating pre-entry communications into a basic post entry probe is then assessed. This assessment covers the disciplines of thermal control, power source, mass properties and design layout.

The final step of the study develops a conceptual design of an electronically despun antenna for use on a Pioneer class of spacecraft.

1

INTRODUCTION

Pre-entry communications is a desirable addition to a basically post entry probe mission such as described in References 1 and 2. In these "baseline" missions, the probe is quiescent from spacecraft release, 30 to 60 days prior to entry, until the probe enters the "sensible" atmosphere. This leaves a void in the space explored between the spacecraft periapsis and the sensible atmosphere. Within this region lie a number of interesting natural phenomenon: the greatest intensity of trapped radiation and the ionosphere, just to mention two. The object of this study is first to define the characteristics of a pre-entry communications link, and second to define the impact of that link on both the probe and the spacecraft.

The communications environment in the vicinity of Jupiter is quite severe. During the pre-entry phase of the mission the communications link will see noise temperatures in the 2000 to 4000 degree Kelvin range due to synchrotron radiation. During entry the communications link will traverse the extensive turbulent ionosphere of Jupiter, resulting quite possibly in an extremely slow fading Rayleigh channel. Despite these formidable difficulties, and the current uncertainty of the Jovian propagation environment, enough information exists to reasonably postulate viable communications links.

Keywords of an outer planet mission design philosophy are "simple, lightweight and reliable". Translated into relay communications terms this means that the antenna patterns are fixed on the vehicles. This in turn implies that the relative geometry between the relay terminals is a critical design element. When pre-entry communications are considered, the relative trajectory prior to entry is as significant as the relative trajectory after entry. In this study relative trajectories before and after entry are selected which maximize the data rate.

The definition of the propagation channel and the definition of the relay geometries forms the basis of the definition of the communications link per se; namely the transmitter powers, receiver sensitivities and the maximum data rate which can be supported. This in turn can be weighed against typical science requirements to establish the overall mission value of the link.

Given the physical characteristics of the science payload and the communications equipments, an assessment can be made of the impact of incorporating a pre-entry communications goal upon a primarily post entry design. This assessment must of necessity encompass a spectrum of engineering disciplines. One discipline is thermal control. The probe of References 1 and 2 is encapsulated in a radio opaque multilayer insulation. What are the effects of removing all or part of this radio opaque insulation and replacing it with a radio transparent insulation? The power source is another discipline. Can the existing battery designs accommodate the additional pre-entry science and radio loads, or must additional capacity be added? Then there is the mass properties discipline. What is the additional mass of the pre-entry equipments? Is the ratio of roll to pitch inertias adequate to maintain stability? Finally, there is mechanical layout. Is there adequate space to place the equipment, and where?

3

The "baseline" designs of References 1 and 2 presupposed a simple spun spacecraft reception antenna. If the spacecraft is a three axis stabilized device, or has a despun platform, obviously a despun reception antenna can be incorporated; for example a parabolic antenna bolted to the spacecraft in an appropriate position. Alternatively, if the spacecraft is roll stabilized and a despun antenna appears desirable, what are the characteristics of that antenna?

These various aspects of the pre-entry communications question will be addressed in turn in the succeeding sections of this report, the factors addressed, and a cogent design developed.

THE JOVIAN PROPAGATION CHANNEL

The definition of the Jovian propagation channel is a challenging task. The basic algorithms are reasonably well in hand. However, in addition to the fundamental uncertainty in the Jovian environment, there is a range of uncertainty in various coefficients of the algorithms. This section will explore in turn synchrotron noise, atmospheric absorption, ionospheric absorption, scintillation, frequency selection and ionospheric entry effects.

Synchrotron Noise

Jupiter is a particularly noisy environment; noise temperatures of 2000 to 4000°K at 0.4 GigaHertz are not uncommon. As a first order approximation, the NASA Jovian SP, Reference 3, models the synchrotron noise temperature as

$$T(°K) = D_{RJ} \, \lambda^2_{cm} \, (.3 \pm .15)$$

where D_{RJ} is the path length in the "synchosphere" in Jovian radii, and λ is the wavelength. The synchrosphere is that region wherein the noise originates. This is a trucated sphere of three radii, two Jovian radii high. Computations based on this model are given in Figure 1 based on the typical communications geometry given in Table 1. From the figure it is seen that the spacecraft beamwidth first intercepts the planet at T - .6 hour. Between T = .1 hour and T + .3 hour the beamwidth totally covers the planet. The synchrotron noise is a minima when the bulk of the synchrosphere is blocked by the planet. The shape and magnitude of the curve is quite similar to a more sophisticated approach given in Reference 4.
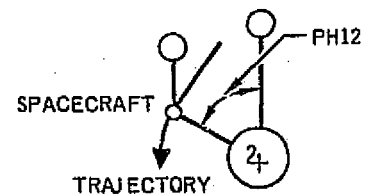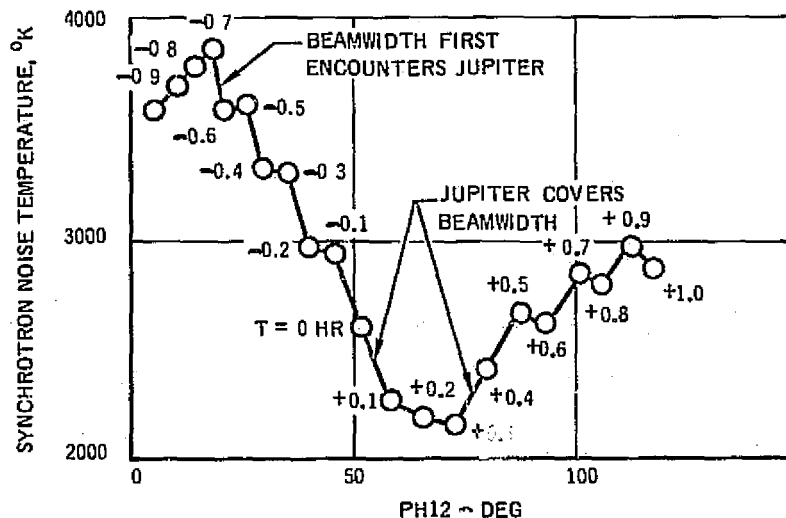
FIGURE 1

SYNCHROTRON NOISE VARIATION
LOOP VEE ANTENNA
400 MHZ

TABLE 1
TYPICAL COMMUNICATIONS GEOMETRY

Time (hr)	Spacecraft View Angle (deg)	Probe View Angle (deg)	Range (radii)
-.3	45.50	57.63	.8608
-.2	41.45	53.58	.8756
-.1	37.58	49.71	.9170
0	34.66	① 46.79 ② 34.89	.9881
.1	43.09	28.90	.9163
.2	52.70	22.91	.8581
.3	63.39	15.84	.8176
.4	74.82	8.057	.7981
.5	86.45	0.812	.8014

① before tip-over

② after tip-over

Absorption

There are two principal absorption mechanisms at Jupiter, atmospheric and ionospheric. Atmospheric absorption on Jupiter is due to the propensity of the nitrogen atom to oscillate between the triad of hydrogen atoms in ammonia. Reference 5 describes the algorithm. Figure 2 compares the loss at the 30 bar level for the three NASA SP Jovian atmospheres and for the Orten-Hunten atmosphere from Reference 6. The Orten-Hunten atmosphere has slightly more loss at 30 bars than the nominal NASA SP model, but is well bracketed by the cool-warm extremes. The relative amount of absorption in all cases is primarily due to the amount of ammonia in the atmospheric model.
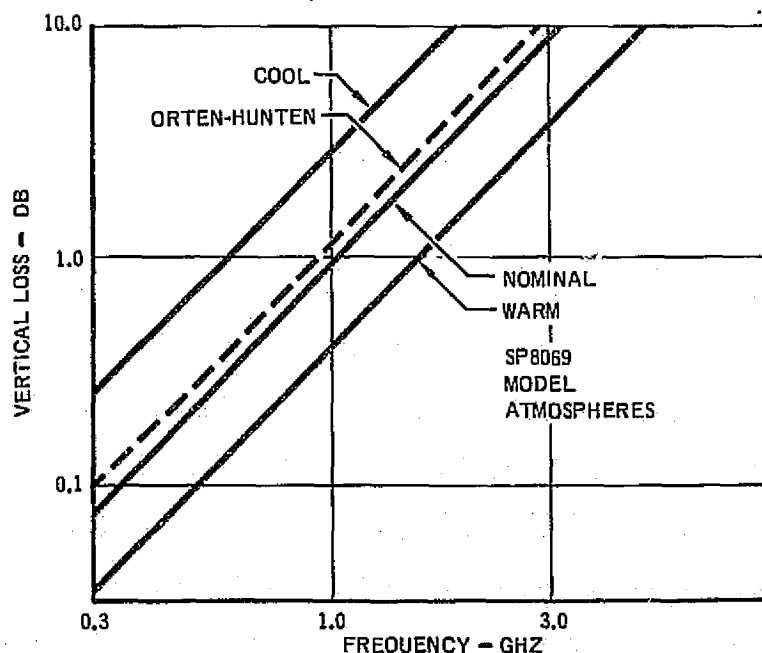
FIGURE 2

JOVIAN ATMOSPHERIC LOSS AT 30 BARS

Ionospheric absorption is due to the interaction of the electromagnetic wave and the free charges in the ionosphere. Reference 7 describes the algorithm. Figure 3 compares the SP Reference 3 values with the Pioneer 10 measurements reported in Reference 8. The Pioneer data indicates that the loss would be between the nominal and minima of the SP reference.
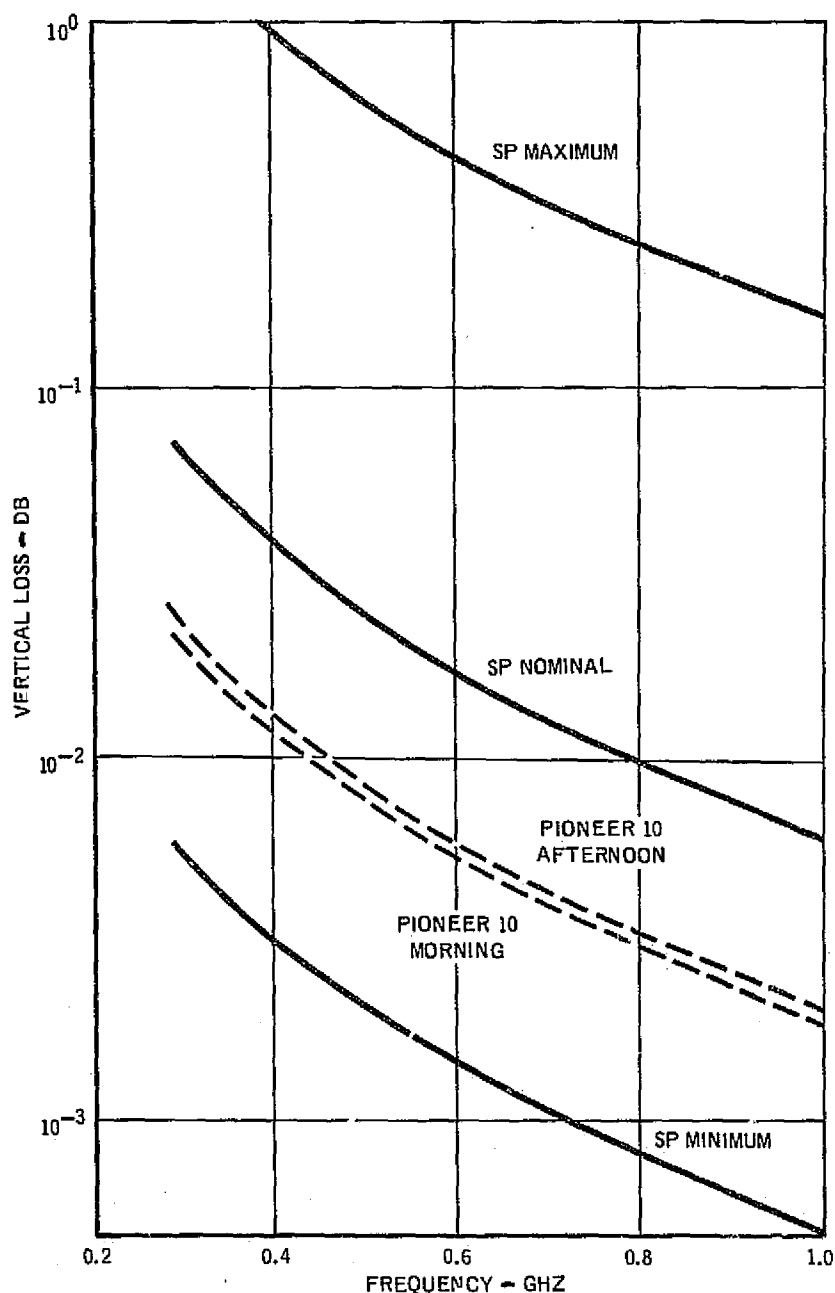
FIGURE 3

JOVIAN IONOSPHERIC LOSS

Scintillation

Scintillation is the effect of the interference of a "direct" path ray by "refracted" rays. The refraction is due to local anomalies in the index of refraction. These anomalies occur both in the atmosphere and the ionosphere. Atmospheric refraction anomalies are due primarily to small variations of temperature; typically less than 1°K. Ionospheric refraction anomalies are due to the temporary "bunching" of the free electronics. References 9 and 10 describe the algorithms. The examples of the latter reference were based on the NASA SP environments from Reference 3. The updated factors on the atmosphere in Reference 6 and the ionosphere in Reference 8 are shown in Figure 4. The dominate scintillation is ionospheric.
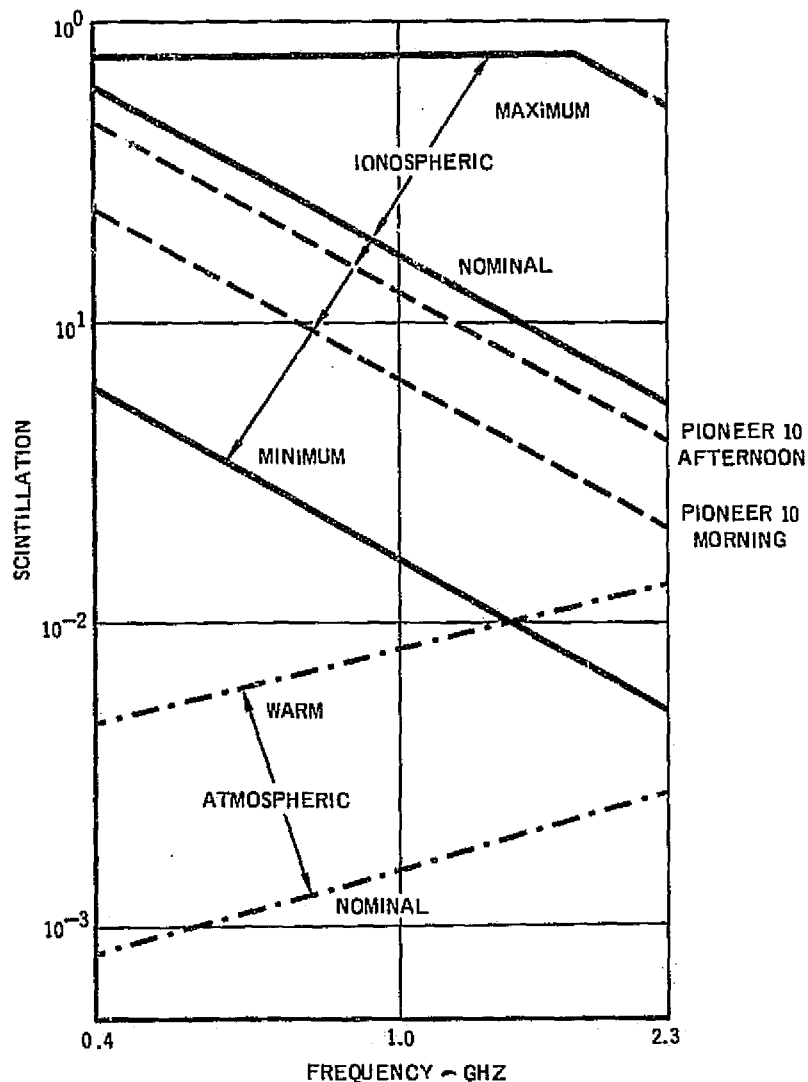
FIGURE 4

30 BAR JOVIAN SCINTILLATION

Scintillation affects the signal phase and amplitude. As the scintillation rates are low, of the order of a few tenths to a few Hertz, the phase variations can be readily tracked out by a loop. The amplitude variations, however, can create potentially deep long term fades. For the usual lognormal distribution the fade depth is $(20 \log_{10} e) V \sigma_x$ where V relates the fade depth, that is V of 1, 2 or 3 is a 15.87, 2.28 or 0.13% time depth. In link table terms the table entry tolerance distributions are often considered uniform, or the "adverse" tolerance is the root three times the standard deviation. Hence V above is root three for standard link computations, or the fade depth is 15 σ_x. A maximally amplitude fading channel is σ_x of .75, thus has an 11.25 decibel fade depth. This corresponds to the worst case NASA SP ionospheric case for all frequencies below 1.7 GigaHertz.

A potential radio frequency experiment is a dual frequency measurement of the electron content of the ionosphere. The scinillation of these frequencies while in the ionosphere is a direct function of the integral of the square of the local electron density.

Carrier Frequency Selection

The preceeding paragraphs reviewed synchrotron noise, which favors high frequencies, atmospheric absorption, which favors low frequencies, ionospheric absorption, which favors high frequencies, atmospheric scintillation, which favors low frequencies and finally ionospheric scintillation, which favors high frequencies. Additional environmental frequency sensitive factors are cosmic noise, which favors high frequencies, and free space attenuation, which favors low frequencies.

In the carrier frequency selection criteria there are also implementation factors. Maximal power for solid state transmitters, transmitter efficiency and receiver noise figure all favor low frequencies, while antenna gain for a fixed aperture favors high frequencies.

There are four configurations of interest: communications before and after entry, and the use of a spun (360 degree clock beamwidth) or a despun spacecraft reception antenna. Figure 5 is a listing of a routine to define the optimal carrier frequency for these configurations. The routine computes a "figure of merit" which includes all of the frequency sensitive factors, and does not include those factors which are nonfrequency sensitive. Table 2 is a generic link table to illustrate the technique, as well as a definition of the salient symbols. All of the nonfrequency sensitive entries are denoted by K, and are left out of the final summation. The data is plotted in Figures 6 and 7.

If a spun spacecraft antenna is employed, the optimal pre-entry frequency is 400 MegaHertz, and the optimal post entry frequency is 550 MegaHertz. If a common 400 MegaHertz carrier were used, the post entry link would be penalized 1.15 dB. If a common 550 MegaHertz carrier were used, the pre-entry link would be penalized .97 dB.

9

```
#LIST CAHFG                    .

CAHFG        12:22 JAN 24, '76

01000$FIXED
01100C       FRQ SELECTION
01200C       ONE JOVIAN POINT:1.8RJ;.5PHASE:T=0
01210        DATA DISH,BWBF,BWAF/3.,11.,52./
01220 5000   PRINT 5001
01230 5001   FORMAT(1X,'DISH,BWBF,BWAF')
01240        READ,DISH,BWBF,BWAF
01250        PRINT 5002,DISH,BWBF,BWAF
01260 5002   FORMAT(1X,3G12.4)
01300        IPO=0
01400        PRINT 1001
01500 1001   FORMAT(5X,'FRQ',7X,'PRESPU',4X,'PREDES',4X,
01501       & 'POSSPU',4X,'POSDES',4X,'PRECDS')
01550        DO 1100 I=1,22
01600        FRQ=(FLOAT(I)+1.)*100.
01700 1100   CALL ANAL(FRQ,IPO,DISH,BWBF,BWAF)
01710        IDTL=0
01720        PRINT 5003
01730 5003   FORMAT(1X,'DETAILS=1')
01740        READ,IDTL
01750        IF(IDTL.EQ.0)GOTO5000
01800        IPO=1
01900        PRINT 1190
02000 1190   FORMAT(//,1X,'FRQ',7X,'XP',7X,'SCINT',/,
02100       &1X,'AION',5X,'ABS',7X,'CN',8X,'TN',8X,'SN',8X,'RN',/,
02200       &1X,'AICNM',4X,'ABSM',6X,'CNM',7X,'TNM',7X,'SNM',7X,'RNM',/,
02300       &5X,'PRESPU',8X,'PREDES',8X,'POSSPU',8X,'POSDES',/,
02350       &1X,'ATS',4X,'ATMS',3X,'ATDS',3X,'ATMDS',2X,'ATS',4X,
02360       & 'ATMS',3X,'ATDS',3X,'ATMDS',/,
02400       &1X,'STS',4X,'STMS',3X,'STDS',3X,'STMDS',2X,
02500       & 'STS',4X,'STMS',3X,'STDS',3X,'STMDS',/,
02600       &1X,'AM1',4X,'ADVT1',2X,'AM2',4X,'ADVT2',2X,'AM3',4X,
02700       & 'ADVT3',2X,'AM4',4X,'ADVT4',/)
02800 1999   PRINT 1200
02900 1200   FORMAT(1X,'ANOTHER FRQ?')
03000        READ,FRQ
03005        IF(FRQ.LT.0.)GOTO5000
03100        IF(FRQ.LT.90.)GOTO9999
03200        CALL ANAL(FRQ,IPO,DISH,BWBF,BWAF)
03300        GOTO1999
03400 9999   END
```

PRESPU= PREENTRY SPUN
PREDES= PREENTRY DESPUN
POSSPU= POST ENTRY SPUN
POSDES= POST ENTRY DESPUN
PRECDS= PREENTRY COMMON
              DESPUN

FIGURE 5
FREQUENCY ANALYSIS LISTING

10

```
03500          SUBROUTINE ANAL(FRQ,IPO,DISH,BWBF,BWAF)
03520          SCINT=7466.26/FRQ**(5./3.) Woo & Yang Afternoon σχ
03530          IF(SCINT.GT..75)SCINT=.75
03540          SCINT=15.04*SCINT FADE DEPTH
03600          XPW=-29.38*FRQ/1000.+71.75 TRANSMITTER WATTS
03700          IF(XPW.GT.60.)XPW=60.
03800          IF(XPW.LT.1.)XPW=1.
03900          XP=10.*ALOG10(XPW/1.E-3) dBm
03930          APPLIM=0.
03940          IF(FRQ.GT.400.)GOTO2000
03950          APPLIM=10.*ALOG10(3.5146E-5*FRQ**2)-7.5
03960C         LIMITING XAG APERTURE LIMITING
03970 2000     CONTINUE
04000          AION=.1301*EXP(-3.0764*FRQ/1000.) IONOSPHERIC LOSS
04100          AIONM=3.5422*EXP(-3.1619*FRQ/1000.) MAXIMUM
04200          ABS=.3941*(FRQ/1000.)**2 ABSORPTION LOSS
04300          ABSM=2.699*(FRQ/1000.)**2 MAXIMUM
04400          TRP1=XP-20.*ALOG10(FRQ)+APPLIM TOTAL RECEIVED POWER
04500          TRP2=XP
04550          TRP22=TRP2
04600          TRP3=TRP1-(AION+ABS)*1.1547
04700          TRP4=TRP2-(AION+ABS)*1.1547
04800C         1.1547=1/COS30 ZENITH ANGLE.
04810          BW=7.E4/(FRQ*DISH) BEAMWIDTH
04815          IF(BW.GT.BWBF)GOTO2001
04820C         BWBF DEG PREENTRY(DISH,FT)
04825          FRQLIM=20.*ALOG10(7.E4/(BWBF*DISH))
04830          TRP2=TRP2-20.*ALOG10(FRQ)+FRQLIM
04835 2001     CONTINUE
04840          IF(BW.GT.BWAF)GOTO2002
04845 C        BWAF DEG POSTENTRY(DISH,FT)
04850          FRQLIM=20.*ALOG10(7.E4/(BWAF*DISH))
04855          TRP4=TRP4-20.*ALOG10(FRQ)+FRQLIM
04860          TRP22=TRP22-20.*ALOG10(FRQ)+FRQLIM
04865 2002     CONTINUE
04900          TRPT1=0. TOTAL RECEIVED POWER TOLERANCE.
05000          TRPT2=TRPT1
05100          TRPT3=(AIONM-AION+ABSM-ABS)*1.1547
05200          TRPT4=TRPT3
05300          CN=10.**(-2.4*ALOG10(FRQ)+8.32) COSMIC NOISE
05350          CN=1.7*(FRQ/1000.)**(-2.721)
05400          CNM=10.**(-2.4*ALOG10(FRQ)+9.) MAXIMUM
05450          CNM=(35.*(FRQ/1000.)**(-2.5455))/3.
05460C         DIVIDE BY 3 FOR BROAD BEAMWIDTHS
05500          AL=ALOG10(3.E4/FRQ)
05600          TN=165.*(AL-2.)+435.          THERMAL NOISE
05700          TNM=155.*(AL-2.)+530.         MAXIMUM
```

FIGURE 5

FREQUENCY ANALYSIS LISTING

(Continued)

```
05800C     D AT T=0=1.5431::X=.3
05900      SN=1.5431*((3.E4/FRQ)**2)*.3  SYNCHROTRON NOISE
06000      SNM=SN*.45/.3                     MAXIMUM
06100      RN=94.2*FRQ**.194  RECEIVER NOISE
06200      RNM=1.122*RN+35.4  MAXIMUM
06300      ATS=SN+CN*.8125+TN*.1875  ANTENNA TEMPERATURE, SPUN
06400      ATDS=SN+TN  DESPUN
06500      ATMS=SNM+CNM*.1875+TNM*.8125 MAXIMUM
06600      ATMDS=SNM+TNM
06700      STS=(ATS+35.4)/1.122+RN  SYSTEM TEMPERATURE  SPUN
06800      STDS=(ATDS+35.4)/1.122+RN  DESPUN
06900      STMS=(ATMS+35.4)/1.122+RNM  MAXIMUM
07000      STMDS=(ATMDS+35.4)/1.122+RNM
07100      SS=-198.63+10.*ALOG10(STS)  SENSITIVITY, SPUN
07200      SDS=-198.63+10.*ALOG10(STDS)  DESPUN
07300      SMS=10.*ALOG10(STMS/STS)      MAXIMUM
07400      SMDS =10.*ALOG10(STMDS/STDS)
07500      ADVT1=TRPT1+SMS    ADVERSE TOLERANCE
07600      ADVT2=TRPT2+SMDS
07700      ADVT3=TRPT3+SMS
07800      ADVT4=TRPT4+SMDS
07850      ADVT3=ADVT3+SCINT
07860      ADVT4=ADVT4+SCINT
07900      AM1=TRP1-SS-ADVT1  MARGIN
08000      AM2=TRP2-SDS-ADVT2
08005      AM22=TRP22-SDS-ADVT2
08100      AM3=TRP3-SS-ADVT3
08200      AM4=TRP4-SDS-ADVT4
08300      IF(IPO.EQ.0)GOTO1000
08400      PRINT 1001,FRQ,XPW,SCINT
08500 1001 FORMAT(/,1X,3F10.2)
08600      PRINT 1002,AION,ABS,CN,TN,SN,RN
08700     &,AIONM,ABSM,CNM,TNM,SNM,RNM
08800 1002 FORMAT(1X,6F10.2,/,1X,6F10.2,/,
08900     &5X,'PRESPU',8X,'PREDES',8X,'POSSPU',8X,'POSDES')
09000      PRINT 1005,ATS,ATMS,ATDS,ATMDS,ATS,ATMS,ATDS,ATMDS
09050 1005 FORMAT(1X,8F7.0)
09060 1003 FORMAT(1X,8F7.2)
09200      PRINT 1009,STS,STMS,STDS,STMDS,STS,STMS,STDS,STMDS
09210 1009 FORMAT(1X,4(F7.0,F7.0))
09300      PRINT 1003,AM1,ADVT1,AM2,ADVT2,AM3,ADVT3,AM4,ADVT4
09400      RETURN
09500 1000 PRINT 1004,FRQ,AM1,AM2,AM3,AM4,AM22
09600 1004 FORMAT(1X,6F10.2)
09700      RETURN
09800      END
```

FIGURE 5

FREQUENCY ANALYSIS LISTING

(Continued)

TABLE 2
GENERIC LINK TABLE

Parameter	Value	Tolerance	Comment
Transmitter Power	$10 \log_{10}(XP/X10^{-3})$	$-1=K$	Maximum for frequency
Transmitter Line	$-.3=K$	$-.1=K$	Assumed
Transmit Antenna	$XAG=K$	$XAGT=K$	Microstrip typical
Free Space	$-K-20 \log_{10} f$	$FST=K$	Entry point
Ionosphere	$AIØN/\cos 30$	$I(MAX-VERT)/\cos 30$	0 for preentry
Scintillation	K	$K/f^{**}(17/12)$	0 for preentry
Atmosphere	$ABS/\cos 30$	$A(MAX-VERT)/\cos 30$	0 for preentry
Receive Antenna	$K+20 \log_{10} f$	$.5=K(post);3=K(pre)$	K for post entry
Polarization	$-.2=K$	$-.1=K$	Assumed
Receiver Line	$-.2=K$	$-.1=K$	Assumed

Total Received Power
1   preentry spun: $K+10 \log_{10}(XP/X10^{-3})-20 \log_{10} f$
2   preentry despun: $K+10 \log_{10}(XP/X10^{-3})$
3   post entry spun: $K+10 \log_{10}(XP/X10^{-3})-20 \log_{10} f - (AIØN+ABS)/\cos 30$
4   post entry despun: $K+10 \log_{10}(XP/X10^{-3})-(AIØN+ABS)/\cos 30$

Parameter	Value	Tolerance	Comment
Cosmic Noise	CN	CNM	Calculated
Thermal Noise	TN	TNM	Calculated
Synchrontron Noise	SN	SNM	Calculated
Receiver Noise	RN	RNM	Calculated
Antenna Temperature	1 and 3 SN+CN(.8125)+TN(.1875); 2 and 4 SN + TN	SNM+CNM (.8125)+TNM(.1875) ; SNM+TNM	
System Temperature	$(AT+35.4)/1.22 + RN$	; $(ATM+35.4)/1.22+RNM$	
Sensitivity (N_0)	1 and 3 $- 198.63 + 10 \log_{10} T_{S1,3}$; 2 and 4 $- 198.63 + 10 \log_{10} T_{S2,4}$;	$10 \log_{10}(T_{SM1,3}/T_{S1,3})$ $10 \log_{10}(T_{SM2,4}/T_{S2,4})$	
Data	$10 \log_{10} R=K$	0	Constant
Receiver Loss	$1.5=K$	$-.2=K$	Assumed
Threshold	$10.6=K$	0	Calculated
Required Data Power	K	K .	Subtotal

Margin(i) = Total Received Power(i) - Sensitivity(i) - Data - Adverse Tolerance(i)

If a despun spacecraft antenna is employed, the optimal pre-entry frequency is 1050 MegaHertz, and the optimal post entry frequency is 550 MegaHertz. If a common 550 MegaHertz carrier were used, the pre-entry link would be penalized 1.6 dB. If a common 1050 MegaHertz carrier were used, the post entry link would be penalized 3.93 dB.
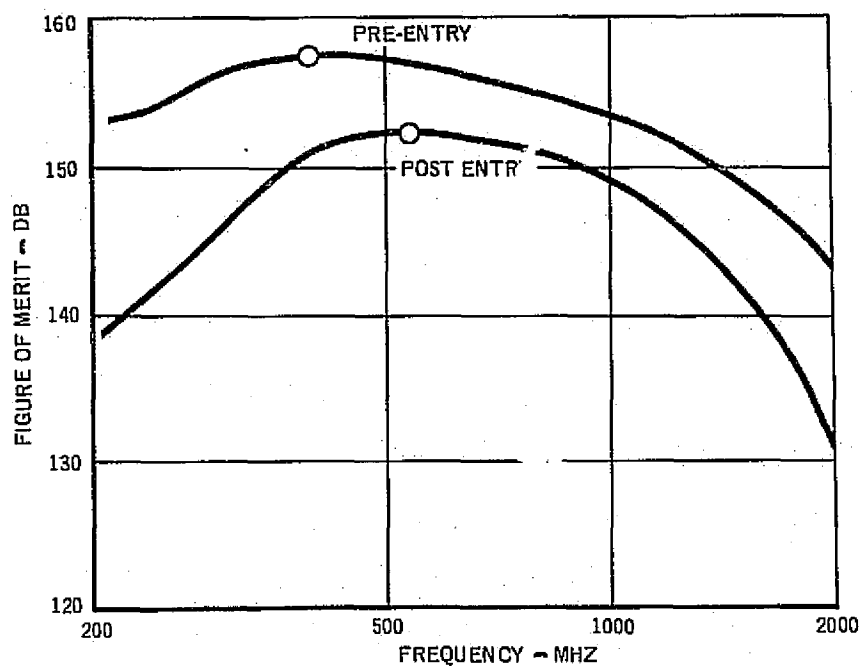
FIGURE 6

FREQUENCY PARAMETRIC SPUN SPACECRAFT ANTENNA
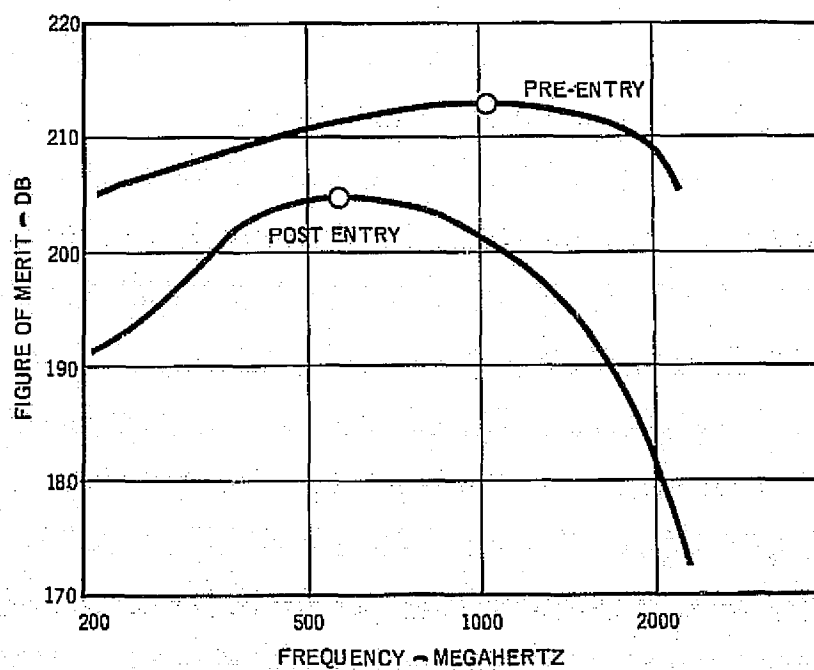
FIGURE 7

FREQUENCY PARAMETRIC DESPUN SPACECRAFT ANTENNA

14

Blackout

A rule of thumb for the initiation of shock/viscous heating (the initiation of blackout) is when the density ratio across the shock (P_∞/P_S) is unity at shock formation, and 1/15 at viscous heating. The density ratio is related to the free stream mean free path (ℓ_∞) by

$$\ell_\infty = (P_\infty/P_S)^{1/2} R_b/10$$

where R_b is the radius of curvature of the body. For a 44.45 cm radius body with a 22.23 cm nose radius, shock formation is between the mean path range of 4.45 cm to 2.23 cm, and viscous heating between 1.15 cm and 0.57 cm. The mean free path is commonly expressed as

$$\ell_\infty = [N_M \; \zeta v]^{-1}$$

where the particle density is

$$N_M = 7.34 \times 10^{21} \; p(atm)/T(°K),$$

The velocity is

$$v = (8kT/\pi m)^{1/2},$$

and

$$\zeta H_2 = 1.3179 \times 10^{-2} \text{ and } \zeta H_E = 8.37 \times 10^{-21}.$$

Table 3 lists the Jovian atmospheric mean free paths.

TABLE 3
JOVIAN MEAN FREE PATHS

p (dyne/cm^2)	COOL			NOMINAL			WARM		
	h(km)	ℓ_∞(cm)	N_M(cc^{-1})	h(km)	ℓ_∞(cm)	N_M(cc^{-1})	h(km)	ℓ_∞(cm)	N_M(cc^{-1})
.2	192.8	59.8	1.4E13	313.4	63.8	1E13	634.8	116.3	2.9E12
.3	187.8	39.8	2E13	304.9	42.6	1.5E13	601.3	75.7	4.6E12
1.	173.0	12.0	6.8E13	279.7	12.8	5.1E13	510.6	21.2	1.8E13
3.	159.5	4.0	2E14	256.6	4.3	1.5E14	438.0	6.6	6.0E13
10.	144.6	1.2	6.8E14	231.4	1.28	5.1E14	368.2	1.9	2.3E13
30.	131.1	.40	2E15	208.3	.43	1.5E15	312.4	.58	7.8E14
100.	116.3	.12	6.8E15	183.1	.13	5.1E15	258.7	.16	3.0E15

Figure 8 illustrates the relationship between the lower edge of the ionosphere, 3 dynes/cm^2, and the anticipated blackout. In all cases, blackout will follow the ionospheric transmission. The duration of one scale height, 500 kilometers, ionospheric transmission for a baseline 7.5 degree entry of 47.1740 km/second relative entry velocity, is 81.20 seconds. The Jovian entry energy is 35.44 times that of a typical Earth entry, and hence every particle will probably be ionized, i.e., the stagnation electron density may be taken as twice (two electrons per particle) the particle density. Using another

rule of thumb (that the wake electron density is 1/10th that of stagnation) the plasma frequency, W_P, below which blackout occurs, is

$$W_p = 2\pi\ 8970\ (2N_M/10)^{1/2}.$$

At earliest viscous heating, approximately 10 dynes/cm^2, the plasma frequencies are 105, 90.6 and 19.2 GigaHertz respectively for the cool, nominal and warm models. All of these plasma frequencies are well above the highest contemplated carrier, hence the wave will definitely be blacked out.
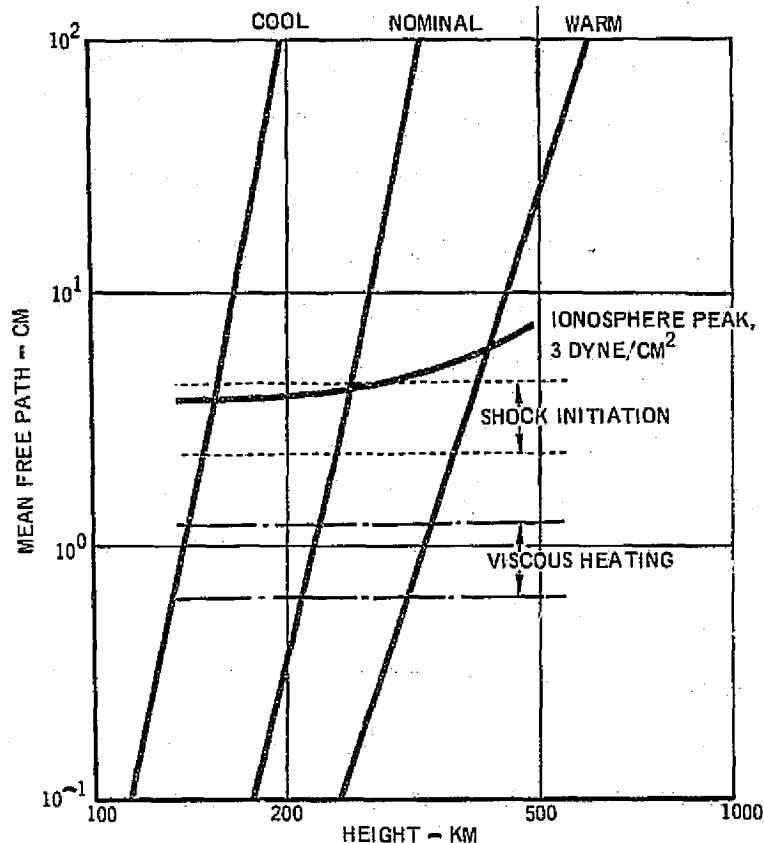
FIGURE 8

RELATIONSHIP OF BLACKOUT TO IONOSPHERE

Summary

The Jovian propagation channel characteristics have been reviewed with current knowledge of the planet and tentative carrier frequency selections were made for various types of links. In particular, if the spacecraft antenna is "spun", i.e., has a 360° clock angle, the optimal pre-entry and post entry frequencies are 400 and 550 MegaHertz respectively. If the spacecraft antenna is despun, the optimal pre-entry and post entry frequencies are 1050 and 550 MegaHertz respectively. It was seen that a radio frequency ionospheric measurement would probably not blackout prior to the peak ionospheric electron density, but would certainly do so shortly thereafter.

TRAJECTORY AND SPACECRAFT ANTENNA SELECTION

The selection of the relative geometry between the spacecraft and the probe, together with the spacecraft antenna pattern, is a critical factor in establishing the relay communications link performance. The general characteristics of the Jovian propagation environment were established in the previous section. Briefly, in that section, the link frequency sensitive parameters established the optimal carrier frequencies for the mission. The remaining factors in defining the links are the data/symbol rates, modem and relative geometry effects. This section establishes the geometric effects.

The geometric effects are the transmission antenna view angle, the transmission distance and the reception antenna view angle. For this study only one transmission antenna is assumed, the microstraip antenna. Basically a high deceleration requirement, coupled with a critical forward center of gravity requirement infers a small flat physical device which a microstrip antenna ideally meets. Further, since the device can provide either an axial or a butterfly pattern dependent upon feed, and these are nearly ideal for post and pre-entry view angles, assuming a microstrip transmission antenna does not penalize a realistic geometric effects analysis.

The remaining geometric factors are the trajectory _per se_, and the radiation pattern of the reception antenna.

Analysis Approach

Margin is used as the measure of link performance. Herein, a geometry investigation, data/symbol rates and modem are constants and hence can be deleted from the discussion. The approach is to equalize the margin at the beginning and end of the transmission period, and by having the reception beam centered between the end point view angles, thus having some greater margin between end points. Mathematically this is

$$A_1 G_1 = A_2 G_2$$

where A represents all of the geometry effects except for receive antenna gain, G is the antenna gain of the receiver (at the respective view angle), and the subscripts 1 and 2 refer to the beginning and end of the transmission period respectively. Further, defining S as the spacecraft aspect angle, and C as the spacecraft angle to the receiving antenna beam center,

$$S_1 \leq C \leq S_2.$$

Figure 9 illustrates the approach. It should be noted that this technique is equivalent for either a spun or despun antenna, for either pre-entry or post entry transmission.

A Gaussian shape is representative of many antenna radiation patterns, hence the reception antenna gain can be expressed as

MARGIN, dB

TIME
BEGIN   END

RADIATION
PATTERN

FROM PROBE
A2 END OF MISSION

EARTH

W

A1
BEGINNING
OF MISSION

SPACE-
CRAFT

S2

C   S1
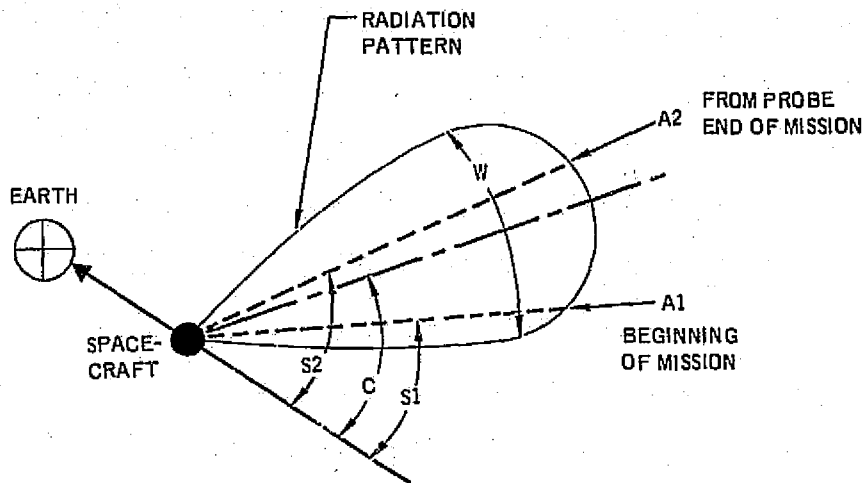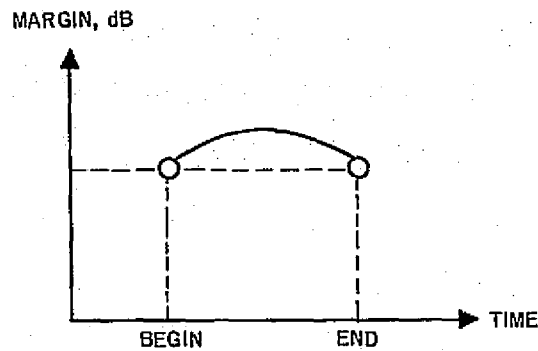
FIGURE 9

TRAJECTORY STUDY APPROACH

$$G = \exp -\frac{1}{2} \left(\frac{1.178\ (c-S)}{W/2} \right)^2$$

where w is the 3 decibel beamwidth, and

$$A_1 \exp{-\frac{1}{2}} \left(\frac{1.178\ (C-S_1)}{W/2} \right)^2 = A_2 \exp{-\frac{1}{2}} \left(\frac{1.178\ (S_2-C)}{W/2} \right)^2$$

which after some algebra yields the form

$$W^2 = \frac{2(1.178)^2}{\ln(A_1/A_2)} [\ S_1{}^2 - S_2{}^2 + 2C\ (S_2 - S_1)]$$

or

$$W^2 = \alpha(-\beta + \gamma C).$$

This is the optimal relationship between the spacecraft reception antenna beamwidth and beam center, W and C, given the trajectory parameters α, β and γ. Figure 10 illustrates the relationship. It should be noted that there are some physical limits on the antenna plane W, C. A typical limit is a minimum beamwidth for a finite physical aperture. The next step is to define the optimal W_i, C_i point for maximal margin. Figure 11 illustrates the approach. Combining the foregoing relationship of the trajectory and beamwidth/beamcenter together with the radiation pattern shape we have an expression of relative margin, or figure of merit.
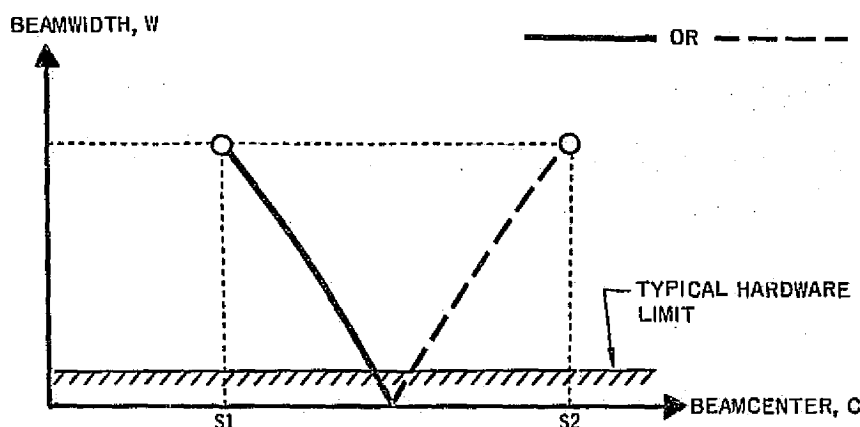
FIGURE 10

OPTIMAL BEAMCENTER BEAMWIDTH RELATIONSHIP

a) GIVEN THE BEAMWIDTH BEAMCENTER RELATION
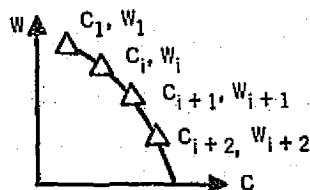
b) DETERMINE THE OPTIMAL MARGIN
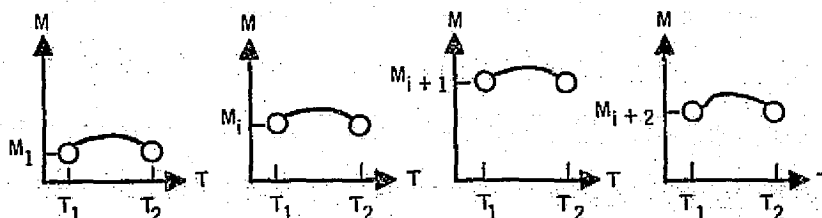
FIGURE 11

OPTIMAL MARGIN CONDITION

$$M = \Gamma \exp -\varsigma (W/\alpha\gamma + \beta/\gamma W - S_1/W)^2$$

where Γ is the peak gain and ς is $(1.178 \times 2)^2/2$. Obviously then the peak margin is at

$$\partial M/\partial W = 0.$$

At this point there are two conditions to investigate. The first is for a despun (quasi-pencil beam radiation pattern) antenna. Herein a simple ratio of areas relationship for directivity is assumed, that is the antenna directivity is the ratio of the area of a unit sphere to the area illuminated on that sphere by the pattern. For the despun case the peak gain is given by

$$\Gamma = \varepsilon/\sin^2(W/4)$$

where ε is the efficiency. The maximal margin for the despun case is at

$$\frac{W^4}{(\alpha\gamma)^2} + \frac{W^3}{4\varsigma \, \text{Tan} \, \frac{W}{4}} = (\frac{\beta}{\gamma} - S_1)^2.$$

Note that the antenna efficiency is irrelevant in this analysis. For the spun (quasi-toroidal radiation pattern) antenna the peak gain is

$$\Gamma = \varepsilon/(\sin C \, \sin(W/2)).$$

Herein the maximal margin is at

$$\frac{W^4}{(\alpha\gamma)^2} + \frac{W^3}{4\varsigma \, \text{Tan} \, \frac{W}{2}} + \frac{W^4}{\alpha\gamma\varsigma \, \text{Tan} \, (\frac{W^2}{\alpha\gamma} + \frac{\beta}{\gamma})} = (\frac{\beta}{\gamma} - S_1)^2.$$

Figure 12 is a computer listing to solve the above expressions by approximation. It should be noted in the routine that the non-reception antenna gain term, A_i, contains antenna view-angle tolerance terms in addition to free space. The routine inputs are the end point trajectory terms of the spacecraft view angle, S, probe view-angle, P, and the range, R, before entry and after entry. The physical despun limit is taken as a .9 meter parabola, and the physical spun limit is taken as a 50 degree beamwidth. The limits are obviously easily modifiable in the routine, but are considered representative for the Jovian analysis.

Baseline Trajectory

The initial estimate of an optimal trajectory was a periapsis of 1.8 radii with a phasing of 0.5 hours at an entry latitude of 3.15 degrees, with

B = BEFORE
A = AFTER
S = S/C ANGLE
P = PROBE ANGLE
R = RANGE
1 = LEAST S
2 = GREATEST S

```
00100$FIXED
00110C        S/C  BW&BC
00120         DATA BS1,BP1,BR1,BS2,BP2,BR2
00130         &/.6049,.8166,.9881,.7941,1.0058,.8608/
00140         DATAAS1,AP1,AR1,AS2,AP2,AR2
00150         &/.6049,.6089,.9881,1.5088,.0142,.804/
00155         DATA RD,PI/57.29577591,3.141592654/
00160 1000 PRINT 1001
00170 1001 FORMAT(///,1X,'PREENTRY S1,P1,R1,S2,P2,R2')
00180         READ,BS1,BP1,BR1,BS2,BP2,BR2
00190         PRINT 1003,BS1,BP1,BR1,BS2,BP2,BR2
00200 1003 FORMAT(1X,3G13.5,/,0X,3G13.5)
00210         PRINT 1002
00220 1002 FORMAT(1X,'POST ENTRY S1,P1,R1,S2,P2,R2')
00230         READ,AS1,AP1,AR1,AS2,AP2,AR2
00240         PRINT 1003,AS1,AP1,AR1,AS2,AP2,AR2
00250         XAGB1=10.*ALOG10(1.36*EXP(-.5*(2.4543*  (TRANSMIT ANTENNA GAIN)
00260         &BP1-.7985))**2))CENTER FED MICROSTRIP
00270         XAGB2=10.*ALOG10(1.36*EXP(-.5*(2.4543*(
00280         &BP2-.7985))**2))  NORMAL MICROSTRIP
00290         XAGA1=10.*ALOG10(5.62*EXP(-.5*(2.0453*AP1)**2))
00300         XAGA2=10.*ALOG10(5.62*EXP(-.5*(2.0453*AP2)**2))
00310         XAGT1=10.*ALOG10(5.62*EXP(-.5*(2.0453*(
00320         &AP1+.0873))**2))    5° WOBBLE TOLERANCE
00330         XAGT2=10.*ALOG10(5.62*EXP(-.5*(2.0453*(
00340         &AP2+.0873))**2))
00350         XAGT1=XAGA1-XAGT1
00360         XAGT2=XAGA2-XAGT2
00370         BA1=10.**((-20.*ALOG10(BR1)-.5+XAGB1)/10.)
00380         BA2=10.**((-20.*ALOG10(BR2)-.5+XAGB2)/10.)
00390         AA1=10.**((-20.*ALOG10(AR1)-XAGT1+XAGA1)/10.)
00400         AA2=10.**((-20.*ALOG10(AR2)-XAGT2+XAGA2)/10.)
```
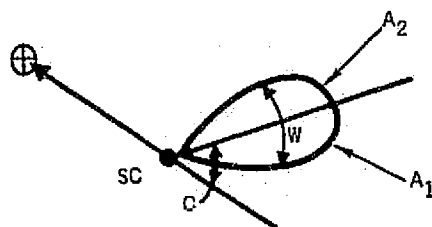

FIGURE 12
TRAJECTORY ANALYSIS COMPUTER LISTING

```
00410C          ALPHA,BETA,GAMMA,B**2
00420           BA=2.7754/ALOG(BA1/BA2)α ⎫
00430           BB=-(BS1*BS1-BS2*BS2) β  ⎪
00440           BG=2.*(BS2-BS1)       γ  ⎬ BEFORE
00450           BB2=(BB/BG-BS1)**2    β²  ⎭
00460           AA=2.7754/ALOG(AA1/AA2)α ⎫
00470           AB<-(AS1*AS1-AS2*@S2)  β  ⎪
00480           AG=2.*(AS2-AS1)        γ  ⎬ AFTER
00490           AB2=(AB/AG-AS1)**2     β²  ⎭
00500           XWB=SQRT(ABS(BA*(BS2-BS1)**2))
00510           XWA=SQRT(ABS(AA*(AS2-AS1)**2))
00515           IF(XWB.GT.2.*PI)XWB=2.*PI
00516           IF(XWA.GT.2.*PI)XWA=2.*PI
00520           PRINT 1010,BA,BB,BG,BB2,XWB,BA1,BA2
00530 1010      FORMAT(1X,'BEFORE A,B,G,@2,XW',/,1X,5G12.4
00531           &,/,7X,2G12.4)
00540           PRINT 1011,AA,AB,AG,AB2,XWA,AA1,AA2
00550 1011      FORMAT(1X'AFTER  A,B,G,B2,XW',/,1X,5G12.4
00551           &,/,7X,2G12.4)
00590           XBD=-9999.
00600           XBS=-9999.
00610           XAD=-9999.
00620           XAS=-9999.
00630           IBD=0
00640           IBS=0
00650           IAD=0
00660           IAS=0
00670C          DIVIDING W INTO 100 PARTS
00680           DO 2000 I=1,100
00690           FI=FLOAT(I)
00700           WB=(FI-1.)/(-99.)*(XWB-.00001)+XWB
00710           WA=(FI-1.)/(-99.)*(XWA-.00001)+XWA
00720           CB=(WB**2/BA+BB)/BG
00730           CA=(WA**2/AA+AB)/AG
00740           XXX=.5*(2.356*(CB-BS1)/WB)**2
00750           IF(XXX.GT.75.)XXX=75. CYBER COMP. LIMIT
00760           RBD=BA1/(SIN(WB/4.)**2)*EXP(-XXX)
00770           RBS=BA1/(SIN(CB)*SIN(WB/2.))*EXP(-XXX) RATIO OF AREAS GAIN
00780           XXX=.5*(2.356*(CA-AS1)/WA)**2
00790           IF(XXX.GT.75.)XXX=75.
00800           RAD=AA1/(SIN(WA/4.)**2)*EXP(-XXX)
00810           RAS=AA1/(SIN(CA)*SIN(WA/2.))*EXP(-XXX)
00820           IF(RBD.GT.XBD)XBD=RBD  ⎫
00830           IF(RBS.GT.XBS)XBS=RBS  ⎬ RESULTANT
00840           IF(RAD.GT.XAD)XAD=RAD  ⎭
00850           IF(RAS.GT.XAS)XAS=RAS
00860           IF(RBD.EQ.XBD)IBD=I
00870           IF(RBS.EQ.XBS)IBS=I
00880           IF(RAD.EQ.XAD)IAD=I
```

$w^2 = \alpha(-\beta + \gamma C)$

RESULTANT { BEFORE { DESPUN / SPUN } ; AFTER }

RESULTANT = A_1 * PEAK * GAUSSIAN SHAPE.

FIGURE 12
TRAJECTORY ANALYSIS COMPUTER LISTING (Continued)

22

```
00890         IF(RAS.EQ.XAS)IAS=I
00900 2000 CONTINUE
00910C        OPTIMALS
00920         WBD=(FLOAT(IBD)-1.)/(-99.)*(XWB-.00001)+XWB
00930         WBS=(FLOAT(IBS)-1.)/(-99.)*(XWB-.00001)+XWB
00940         WAD=(FLOAT(IAD)-1.)/(-99.)*(XWA-.00001)+XWA
00950         WAS=(FLOAT(IAS)-1.)/(-99.)*(XWA-.00001)+XWA
00960         CBD=(WBD**2/BA+BB)/BG
00970         CBS=(WBS**2/BA+BB)/BG
00980         CAD=(WAD**2/AA+AB)/AG
00985         CAS=(WAS**2/AA+AB)/AG
00986         PRINT 9999,WBS,CBS,IBS,WAS,CAS,IAS
00987 9999 FORMAT(1X,'****',2G12.4,I6,2G12.4,I6)
00991         IF(WBS/2..GT.CBS)GOTO2800
00992 2810 CONTINUE
00993         IF(WAS/2..GT.CAS)GOTO2820
00994 2830 CONTINUE
00995         IF(ABS(ALOG10(BA1)-ALOG10(BA2)).LT..1)GOTO2500
00996 2502 IF(ABS(ALOG10(AA1)-ALOG10(AA2)).LT..1)GOTO2600
00997 2700 CONTINUE
01000C        THREE FOOT PARABOLA      W0 = TE4/(FRQ * DISH)
01010         WB3=.3879        1050 MHz
01020         WA3=.7404         550 MHz
01030         CB3=(WB3**2/BA+BB)/BG
01035         IF(CB3.LT.BS1)CB3=BS1
01036         IF(CB3.GT.BS2)CB3=BS2
01040         CA3=(WA3**2/AA+AB)/AG
01045         IF(CA3.LT.AS1)CA3=AS1
01046         IF(CA3.GT.AS2)CA3=AS2
01050         RBD3=BA1*1./(SIN(WB3/4.))**2*EXP(-.5*(2.356*
01060       &(CB3-BS1)/WB3)**2)
01062         RBD39=BA2/(SIN(WB3/4.))**2*EXP(-.5*(2.356*
01063       &(CB3-BS2)/WB3)**2)
01064         IF(RBD39.LT.RBD3)RBD3=RBD39
01070         RAD3=AA1*1./(SIN(WA3/4.))**2*EXP(-.5*(2.356*
01080       &(CA3-AS1)/WA3)**2)
01082         RAD39=AA2/(SIN(WA3/4.))**2*EXP(-.5*(2.356*
01083       &(CA3-AS2)/WA3)**2)
01084         IF(RAD39.LT.RAD3)RAD3=RAD39
01090C        LOOP VEE LIMITS;FIX W ; VARY C
01100         WV=.8727
01110         CVB=(WV**2/BA+BB)/BG
01115         IF(CVB.LT.BS1)CVB=BS1
01116         IF(CVB.GT.BS2)CVB=BS2
01117         IF(CVB.LT..4363)CVB=.4363
01120         CVA=(WV**2/AA+AB)/AG
01125         IF(CVA.LT.AS1)CVA=AS1
01126         IF(CVA.GT.AS2)CVA=AS2
01127         IF(CVA.LT..4363)CVA=.4363
```

FIGURE 12

TRAJECTORY ANALYSIS COMPUTER LISTING (Continued)

```
01130        RBV=BA1*1./(SIN(CVB)*SIN(WV/2.))*EXP(-.5*(2.356*
01140       &(CVB-BS1)/WV)**2)
01142        RBV9=BA2/(SIN(CVB)*SIN(WV/2.))*EXP(-.5*(2.356*
01143       &(CVB-BS2)/WV)**2)
01144        IF(RBV9.LT.RBV)RBV=RBV9
01150        RAV=AA1*1./(SIN(CVA)*SIN(WV/2.))*EXP(-.5*(2.356*
01160       &(CVA-AS1)/WV)**2)
01162        RAV9=AA2/(SIN(CVA)*SIN(WV/2.))*EXP(-.5*(2.356*
01163       &(CVA-AS2)/WV)**2)
01164        IF(RAV9.LT.RAV)RAV=RAV9
01170C       HUMAN UNITS
01190        WBS=WBS*RD
01200        WV=WV*RD
01210        WBD=WBD*RD
01215        WB3=WB3*RD
01220        CBS=CBS*RD
01225        CBD=CBD*RD
01230        CVB=CVB*RD
01240        CB3=CB3*RD
01250        WAS=WAS*RD
01260        WAD=WAD*RD
01270        WA3=WA3*RD
01280        CAS=CAS*RD
01290        CVA=CVA*RD
01300        CAD=CAD*RD
01310        CA3=CA3*RD
01320        XBS=10.*@LOG10(ABS(XBS))
01330        RBV=10.*ALOG10(ABS(RBV))
01340        XBD=10.*ALOG10(XBD)
01350        RBD3=10.*ALOG10(RBD3)
01360        XAS=10.*ALOG10(ABS(XAS))
01370        RAV=10.*ALOG10(RAV)
01380        XAD=10.*ALOG10(XAD)
01390        RAD3=10.*ALOG10(RAD3)
01400        PRINT 3000
01410 3000   FORMAT(1X,'PREENTRY',3X,'W',5X,'C',3X,'MERIT')
01420        PRINT 3001,WBS,CBS,XBS
01430 3001   FORMAT(2X,'SPUN     ',F5.1,F6.1,F6.2)
01440        PRINT 3002,WV,CVB,RBV
01450 3002   FORMAT(2X,'LOOPVEE ',F5.1,F6.1,F6.2)
01460        PRINT 3003,WBD,CBD,XBD
01470 3003   FORMAT(2X,'DESPUN   ',F5.1,F6.1,F6.2)
01480        PRINT 3004,WB3,CB3,RBD3
01490 3004   FORMAT(2X,'3 FOOT  ',F5.1,F6.1,F6.2)
01500        PRINT 3005
01510 3005   FORMAT(1X,'POSTENTRY',2X,'W',5X,'C',3X,'MERIT')
01520        PRINT 3001,WAS,CAS,XAS
01530        PRINT 3002,WV,CVA,RAV
01540        PRINT 3003,WAD,CAD,XAD
```

PREENTRY	W	C	A.G.
SPON	WBS	CBS	XBS
VEE	WV	CVB	RBV
DESPON	WBD	CBD	XBD
3'	WB3	CB3	RBD3
POSTENTRY			
SPON	WAS	CAS	XAS
VEE	WV	CVD	RAV
DESPON	WAD	CAD	XAD
3'	WA3	CA3	RAD3

FIGURE 12
TRAJECTORY ANALYSIS COMPUTER LISTING (Continued)

```
01550          PRINT 3004, WA3, CA3, RAD3
01560          GOTO1000
01570 2500 CONTINUE
01580C         BEFORE AND CENTERED WITHIN 1DB
01590          WB=BS2-BS1
01600          CB=(BS2+BS1)/2.
01610          XXX=.5*(2.356*(CB-BS1)/WB)**2
01620          IF(XXX.GT.75.)XXX=75.
01630          ZRBD=BA1/(SIN(WB/4.)**2)*EXP(-XXX)
01640          ZRBS=BA1/(SIN(CB)*SIN(WB/2.))*EXP(-XXX)
01650          WB=WB*RD
01660          CB=CB*RD
01670          ZRBD=10.*ALOG10(ZRBD)
01680          ZRBS=10.*ALOG10(ZRBS)
01690          PRINT 2501,CB,WB,ZRBD,ZRBS
01700 2501 FORMAT(1X, BEFORE AND CENTERED WITHIN 1DB ,/,
01710          &1X, BC= ,G12.4, BW= ,G12.4,/,
01720          &1X, DESPUN= ,G12.4, SPUN= ,G12.4)
01730          GOTO2502
01740 2600 CONTINUE
01750C         AFTER AND CENTERED WITHIN 1DB
01760          WA=AS2-AS1
01770          CA=(AS2+AS1)/2.
01780          XXX=.5*(2.356*(CA-AS1)/WA)**2
01790          IF(XXX.GT.75.)XXX=75.
01800          ZRAD=AA1/(SIN(WA/4.)**2)*EXP(-XXX)
01810          ZRAS=AA1/(SIN(CA)*SIN(WA/2.))*EXP(-XXX)
01820          WA=WA*RD
01830          CA=CA*RD
01840          ZRAD=10.*ALOG10(ZRAD)
01850          ZRAS=10.*ALOG10(ZRAS)
01860          PRINT 2601,CA,WA,ZRAD,ZRAS
01870 2601 FORMAT(1X, AFTER AND CENTERED WITHIN 1DB ,/,
01880          &1X, BC= ,G12.4, BW= ,G12.4,/,
01890          &1X, DESPUN= ,G12.4, SPUN= ,G12.4)
01900          GOTO 2700
01910 2800 CONTINUE
01920C         SPUN LIMIT: W**2=A(-B+G*C) &W=2*C
01925          YYY=BA*(-BB+BG*BS1)
01926          YYY=SIGN(1.,YYY)
01930          CBS=BA*BG/8.+YYY*SQRT((BA*BG/8.)**2-BA*BB/4.)
01940          WBS=2.*CBS
01950          XXX=.5*(2.356*(CBS-BS1)/WBS)**2
01960          IF(XXX.GT.75.)XXX=75.
01970          XBS=BA1/(SIN(CBS)*SIN(WBS/2.))*EXP(-XXX)
01975          PRINT 2899
01976 2899 FORMAT(1X, ***** BEFORE SPUN LIMIT )
01980          GOTO2810
01990 2820 CONTINUE
```

FIGURE 12

TRAJECTORY ANALYSIS COMPUTER LISTING (Continued)

```
01995        YYY=AA*(-AB+AG*ASI)
01996        YYY=SIGN(I.,YYY)
02000        CAS=AA*@G/8.+YYY*SQRT((AA*@G/8.)**2-AA*@B/4.)
02010        WAS=2.*CAS
02020        XXX=.5*(2.356*(CAS-ASI)/WAS)**2
02030        IF(XXX.GT.75.)XXX=75.
02040        XAS=AAI/(SIN(CAS)*SIN(WAS/2.))*EXP(-XXX)
02045        PRINT 2898
02046 2898   FORMAT(IX,'***** AFTER SPUN LIMIT')
02050        GOTO2830
02060        END
```

FIGURE 12
TRAJECTORY ANALYSIS COMPUTER LISTING (Continued)

the probe roll axis algined to Earth at probe spacecraft separation and a
launch date of 2446028.6 Julian. For this analysis 25 trajectories were
defined covering the matrix of periapsis from 1.6 to 2.0 in 0.1 radii steps
and of phasings from 0.3 to 0.7 in 0.1 hour steps.

The temporal relationship between the probe and spacecraft trajectories
herein is termed phase time. This is the time from probe entry to the minimum
transmission range. Another relationship is termed lead time. This is the
time from probe entry to spacecraft periapsis. Reference 11 provides algorithms
to relate these various definitions. Over the range of periapsis herein, for
the baseline mission, the lead time, LT, may be related to the phasing TT by

$$LT = ((5.14)TT + (-.2553 \; RP^2 - 1.3589 \; RP + 4.4731))/10$$

where RP is the periapsis.

For each of these trajectories, the optimum (within the specified physi-
cal limits) reception antenna (both spun and despun) was defined and a figure
of merit (quasi-margin) identified. The two computer runs thus define points
on a three dimensional trajectory/margin surface. One such surface is the pre-
entry case, and another is the post entry case. Figure 13 illustrates the
surfaces. The optimal trajectory for each case is just the maximum margin
point. As one might expect, the optimal pre-entry communications trajectory
is not the optimal post entry communications trajectory. The intersection of
the two surfaces is the best joint trajectory loci, and the maximum margin of
this three dimensional curve is the optimal joint trajectory. It should also
be noted that before the joint trajectory comparison can be made, the maximum
figures of merit for both cases must be normalized. Recall that the figure
of merit is a partial derivative, and hence is meaningful only to that case.
Herein, both pre-entry and post entry cases were normalized to unity, thus
equating the importance of each. Of course other normalizations might be
suitable also.

A summary of the "raw" data is given in Table 4. For both the spun cases
cases, and for the despun pre-entry case the maximum point is apparent, that
is the normalization point. For the post entry despun case the maxima of the
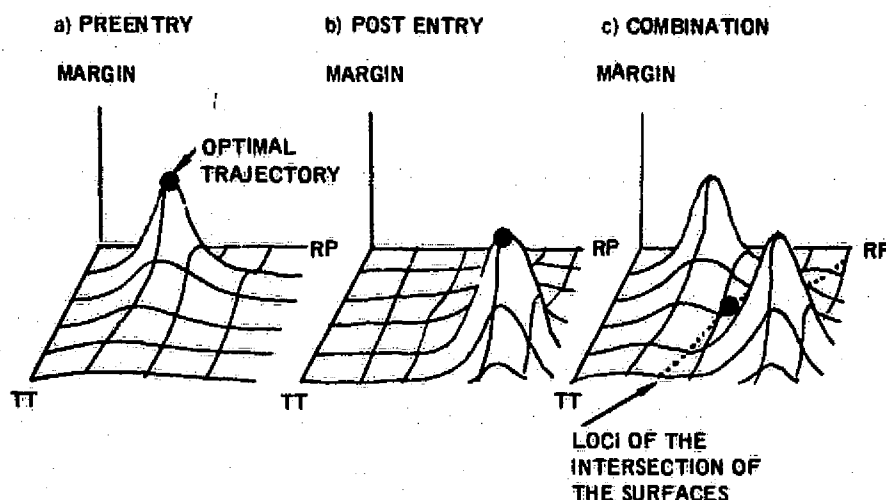
26

FIGURE 13
OPTIMAL TRAJECTORY ANALYSIS

table is at a corner of the matrix, and thus may not be the true maxima. The trajectories were extrapolated, with the raw data summarized in Table 5.

Contour plots of the data are given in Figures 14 and 15. For the spun spacecraft antenna case the best joint trajectory appears to be in the vicinity of a 1.65 radii periapsis, 0.4 hour phasing, while for the despun spacecraft antenna case the best joint trajectory appears to be in the vicinity of a 1.8 radii periapsis, 0.4 hour phasing. Although contour plots provide the best visualization of the problem, their accuracy is a function of the accuracy of the contours. An alternative scheme which provides accuracy, but leaves something to be desired in terms of visualization are carpet plots; Figures 16 and 17. It is seen that for either antenna the optimum trajectory phasing is 0.4 hour, and for the spun spacecraft antenna the optimum periapsis is 1.63 radii, and for the despun spacecraft antenna the optimum periapsis is 1.79 radii.

Table 6 summarizes the trajectory selected, together with the associated spacecraft antenna characteristics.

High Periapsis Trajectories

In a Jupiter Orbiter with Probe mission the spacecraft would remain in orbit long after the completion of the probe mission. As Jupiter has severe radiation belts, the accumulated dosage is significant, particularly within a few radii. An obvious method to reduce the dosage is to increase the initial spacecraft periapsis, where a large fraction of the dosage occurs. Higher initial (probe related) periapsis would also significantly reduce the shielding penalty (a fixed fraction of the total electronics weight) for larger spacecraft. Therefore a secondary task was to optimize the communication system design for higher periapsis.

TABLE 4

OPTIMAL ANTENNA FIGURES OF MERIT, DECIBELS

PERIAPSIS	PHASING	SPUN		DESPUN	
		PREENTRY	POST ENTRY	PREENTRY	POST ENTRY
1.6	.7	3.68	1.73	17.49	9.79
	.6	5.93	4.58	19.19	11.31
	.5	7.99	6.02	20.87	12.28
	.4	9.24**	6.85	22.4***	13.31
	.3*	9.46	7.09	23.12	19.97
1.7	.7	5.82	4.88	18.87	11.97
	.6	7.32	6.64	20.14	13.43
	.5	8.04	7.37	21.3	14.44
	.4	8.19	7.77	21.91	15.15
	.3	7.07	7.63	21.68	15.60
1.8	.7	6.83	6.82	19.65	13.98
	.6	7.02	7.40	20.47	15.07
	.5	7.11	7.89	20.87	15.95
	.4	6.35	8.02	20.77	16.47
	.3	4.76	7.87	20.12	16.73
1.9	.7	6.13	7.23	19.78	15.38
	.6	6.14	7.62	19.99	16.24
	.5	5.44	7.91	18.89	16.96
	.4	4.16	8.04	19.42	17.38
	.3	2.84	8.05	18.59	17.60
2.0	.7	5.12	7.38	19.17	16.36
	.6	4.34	7.71	19.01	17.00
	.5	3.35	7.99	18.63	17.54
	.4	2.34	8.10***	18.02	17.87
	.3	1.15	8.09	17.15	18.03***

* Spacecraft view angle in excess of 105 degrees

** Maxima

*** Quasi-Maxima

Higher periapses incur longer transmission ranges, but one would antici-
pate that the additional free space loss could be offset by the higher gain
of narrow beam antennas. Also, for a given antenna size, a higher carrier
frequency increases the antenna gain. The first step therefore is to rein-
vestigate the optimal carrier frequency for the higher periapsis trajectories
with despun spacecraft antennas. Figure 18 is a data dump from the carrier
frequency analysis routine of the previous section. It is apparent from the
figure that the optimal transmission frequency varies with the assumed recep-
tion dish size, and the trajectory. An apparent lower "bound" in the vicinity
of 550 MegaHertz exists, due to synchrotron and cosmic noise effects; while

TABLE 5
EXTRAPOLATED TRAJECTORY DATA

PERIAPSIS	PHASING	SPUN		DESPUN	
		PRE-ENTRY	POST-ENTRY	PRE-ENTRY	POST-ENTRY
2.1	.3	-.59	8.42	15.62	18.64
2.2	.3	-2.15	8.50*	14.18	18.93*
2.3	.3	-3.85	8.23	12.56	18.83
2.0	.2	-.04	7.99	16.21	18.05
2.0	.1	-1.48	7.68	14.91	17.80
2.0	.0	-2.89	7.33	13.57	17.43
2.1	.2	-2.71	7.87	13.68	18.17
2.2	.1	-6.56	7.18	9.94	17.75
2.3	.0	-10.73	6.02	5.81	16.73

* MAXIMA
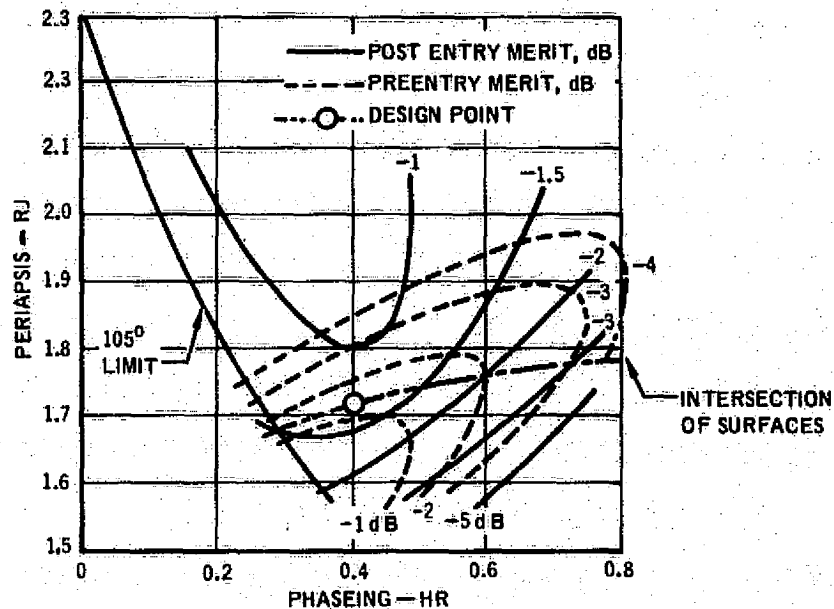
FIGURE 14

SPUN SPACECRAFT ANTENNA TRAJECTORY SELECTION
CONTOUR PLOT

an apparent upper "bound" of 850 to 1050 MegaHertz exists due to transmission efficiency, noise figure and free space. Thus, in this range, the frequency is that which provides the required beamwidth for a specified dish size. The assumption, of course, is that the beam is not steered during the mission.
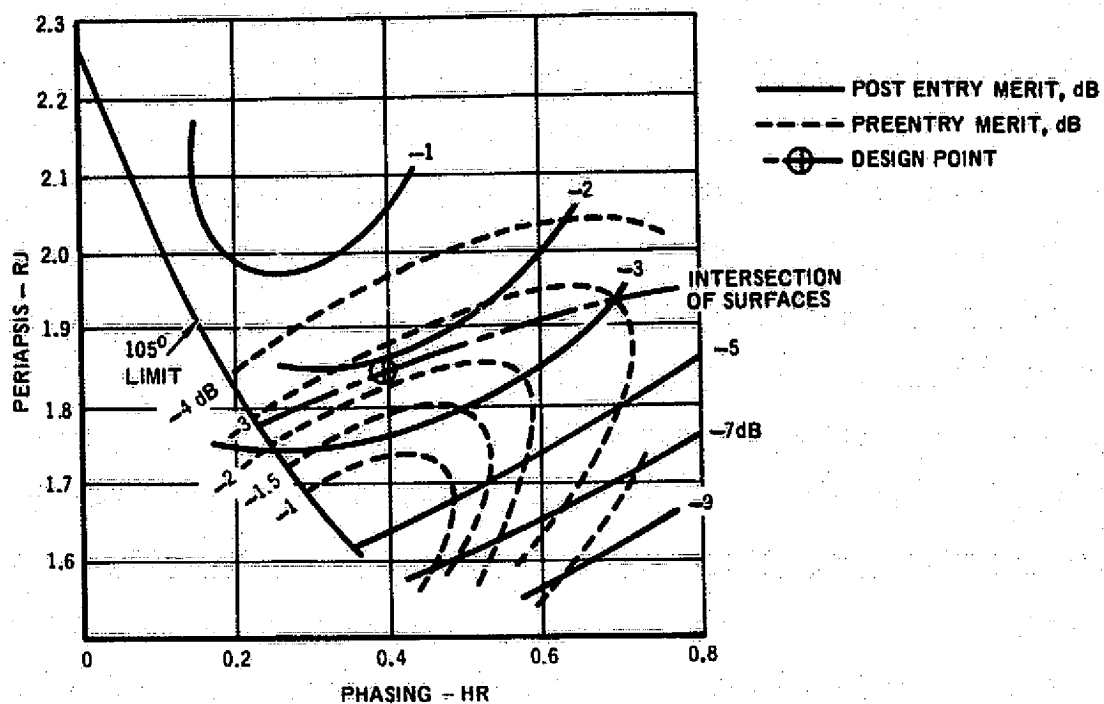
FIGURE 15

DESPUN SPACECRAFT ANTENNA TRAJECTORY
SELECTION CONTOUR PLOT
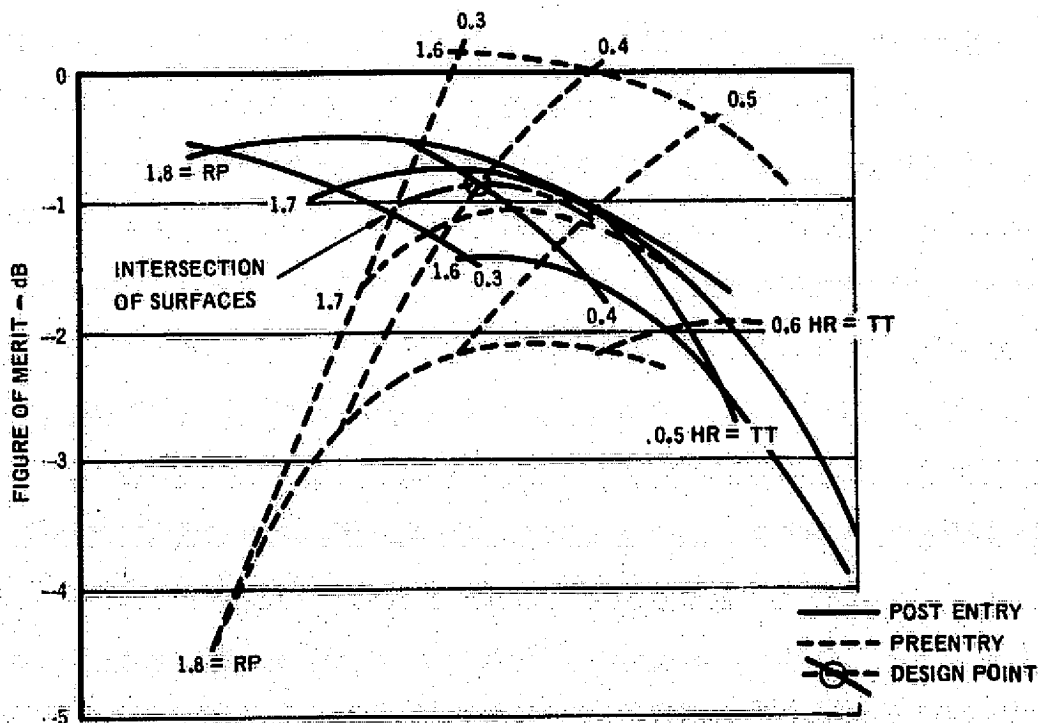
FIGURE 16

SPUN SPACECRAFT ANTENNA TRAJECTORY
SELECTION CARPET PLOT

FIGURE OF MERIT – dB

POST ENTRY
PREENTRY
DESIGN POINT

INTERSECTION OF SURFACES

2.0 = RP

0.6 HR = TT

0.7 HR = TT
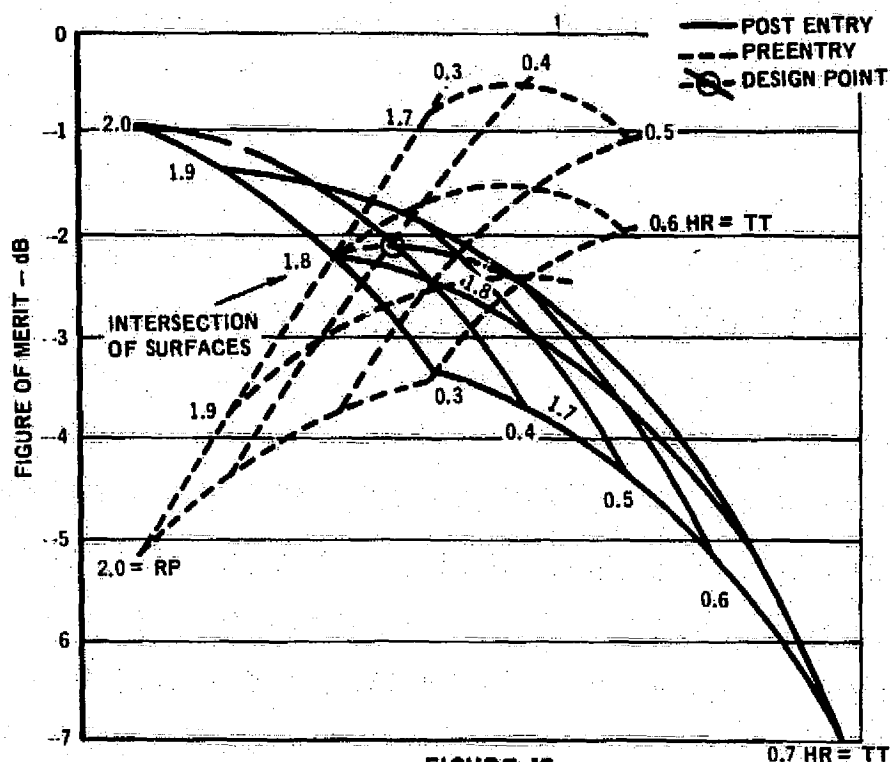
FIGURE 17
DESPUN SPACECRAFT ANTENNA TRAJECTORY SELECTION
CARPET PLOT

TABLE 6
TRAJECTORY SELECTION SUMMARY

A) INDIVIDUAL TRAJECTORIES (OPTIMAL FOR EACH CASE)

	SPUN		DESPUN	
	PREENTRY	POST ENTRY	PREENTRY	POST ENTRY
RP	1.6	2.2	1.6	2.2
TT	.4	.3	.4	.3
W	50°	50°	22.2°	42.4
C	27.5°	74.6°	27.7°	74.9

B) JOINT TRAJECTORIES (OPTIMAL FOR EACH SPACECRAFT ANTENNA TYPE

	SPUN	DESPUN
RP	1.686	1.836
TT	.4	.4

	PREENTRY	POST ENTRY	PREENTRY	POST ENTRY
W	50°	79.2°	22.2°	42.4°
C	32.5°	39.6°	47.8°	62.1°

TRAJ. 1.8; 0.5   BWBF= 11. , BWAF= 52

DISH, FT

	3	6	9	12
FRQ	PREDFS	PREDFS	PREDFS	PREDFS
200.00	204.71	204.71	204.71	204.71
300.00	207.93	207.93	207.93	207.93
400.00	210.04	210.04	210.04	210.04
500.00	211.29	211.29	211.29	211.29✔
600.00	212.14	212.14	212.14	211.07
700.00	212.71	212.71	212.71✔	210.30
800.00	213.07	213.07	211.99	209.48
900.00	213.27	213.27	211.17	208.68
1000.00	213.35✔	213.35✔	210.34	207.94
1100.00	213.34	213.09	209.50	207.00
1200.00	213.24	212.17	208.65	206.15
1300.00	213.09	211.31	207.79	205.29
1400.00	212.84	210.43	206.90	204.41
1500.00	212.53	209.52	206.00	203.50
1600.00	212.16	208.58	205.06	202.55
1700.00	211.70	207.60	204.09	201.59
1800.00	211.15	206.56	203.03	200.53
1900.00	210.48	205.42	201.90	199.40
2000.00	209.65	204.14	200.62	198.19
2100.00	208.58	202.65	199.13	196.63
2200.00	206.91	200.79	197.27	194.77
2300.00	204.15	199.13	194.61	192.11
FRQ	POSDFS	POSDFS	POSDFS	POSDFS
200.00	191.14	191.14	188.61	186.11
300.00	197.71	195.18	191.67	189.17
400.00	203.21	197.19	194.67	192.17
500.00	205.17	199.15	195.63	193.13
600.00	205.25✔	199.03✔	195.71✔	193.21✔
700.00	204.94	199.91	195.99	192.79
800.00	204.09	198.07	194.55	192.05
900.00	203.19	197.10	193.59	191.09
1000.00	201.99	195.96	192.44	189.94
1100.00	200.70	194.68	191.15	188.66
1200.00	199.59	193.27	190.75	187.05
1300.00	197.79	191.76	188.03	185.74
1400.00	196.16	190.14	186.61	184.19
1500.00	194.43	188.41	184.90	182.30
1600.00	192.60	186.57	183.05	180.55
1700.00	190.64	184.69	181.10	178.50
1800.00	188.55	182.53	179.01	176.51
1900.00	186.30	180.29	176.75	174.26
2000.00	183.84	177.82	174.30	171.80
2100.00	181.11	175.09	171.56	169.07
2200.00	177.93	171.91	168.30	165.80
2300.00	173.89	167.87	164.34	161.85

FIGURE 18
HIGH PERIAPSIS CARRIER FREQUENCY ANALYSIS

	DISH, FT			
	3	6	9	12
FPO	PREDES	PREDES	PREDES	PREDES
200.00	204.71	204.71	204.71	204.71
300.00	207.93	207.93	207.93	207.93
400.00	210.04	210.04	210.04	210.04
500.00	211.29	211.29	211.29	211.29
600.00	212.14	212.14	212.14	212.14
700.00	212.71	212.71	212.71	212.19✓
800.00	213.07	213.07	213.07✓	211.38
900.00	213.27	213.27	213.06	210.56
1000.00	213.35✓	213.35✓	212.23	209.73
1100.00	213.34	213.34	211.39	208.89
1200.00	213.24	213.24	210.54	208.04
1300.00	213.09	213.09	209.67	207.19
1400.00	212.94	212.39	208.79	206.29
1500.00	212.53	211.41	207.79	205.39
1600.00	212.16	210.47	206.85	204.45
1700.00	211.70	209.49	205.97	203.47
1800.00	211.15	208.44	204.92	202.42
1900.00	210.48	207.31	203.79	201.39
2000.00	209.55	206.03	202.51	200.01
2100.00	208.59	204.54	201.09	198.59
2200.00	207.13	202.68	199.15	196.66
2300.00	204.85	200.09	196.49	194.00
FPO	POSDES	POSDES	POSDES	POSDES
200.00	191.14	191.14	191.14	191.14
300.00	197.71	197.71	197.71	197.71
400.00	203.21	203.21	203.21	202.41
500.00	206.11	206.11	205.86	203.36
600.00	207.79	207.79	205.95✓	203.45✓
700.00	208.70	208.70✓	205.53	203.03
800.00	209.19	208.31	204.79	202.29
900.00	209.17✓	207.34	203.92	201.32
1000.00	208.94	206.30	202.69	200.19
1100.00	207.69	204.91	201.39	198.89
1200.00	207.94	203.51	199.99	197.49
1300.00	207.09	201.99	198.47	195.97
1400.00	205.94	200.37	196.85	194.35
1500.00	204.57	198.65	195.13	192.63
1600.00	202.93	196.81	193.29	190.79
1700.00	200.99	194.85	191.34	188.84
1800.00	198.79	192.77	189.25	186.75
1900.00	196.54	190.59	186.99	184.50
2000.00	194.02	188.06	184.54	182.04
2100.00	191.35	185.39	181.90	179.30
2200.00	188.17	182.15	178.59	176.13
2300.00	184.19	178.19	174.59	172.09

FIGURE 18
HIGH PERIAPSIS CARRIER FREQUENCY ANALYSIS (Continued)

DISH, FT

FRQ	3	6	9	12
	PREDES	PREDES	PREDES	PREDES
200.00	204.71	204.71	204.71	204.71
300.00	207.03	207.03	207.03	207.03
400.00	210.04	210.04	210.04	210.04
500.00	211.29	211.29	211.29	211.29
600.00	212.14	212.14	212.14	212.14
700.00	212.71	212.71	212.71	212.71
800.00	213.07	213.07	213.07	213.07
900.00	213.27	213.27	213.27	213.27
1000.00	213.35	213.35	213.35	213.35
1100.00	213.34	213.34	213.34	213.34
1200.00	213.24	213.24	213.24	213.24
1300.00	213.09	213.09	213.09	212.69
1400.00	212.94	212.94	212.94	211.74
1500.00	212.53	212.53	212.53	210.83
1600.00	212.16	212.16	212.15	209.80
1700.00	211.70	211.70	211.41	208.01
1800.00	211.15	211.15	210.36	207.07
1900.00	210.48	210.48	209.93	206.73
2000.00	209.65	209.65	207.95	205.45
2100.00	208.59	208.59	205.46	203.96
2200.00	207.13	207.13	204.60	202.10
2300.00	204.85	204.85	201.94	199.44
FRQ	POSDES	POSDES	POSDES	POSDES
200.00	191.14	191.14	191.14	191.14
300.00	197.71	197.71	197.71	197.71
400.00	203.21	203.21	203.21	203.21
500.00	206.11	206.11	206.11	206.11
600.00	207.79	207.79	207.79	207.79
700.00	208.70	208.70	208.70	208.70
800.00	209.12	209.12	209.12	209.12
900.00	209.17	209.17	209.17	209.17
1000.00	208.94	208.94	208.94	208.94
1100.00	208.49	208.49	208.49	208.49
1200.00	207.84	207.84	207.84	207.84
1300.00	207.09	207.09	207.09	207.09
1400.00	206.04	206.04	206.04	206.04
1500.00	204.91	204.91	204.91	204.91
1600.00	203.64	203.64	203.64	203.64
1700.00	202.21	202.21	202.21	202.01
1800.00	200.62	200.62	200.62	200.41
1900.00	198.83	198.83	198.83	198.16
2000.00	196.83	196.83	196.83	195.70
2100.00	194.51	194.51	194.51	192.96
2200.00	191.74	191.74	191.74	189.70
2300.00	188.09	188.09	188.09	185.74

FIGURE 18
HIGH PERIAPSIS CARRIER FREQUENCY ANALYSIS (Continued)

Table 7 summarizes the high periapsis trajectories. Figure 19 summarizes the best carrier frequency for any periapsis and dish size. Figure 20 summarizes the link figures of merit. The trajectories shown are for a phasing of 0.5 hour, and the maximum merits are for the optimal trajectories of the previous section. At the higher periapses, the phasing is a much less critical parameter. It is seen that for pre-entry communications, the link merit montonically decreases with increasing periapsis for all antenna sizes investigated. For example at six radii, the merit is -1.05 dB, or 24.47 dB below the baseline with a .9 meter parabola. This translates to an equivalent 1/279.7 reduction in date rate. At a 3.66 meter reception parabola, outside reality, the merit is 8.1 dB or 15.3 dB below the baseline, or a 1/33.88 data rate reduction.

TABLE 7
HIGH PERIAPSIS TRAJECTORY CONDITIONS
TT = 0.5 HR

| RP | t = -.3 HR | | P | T + 0 HR | | P* | T = +.5 HR | | P |
	R	S		R	S		R	S	
1.6	.7258	27.57	36.14	.9093	20.80	29.36/49.70	.5989	86.47	9.655
1.8	.8608	45.51	54.09	.9879	34.67	43.25/34.89	.8014	86.47	0.812
2.0	1.041	57.35	65.93	1.111	45.49	54.07/23.46	1.0044	86.47	0.7212
3.0	2.1	79.33	87.91	1.999	70.48	79.06/2.10	2.028	86.46	0.539
4.0	3.17	84.88	93.47	3.01	78.13	86.71/9.78	3.067	86.46	0.4784
5.0	4.254	86.96	95.55	4.057	81.42	90./13.08	4.12	86.46	0.448
6.0	5.34	87.87	96.46	5.126	83.14	91.73/14.80	5.199	86.46	0.430

R IN PLANET RADII
S AND P IN DEGREES

* AA/BB; AA = P (t = 0-); BB = P(t = 0+)

The post entry situation is less severe for small spacecraft parabolas; being 11.6 dB or 7.6 dB below the baseline for a .9 meter dish, that is an equivalent 1/5.81 data rate reduction. Moderate increases in allowable reception dish sizes in conjunction with higher periapsis can provide more post entry data, but with the corresponding pre-entry data penalty.

A completely different alternate approach is possible if the groundrules of simple, lightweight and inexpensive no longer apply. That would be the use of a monopulse tracking antenna to steer the beam during the mission. Of course in addition to a more complex antenna and receiver (plus the angular acquisition and tracking designs) the system would have to operate at low signal energy to noise density ratios in the presence of severe signal scintillation (long time constant Rayleigh fading). Assuming such a reception

TT = 0.5 HR

a) PREENTRY

DISH – M

b) POST ENTRY

DISH – M
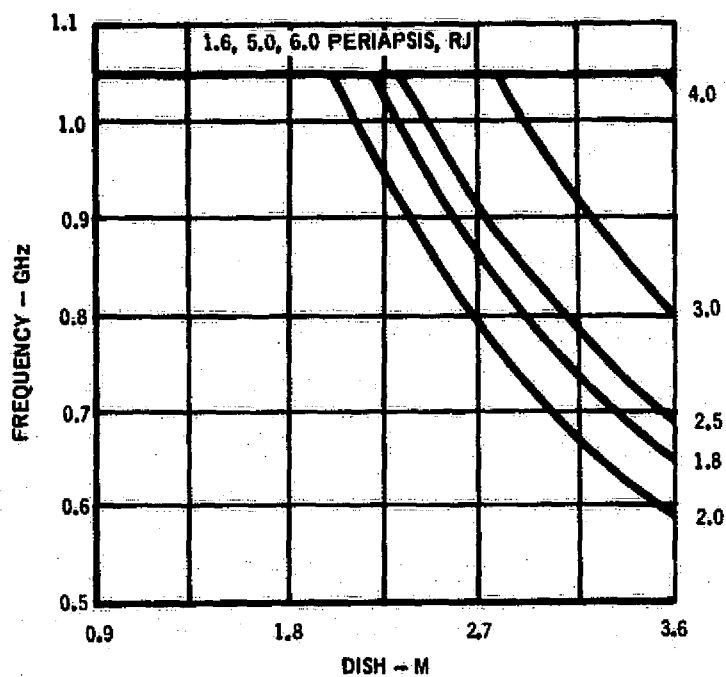
FIGURE 19

OPTIMUM TRANSMISSION FREQUENCY

A) PREENTRY

B) POST ENTRY

FIGURE 20

HIGH PERIAPSIS LINK MERIT

TT = 0.5 HR

system, the link figure of merit is just the logarithm of the product of the pointed antenna gain and the other non-pointed antenna gain factors. The net result of the latter factors is just the minimum A of the first paragraphs of this section. Figure 21 summarizes the effect. Although the p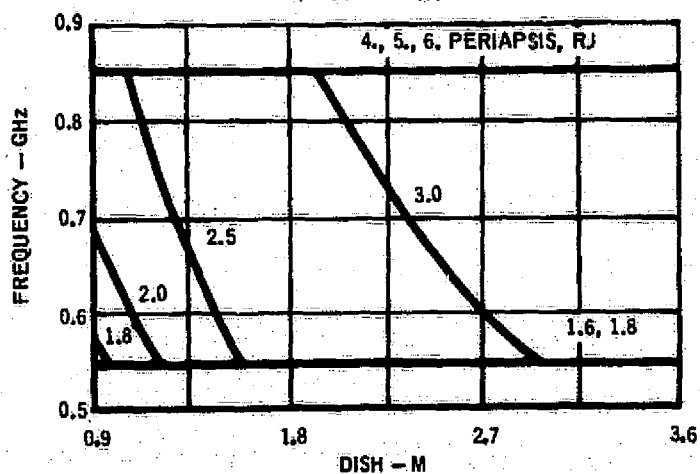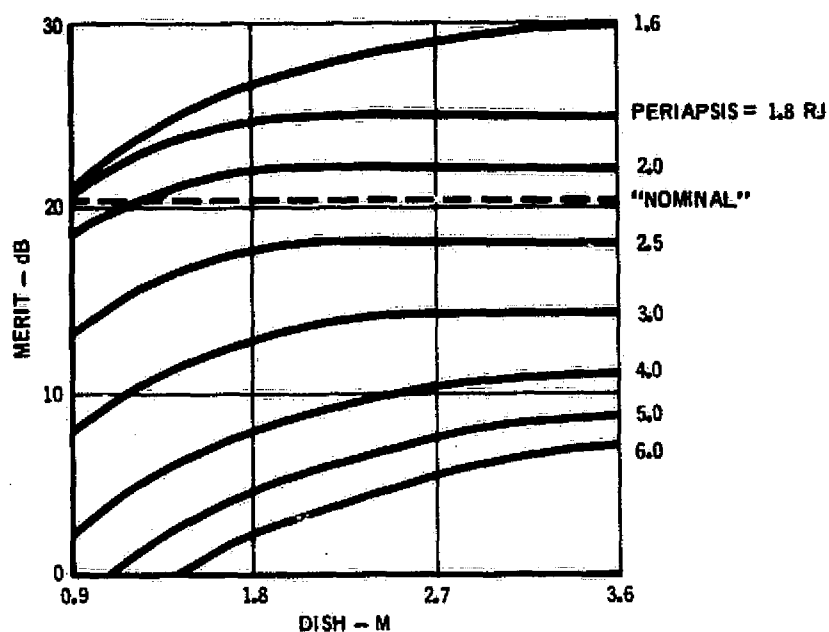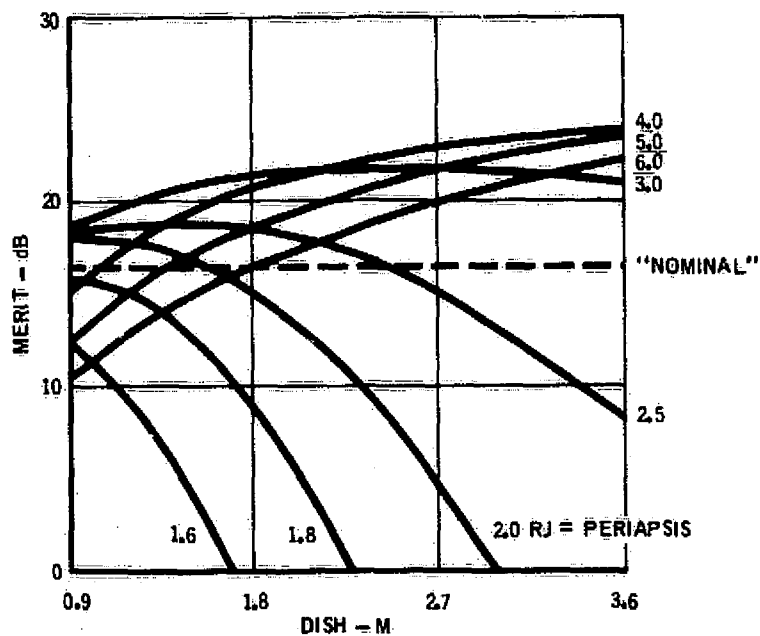ost entry link could tolerate higher radii periapsis for equivalent baseline results, the more complex system only allows a slightly greater periapsis for equivalent pre-entry data.

A high periapsis spacecraft trajectory will penalize the probe mission fairly significantly unless either a large dish is available on the spacecraft to receive the probe signals, or a sophisticated tracking system is employed.

High Latitude Trajectories

A second technique to reduce the radiation dosage, particularly for the probe but also probably applicable for the spacecraft, was pointed out in Reference 13. This is to enter at a higher latitude than the "nominal" 3.15°.

A minor variant of this trajectory of a 1068.6 day trip time is a 1207 day trip time which provides a slightly earlier local time entry. (That is one with entry meridians of 29 and 44 degrees from the terminator respectively.) To support this analysis, 12 trajectories were constructed to cover the two trip times, and to parametrically investigate entry latitude from zero to 20 degrees. Note that at much higher latitudes the entry heating, which varies with the secant squared, becomes significantly greater.

The trajectories are summarized in Tables 8 and 9. The figure of merit data are summarized in Table 10 and 11. In all cases there is relatively little effect out to approximately a 10 degree latitude, but at higher latitudes the merit drops quite rapidly.

Special Angle of Attack Trajectories

Two additional trajectory variants are a) to align the probe roll axis to Earthline at the time of entry and b) to align the probe roll axis to zero angle of attack at entry. The former would be the case if a direct to Earth pre-entry communications link were to be attempted, and the latter is an exercise to define link effects if entry angle of attack were critical. The entry angle of attack for the Earthline at entry situation is 12.16°, greater than the 3° typical of the reference mission, but within the maximum allowable of 15°. Table 12 summarizes the trajectory data. Table 13 summarizes the merit data. There is negligible effect for a despun antenna. The worst case degradation for a spun antenna is 0.5 dB for an Earthline at entry.

Summary

The geometric effects of a Jovian entry relay link have been investigated. It was found that the relative geometry between the trajectories has a signifi-

PRE-ENTRY
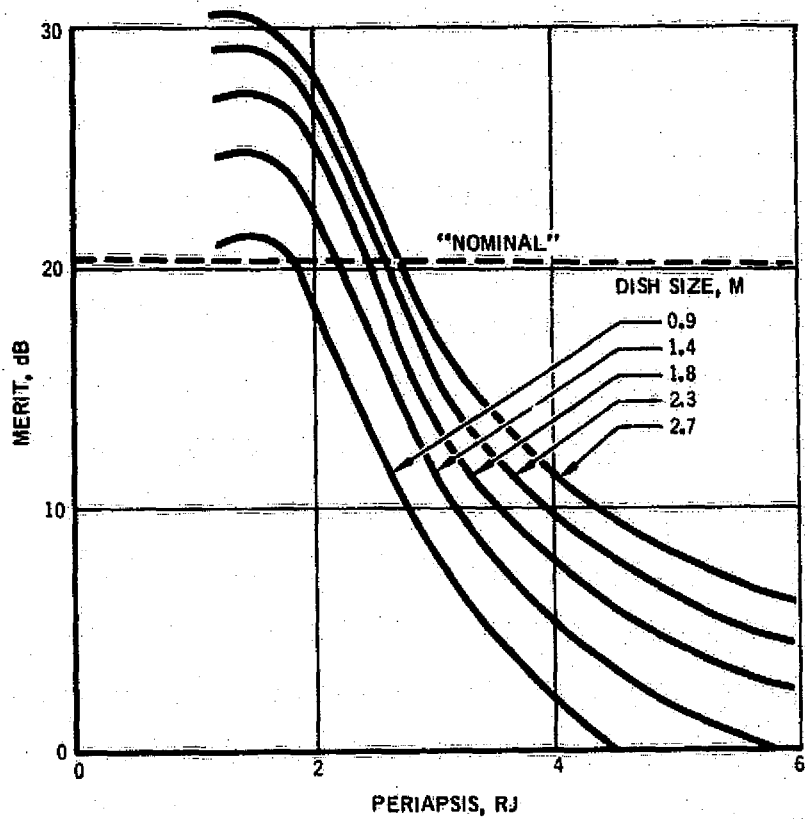
POST ENTRY
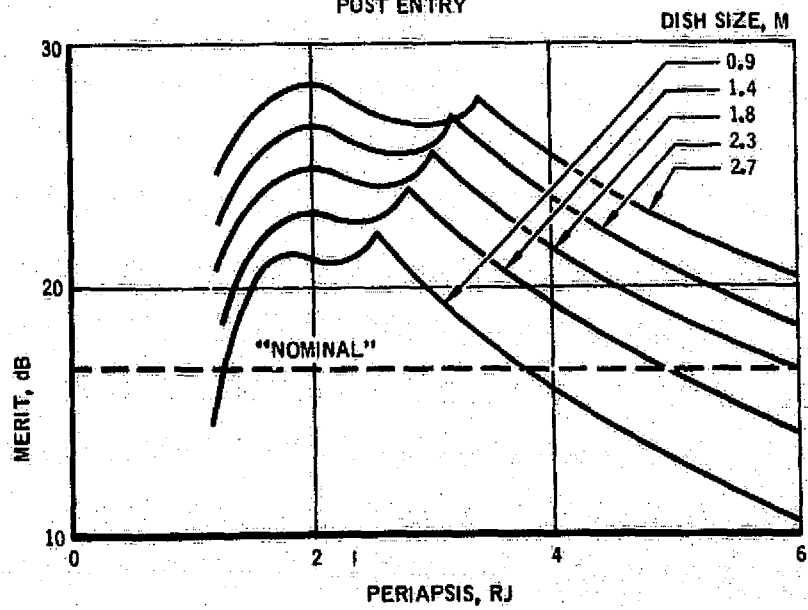
FIGURE 21

PERFECT MONOPULSE TRACKING PERFORMANCE

TABLE 8
1068.6 DAY ENTRY LATITUDE TRAJECTORY DATA (EQUATORIAL SPACECRAFT)
TT = 0.5

LATITUDE (DEG)	TIME (HR)	RANGE (RADII)	S (DEG)	P* (DEG)
0	-.3 0 +.5	.8798 .9889 .8065	46.68 35.21 86.81	54.93 43.69/35.29 8.21
3.15	-.3 0 +.5	.8608 .9879 .8014	45.51 34.67 86.47	54.09 43.25/34.89 0.81
5	-.3 0 +.5	.8675 .9891 .8023	45.53 34.65 86.44	54.10 43.24/35.11 3.54
10	-.3 0 +.5	.9477 .9986 .8187	47.78 35.66 87.02	55.70 44.17/37.48 15.13
15	-.3 0 +.5	1.1019 1.016 .8555	51.14 38.16 88.59	58.14 46.45/42.06 26.13
20	-.3 0 +.5	1.309 1.039 .9128	53.83 42.22 91.38	60.13 50.25/48.11 36.20
-5	-.3 0 +.5	.9827 .9980 .8314	50.52 37.31 88.2	57.72 45.52/38.07 19.66
-10	-.3 0 +.5	1.1571 1.0154 .8770	54.45 40.93 90.49	60.65 48.80/43.17 30.38
-15	-.3 0 +.5	1.3862 1.0383 .9451	57.23 46.33 94.30	62.77 53.87/49.70 40.03

AA/BB IS P(t=0-) = AA; BB = P(t=0+)

TABLE 9
1207 DAY ENTRY LATITUDE TRAJECTORY DATA

LATITUDE (DEG)	TIME (HR)	RANGE (RADII)	S (DEG)	P* (DEG)
0	-.3	.8694	14.66	56.61
	0	.9878	4.30	44.91/35.20
	+.5	.8048	52.77	6.25
3.15	-.3	.8599	11.27	54.47
	0	.9875	.99	43.72/35.03
	-.5	.8019	52.39	1.13
5	-.3	.8715	12.83	56.10
	0	.9891	1.25	44.64/35.39
	+.5	.8040	52.45	5.46
10	-.3	.9616	22.66	68.04
	0	.9997	6.25	52.42/38.05
	+.5	.8238	53.58	16.95
15	-.3	1.1207	31.45	84.07
	0	1.0184	11.84	65.74/42.87
	+.5	.8636	56.07	27.79
20	-.3	1.3301	37.13	100.72
	0	1.0428	17.32	82.98/49.03
	+.5	.9241	59.89	37.67

$*$ AA/BB IS P(t = 0-) = AA; P(t = 0+) = BB

cant impact on the link performance. After defining an optimal set of space-craft antenna characteristics for each point on a periapsis phasing trajectory plane, the optimal point on that plane was found to maximize the data rate. This was done for both the case of a 360 degree clock angle of spun spacecraft antenna, and a pointed despun spacecraft antenna.

After the definition of the optimal geometries, two variant cases were investigated: high periapsis trajectories and high entry latitude trajectories. In the case of high periapsis trajectories it was found that they could provide slightly greater post entry margins if slightly larger despun spacecraft antenna dish sizes were available than assumed in the nominal case. However, the preentry margins uniformly degrade with higher periapses. In the case of high latitude trajectories it was found that relatively little communications link penalty accured on moving up to ten degrees latitude, but that the penalty becomes increasingly severe at still higher latitudes.

TABLE 10
INCLINED SPACECRAFT TRAJECTORY DATA FOR LATITUDE
RP = 1.8, TT = 0.5

LATITUDE (DEG)	TIME (HR)	RANGE (RADII)	S (DEG)	P* (DEG)
5	-.3	.8749	48.88	56.78
	0	.9929	37.08	45.08/35.67
	+.5	.8011	86.52	0
10	-.3	1.0771	77.81	82.12
	0	1.0684	59.57	64.63/45.88
	+.5	.7982	87.34	0
15	-.3	1.2777	100.03	102.76
	0	1.1708	80.32	83.38/55.34
	+.5	.7947	89.16	0
20	-.3	1.3967	115.60	117.44
	0	1.2669	96.09	98.10/61.27
	+.5	.7938	92.21	0
-5	-.3	1.1991	86.85	90.97
	0	1.1180	67.41	71.96/51.24
	+.5	.7968	87.70	0
-10	-.3	1.3742	105.84	108.74
	0	1.2224	86.04	89.27/59.31
	+.5	.7939	89.87	0
-15	-.3	1.4684	120.02	122.36
	0	1.3192	100.90	103.17/64.23
	+.5	.7950	93.52	0
-20	-.3	1.5037	134.32	135.45
	0	1.4262	115.94	117.19/67.45
	+.5	.8054	100.14	0

*AA/BB is P(t = 0-) = AA; P(t = 0+) = BB

TABLE 11

INCLINED SPACECRAFT TRAJECTORY DATA FOR PHASING

LATITUDE (DEG)	PHASING (HR)	TIME (HR)	RANGE (RADII)	S (DEG)	P* (DEG)
+10	.1	-.3	.8606	75.52	83.93
		0	.8270	62.79	71.11/8.68
		+.5	.9284	112.93	31.34
	.2	-.3	.8514	70.68	78.78
		0	.8580	57.17	65.17/10.51
		+.5	.8816	106.57	25.03
	.3	-.3	.8673	67.89	75.32
		0	.9041	53.58	60.99/26.03
		+.5	.8428	99.76	17.93
	.4	-.3	.9276	69.36	75.53
		0	.9696	53.54	59.90/35.18
		+.5	.8140	92.94	9.81
-10	.1	-.3	.8632	80.06	88.34
		0	.8314	67.59	75.65/10.67
		+.5	.9621	107.08	38.17
	.2	-.3	.8774	80.60	88.11
		0	.8756	65.95	73.25/11.07
		+.5	.9054	100.92	31.92
	.3	-.3	.9518	85.36	91.53
		0	.9489	68.27	74.41/34.19
		+.5	.8542	94.98	24.04
	.4	-.3	1.112	94.29	98.80
		0	1.0609	75.13	79.82/46.65
		+.5	.81331	90.51	13.72

*AA/BB is P(t = 0-) = AA; P(t = 0+) = BB

TABLE 12
PROBE ATTITUDE TRAJECTORY DATA

CASE	TIME (HR)	RANGE (RADII)	S (DEG)	P* (DEG)
EARTHLINE AT SEPARATION	-.3 0 -.5	.8608 .9879 .8014	45.51 34.67 86.47	54.09 43.25/34.89 .81
EARTHLINE AT ENTRY	-.3 0 +.5	.8608 .9879 .8014	45.51 34.67 86.47	45.51 34.67/34.89 .81
ZERO ANGLE OF ATTACK	-.3 0 -.5	.8608 .9879 .8014	45.51 34.67 86.47	57.65 46.80/34.89 .81

** AA/BB IS $P(t = 0-) = AA$; $P(t = 0+) = BB$

TABLE 13
PREENTRY ATTITUDE FIGURE OF MERIT SUMMARY, dB

CASE	SPUN	DESPUN
EARTHLINE AT SEPARATION	8.11	21.87
EARTHLINE AT ENTRY	7.64	21.61
ZERO ANGLE OF ATTACK	8.13	21.78

PRE-ENTRY COMMUNICATIONS LINK DESIGN

The first section of this report reviewed the propagation environment about Jupiter, and selected "optimal" transmission frequencies for the various types of relay links. The selections were for a "baseline" spacecraft trajectory with a periapsis of 1.8 Jovian radii and a phasing of 0.5 hr. The second section of this report investigated a number of trajectories and selected "otpimal" trajectories to maximize the data return. This section combines the propagation information with the geometric effects of the trajectories into link tables to define the allowable data rates.

The first step is to define the allowable data rates. This is given for both the case of no dual frequency Doppler experiment, and for the case with the experiment. Following this, margin histories are presented. Antennas other than the "optimals" are then explored. Finally, follows two special cases: a direct to Earth pre-entry link, and a nonoptimal six Jovian radii spacecraft periapsis case.

The trajectories previously selected were a periapsis of 1.685 radii with an 0.4 hr phasing (herein in shorthand 1.685; .4) for the case of a "spun" (360° clock angle) spacecraft reception pattern, and a 1.836; .4 trajectory for a despun (pointed) spacecraft antenna pattern. The geometric characteristics of these trajectories is given in Table 14. In the table, T is the time from entry, R is the transmission range, S is the spacecraft view angle, P is the probe view angle, RHØ is the spacecraft altitude from the center of the planet, and PHI2 is the planet subtended Earth spacecraft angle.

TABLE 14

OPTIMAL JOINT TRAJECTORIES

	T (hr)	R (radii)	S (deg)	P (deg)	RHØ (radii)	PHI2 (deg)
(a) Spun Spacecraft Antenna, 1.685; .4	-.3	.738	43.5	52.	1.99	33.
	0	.868	32.5	41./37.	1.785	52.
	+.5	.7	96.5	10.	1.7	91.
(b) Despun Spacecraft Antenna, 1.836; .4	-.3	.875	54.	62.	2.095	37.5
	0	.955	41.	50.5/ 27.5	1.915	55.
	+.5	.845	93.5	7.	1.855	90.

The optimal spacecraft antenna patterns are a 50° beamwidth 32.5° beam center for the spun case, and a 22.2° beamwidth 47.8° beamcenter for the despun case.

Data Links

The pre-entry data load, from Reference 13, is summarized in Table 15.

TABLE 15
PREENTRY DATA LOAD

Instrument	Data Rate (3 RJ - 1000 km)	Data Rate (below 1000 km)
Magnetometer	.27 BPS	5.33 BPS
Particle Detector	.53 BPS	10.67 BPS
Retarding Pot. Analyzer	.13 BPS	8.0 BPS
Radio Spec Analyzer	1.33 BPS	8.0 BPS
Clock	.13 BPS	8.0 BPS
Langmuir Probe	N/A	8.0 BPS
Neutral Mass Spec	N/A	24.0 BPS
Ion Mass Spec	N/A	16.0 BPS

The 3 RJ to 1000 km data is labeled "stored." in Reference 13, and the 1000 km to termination data is "real-time". Three Jovian radii on a 1.8; .5 trajectory is 1.1763 hr from entry. The time in the ionosphere, 1000 km, is

$$((R+250) \cos 97.5 + (((R+250) \cos 97.5)^2 - (R+250)^2 + (R+1000)^2)^{1/2})/59.6614 \text{ or}$$

77.61 secs for a 7.5° entry at 59.6614 km/sec. The "minimum" storage is thus

$$(2.4)(1.1763)(60)^2 = 10,163.23 \text{ bits.}$$

The pre-entry link from Reference 15 shall provide 10^4 bits minimum in the one to two minutes prior to entry, that is 83-1/3 to 166 2/3 bits per second. It shall also provide some capability for 20 minutes prior to entry.

Combining the requirements from References 13 and 15 it appears reasonable to collect and store from 3 RJ to T-20 minutes (1.1763 hr - 20 minutes) x (2.4 BPS) x (1.15 for synchronization and formatting) or 8375.72 bits; and then at T-20 minutes to switch to the high rate and dump the storage. The resultant rate, again with a 1.15 synchronization and formatting factor is 108.18 bits per second.

The bulk of the pre-entry link transmission is prior to the ionosphere, thus a coherent phase shift keyed modulation will provide the maximal data return. During the 77.61 seconds of ionospheric data the coherent link may well degrade, but any loss of data can be repeated in the post entry transmission.

Tables 16 and 17 are the preentry link tables. Each table is really two tables in order to define the end points of the transmission. In the tables the data rate is adjusted such that one of the end points of the mission has zero excess margin. Table 18 compares the "required" data rates, with those "available". The "excess" capability may be used for data, margin, or to reduce the transmitter size. An estimate of the physical characteristics of the transmitters and associated battery is given in Table 19. The despun system is 1.31 kg heavier, but provides 6.76 times more data.

TABLE 16
PREENTRY SPUN LINK TABLE

PARAMETER	VALUE		TOLERANCE		SOURCE
	T = -.3	T = 0	T = -.3	T = 0	
Total Transmitter Power	47.8	47.8	-1.	-1.	60 watts
Transmitting Circuit Loss	-.3	-.3	-.1	-.1	Assumed
Transmitting Antenna Gain	1.2	1.3	-.5	-.5	Centerfed microstrip
Space Loss (.4 GHz)	-178.9	-180.3	0	0	1.685; .4 trajectory
Ionospheric Loss	0	0	0	-1.	Theoretical
Polarization Loss	-3.	-3.	-.5	-.5	Assumed
Receiving Antenna Gain	4.2	4.7	-.5	-.5	Optimal antenna
Receiving Circuit Loss	-.5	-.5	-.1	-.1	Assumed
Total Received Power	-129.5	-130.3	-2.7	-3.7	Subtotal
Receiver Noise Spectral Density	-163.2	-162.7	1.7	1.7	1.685; .4 trajectory
Received Data Power	33.7	32.4	-4.4	-5.4	Subtotal
Bit Rate (134.9 BPS)	21.3	21.3	0	0	Calculated
Required Data Signal/N_0	4.5	4.5	0	0	PSK Rate 1/2
Receiver Loss	1.0	1.0	-.2	-.2	Assumed
Threshold Data Power	6.9	5.6	-4.6	-5.6	Subtotal
Performance Margin	2.3	0			Total

TABLE 17
PREENTRY DESPUN LINK TABLE

PARAMETER	VALUE		TOLERANCE		SOURCE
	T = -.3	T = 0	T = -.3	T = 0	
Total Transmitter Power	46.1	46.1	-1.	-1.	40.9 watts
Transmitting Circuit Loss	-.3	-.3	-.1	-.1	Assumed
Transmitting Antenna Gain	.3	1.3	-.5	-.5	Centerfed microstrip
Space Loss (1.05 GHz)	-188.8	-189.6	0	0	1.836; .4 trajectory
Ionospheric Loss	0	0	0	-.1	Theoretical
Polarization Loss	-3.	-3.	-.5	-.5	Assumed
Receiving Antenna Gain	16.8	16.6	-.5	-.5	Optimal Antenna
Receiving Circuit Loss	-.5	-.5	-.1	-.1	Assumed
Total Received Power	-129.4	-129.4	-2.7	-2.8	Subtotal
Receiver Noise Spectral Density	-168.6	-168.7	1.2	1.2	1.836; .4 trajectory
Received Data Power	39.2	39.3	-3.9	-4.0	Subtotal
Bit Rate (912 BPS)	29.6	29.6	0	0	Calculated
Required Data Signal/N_0	4.5	4.5	0	0	PSK Rate 1/2
Receiver Loss	1.0	1.0	-.2	-.2	Assumed
Threshold Data Power	4.1	4.2	-4.1	-4.2	Subtotal
Performance Margin	0	0			Total

TABLE 18
DATA RATE COMPARISON – DATA LINKS ONLY

	Spun	Despun
Available, BPS	134.9	912.
Required, Ref (13), BPS	83-1/3 to 166-2/3	
Excess, Ref (13), dB	-.9 to +2.1	7.4 to 10.4
Required, Table 15, BPS	108.18	
Excess, Table 15, dB	+1.	9.3

TABLE 19
PHYSICAL CHARACTERISTICS – DATA LINKS ONLY

	Spun	Despun
Transmitter Output (w)	60	40.9
Transmitter Input (w)	135.4	162.73
Transmitter Weight (kg)	1.48	2.60
Battery Weight (44.1 WH/kg)	.92	1.11
Total Probe Weight (kg)	2.40	3.71

Dual Frequency Differential Doppler Links

A dual frequency differential Doppler system measures the electron content of the propagation medium. In such an experiment the carrier frequencies should be of the order of an octave apart. To incorporate this experiment it is only necessary to (a) add the octave link, and (b) split off some of the power from the data link to provide accurate carrier tracking. The tracking loop bandwith 2 B_L is just 1.06 (2 ω_{DR})$^{1/2}$ where the angular Doppler rate ω_{DR} is $2\pi(V_D/C)F$ and V_D is the deceleration, C is the velocity of light and F is the carrier frequency. For the spun trajectory, the 1.685 periapsis, the maximum pre-entry deceleration is 15.5 m/sec^2, and the maximum post entry deceleration is 33 m/sec^2. For the despun trajectory, the 1.836 periapsis, the maximum pre-entry deceleration is 18 m/sec^2, and the maximum post entry deceleration is 22 m/sec^2. Tables 20 to 23 are the link tables for the various links. As before, the data link tables are really two tables to define the end points of the transmission. The tone links are of course only of import at t = 0- when the channel contains the ionosphere.

TABLE 20
PREENTRY SPUN DOPPLER LINK TABLE

PARAMETER	VALUE	TOLERANCE	SOURCE
Total Transmitter Power	45.0	-1.	31.84 watts
Transmitting Circuit Loss	-.3	-.1	Assumed
Transmitting Antenna Gain	1.3	-.5	Centerfed microstrip
Space Loss (.8 GHz)	-186.3	0	1.685; .4 trajectory
Ionospheric Loss	0	-.3	Theoretical
Polarization Loss	-3.	-.5	Assumed
Receiving Antenna Gain	4.7	-.5	Optimal Antenna
Receiving Circuit Loss	-.5	-.1	Assumed
Total Received Power	-139.1	-3.0	Subtotal
Receiver Noise Spectral Density	-167.4	1.5	1.685; .4 trajectory
Received Carrier Power	28.3	-4.5	Subtotal
Noise Bandwidth ($2B_{LO}$=24.16)	13.8	0	Calculated
Threshold SNR in $2B_{LO}$	10.	0	Requirement
Threshold Carrier Power	4.5	-4.5	Subtotal
Performance Margin	0		Total

TABLE 21
PREENTRY DESPUN DOPPLER LINK TABLE

PARAMETER	VALUE	TOLERANCE	SOURCE
Total Transmitter Power	38.3	-1.	6.82 watts
Transmitting Circuit Loss	-.3	-.1	Assumed
Transmitting Antenna Gain	1.3	-.5	Centerfed microstrip
Space Loss (.525 GHz)	-183.6	0.	1.836; .4 trajectory
Ionospheric Loss	0	-.6	Theoretical
Polarization Loss	-3.	-.5	Assumed
Receiving Antenna Gain	10.6	-.5	Optimal Antenna
Receiving Circuit Loss	-.5	-.1	Assumed
Total Received Power	-137.2	-3.3	Subtotal
Receiver Noise Spectral Density	-164.9	1.5	1.836; .4 trajectory
Received Carrier Power	27.7	-4.5	Subtotal
Noise Bandwidth ($2 B_{LO}$=21.09)	13.2	0	Calculated
Threshold SNR in $2 B_{LO}$	10.	0	Requirement
Threshold Carrier Power	4.5	-4.5	Subtotal
Performance Margin	0		Total

TABLE 22

PREENTRY SPUN WITH DOPPLER LINK TABLE

PARAMETER	VALUE		TOLERANCE		SOURCE
	T = -.3	T = 0	T = -.3	T = 0	
Total Transmitter Power	47.8	47.8	-1.	-1.	60 watts
Transmitting Circuit Loss	-.3	-.3	-.1	-.1	Assumed
Transmitting Antenna Gain	1.2	1.3	-.5	-.5	Centerfed microstrip
Space Loss (.4 GHz)	-178.9	-180.3	0	0	1.685; .4 trajectory
Ionospheric Loss	0	0	0	-1.	Theoretical
Polarization Loss	-3.	-3.	-.5	-.5	Assumed
Receiving Antenna Gain	4.2	4.7	-.5	-.5	Optimal Antenna
Receiving Circuit Loss	-.5	-.5	-.1	-.1	Assumed
Total Received Power	-129.5	-130.3	-2.7	-3.7	Subtotal
Receiver Noise Spectral Density	-163.2	-162.7	1.7	1.7	1.685; .4 trajectory
Carrier Modulation Loss	4.1	4.1	-.6	-.6	Index=.673$\pm$.05 radians
Received Carrier Power	29.6	28.3	-5.0	-6.0	Subtotal
Noise Bandwidth (2 B_{LO}=17.08)	12.3	12.3	0	0	Calculated
Threshold SNR in 2 B_{LO}	10	10	0	0	Requirement
Thrshold Carrier Power	7.3	6.0	-5.0	-6.0	Subtotal
Performance Margin	2.3	0			Total
Data Modulation Loss	2.1	2.1	-.4	-.4	Index=.673$\pm$.05 radians
Received Data Power	31.6	30.3	-4.8	-5.8	Subtotal
Bit Rate (75.84 BPS)	18.8	18.8	0	0	Calculated
Required Data Signal/N_o	4.5	4.5	0	0	PSK Rate 1/2
Receiver Loss	1.	1.	-.2	-.2	Assumed
Threshold Data Power	7.3	6.0	-5.0	-6.0	Subtotal
Performance Margin	2.3	0			Total

TABLE 23

PREENTRY DESPUN WITH DOPPLER LINK TABLE

PARAMETER	VALUE		TOLERANCE		SOURCE
	T = -.3	T = 0	T = -.3	T = 0	
Total Transmitter Power	46.1	46.1	-1.	-1.	
Transmitting Circuit Loss	-.3	-.3	-.1	-.1	Assumed
Transmitting Antenna Gain	.3	1.3	-.5	-.5	Centerfed
					microstrip
Space Loss (1.05 GHz)	-188.8	-189.6	0	0	1.836; .4
					trajectory
Ionospheric Loss	0	0	0	-.1	Theoretical
Polarization Loss	-3.	-3.	-.5	-.5	Assumed
Receiving Antenna Gain	16.8	16.6	-.5	-.5	Optimal Antenna
Receiving Circuit Loss	-.5	-.5	-.1	-.1	Assumed
Total Received Power	-129.4	-129.4	-2.7	-2.8	Subtotal
Receiver Noise Spectral	-168.6	-168.7	1.2	1.2	1.836; .4
					trajectory
Density					
Carrier Modulation Loss	-9.2	-9.2	-1.3	-1.3	Index=.353+.05
					radians
Received Carrier Power	30.0	30.1	-5.2	-5.3	Subtotal
Noise Bandwidth (2 B_{LO}=29.83)	14.8	14.8	0	0	Calculated
Threshold SNR in 2 B_{LO}	10	10	0	0	Requirement
Thrshold Carrier Power	5.2	5.3	-5.2	-5.3	Subtotal
Performance Margin	0	0			Total
Data Modulation Loss	-.6	-.6	-.2	-.2	Index=.353+.05
					radians
Received Data Power	38.6	38.7	-4.1	-4.2	Subtotal
Bit Rate (758.58 BPS)	28.8	28.8	0	0	Calculated
Required Data Signal/N_0	4.5	4.5	0	0	PSK Rate 1/2
Receiver Loss	1.	1.	-.2	-.2	Assumed
Threshold Data Power	4.3	4.4	-4.3	-4.4	Subtotal
Performance Margin	0	0			Total

Table 24 compares the required and available data rates when the doppler links are added. The spun pre-entry link falls short of supporting the maximum rate of Reference 13, but almost meets the rate requirements of Table 15. The despun link has excess capability in all cases.

The physical characteristics of the links are given in Table 25. The despun system is approximately the same weight, and provides 10 times more data. The "cost" of the Doppler experiment is 2.73 probe kg and 6.38 x 10^4 bits for the spun approach, and 1.4 probe kg and 1.66 x 10^5 bits for the despun approach. The additional spacecraft receiver is estimated at 1.9 kg.

TABLE 24

DATA RATE COMPARISON – WITH A DOPPLER LINK

	Spun	Despun
Available, BPS	75.84	758.58
Required, Ref (13), BPS	83-1/3 to 166-2/3	
Excess, Ref (13), dB	-3.4 to -.4	6.6 to 9.6
Required, Table 15, BPS	108.18	
Excess, Table 15, dB	-1.6	8.5

TABLE 25

PHYSICAL CHARACTERISTICS – WITH A DOPPLER LINK

	Spun		Despun	
	Preentry	Doppler	Preentry	Doppler
Transmitter Output (w)	60	31.84	40.9	6.82
Transmitter Input (w)	135	108	163.	18.
Transmitter Weight (kg)	1.48	2.0	2.60	1.28
Battery Weight (44.1 wh/kg)	.92	.73	1.11	.12
Total Probe Weight (kg)	2.40	2.73	3.71	1.40

Margin Histories

The mathematics generated in the trajectory selection section attempted to equalize and maximize the margins at the beginning and end of the mission, and as the margin could be equal or greater in the middle of the mission. Table 26 summarizes the geometry of the missions. The margin histories are given in Figure 22. As expected the margins are nearly equal at the ends of the mission, and greater between.

TABLE 26

COMMUNICATIONS GEOMETRY

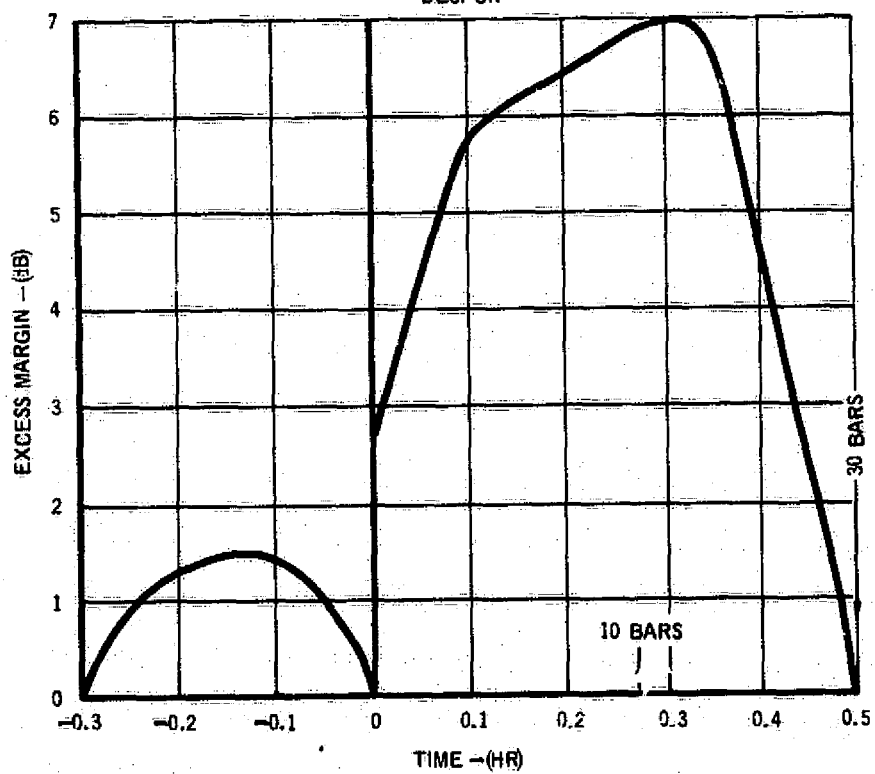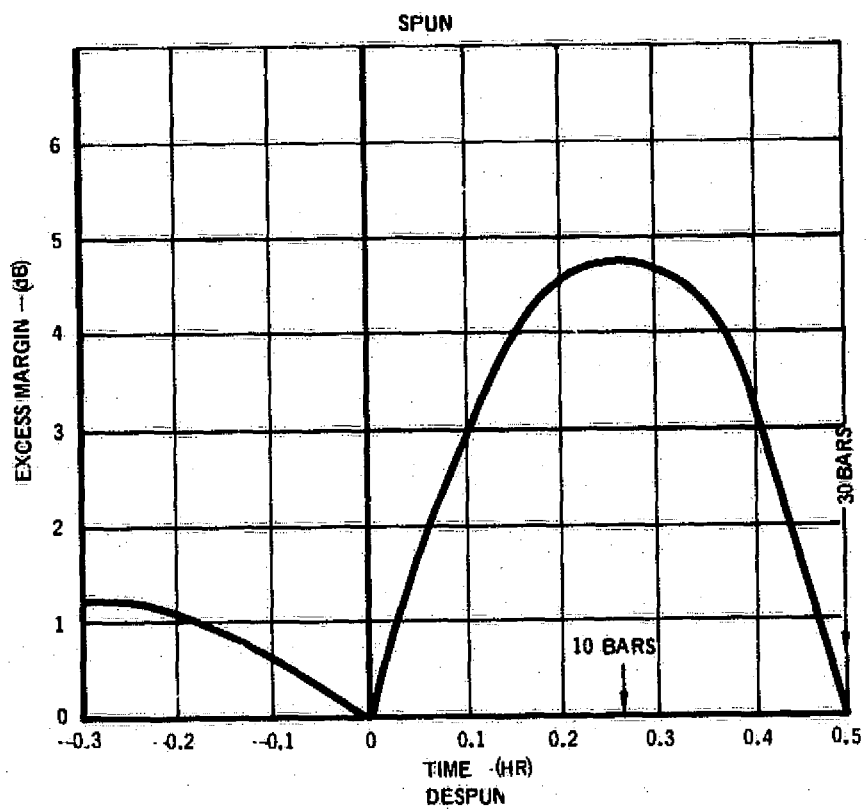| T (hr)	1.685 RJ Mission (Spun)			1.836 RJ Mission (Despun)		
	S (deg)	P (deg)	R (radii)	S (deg)	P (deg)	R (radii)
-.3	43.5	52.	.738	54.	62.	.875
-.2	39.5	47.5	.782	50.	58.5	.870
-.1	36.	44.	.795	45.5	54.	.9
0-	32.5	41.	.868	41.	50.5	.955

FIGURE 22
LINK MARGIN HISTORIES

Alternate Antennas

In the baseline analysis the transmission antennas were assumed to be microstrip antennas, and the reception spun antenna was a 50 deg beamwidth maximum, variable beam center antenna. This section investigates the effects of other candidate antennas from the link viewpoint.

The other pre-entry antennas are given in Table 27. The two alternates to the baseline transmission center fed microstrip are a 3/4 turn quadrafilar and the Loop Vee. The center fed microstrip is a linearly polarized antenna with a beamwidth of 55°, and a beam center of 45.75°. The 3/4 turn quadrifilar has a beam center of 42.5°, and a beamwidth of 85°. The Loop Vee has a beam center of 65°, and a beamwidth of 50°. Both of the alternative antennas have a link advantage over the microstrip. The microstrip has the physical advantage however, being much smaller.

TABLE 27

OTHER PREENTRY ANTENNAS

Parameter	Spun Design		Despun Design	
	T = -.3	T = 0-	T = -.3	T = 0-
(a) Transmission Antenna				
View Angles	52°	41°	62°	50.5°
Reference Microstrip Gain	1.18 dB	1.25 dB	0.29 dB	1.25 dB
3/4 Turn Quadrafilar Advantage	4.08 dB	4.16 dB	4.49 dB	4.05 dB
Loop Vee Advantage	3.52 dB	1.48 dB	5.18 dB	3.25 dB
(b) Spun Reception Antenna				
View Angles	43.5°	32.5°		
Reference Spun Gain	4.16 dB	4.74 dB		
Loop Vee Advantage	-3.86 dB	-7.30 dB		
3/4 Turn Quadrafilar Advantage	-1.76 dB	-2.50 dB		
90° Quadrafilar Advantage	-.82 dB	-.16 dB		
66° Microstrip Advantage	-1.90 dB	-.16 dB		

Four alternatives are given for the pre-entry reception spun antenna baseline of a 50° beamwidth, and a 32.5° beam center. In addition to the 3/4 turn quadrafilar and the Loop Vee, there is the 90° quadrafilar and the 66° microstrip. The 90° quadrafilar has a 90° beamwidth, and a 0° beam center. The 66° microstrip has a 66° beamwidth, and a 0° beam center. Of the four alternatives the 90° quadrafilar most nearly approaches the reference antenna performance.

High Periapsis Links

There may be overriding considerations to force the spacecraft into much higher periapses than those predicted by the communications trades. A "typical" high periapsis is six Jovian radii. Tables 28 and 29 are the link tables

for both a .9 meter parabolic reception dish and a 1.8 meter parabolic dish. A spun reception antenna obviously is not viable at these transmission ranges.

TABLE 28
PREENTRY SIX RADII .9 METER PARABOLA

PARAMETER	VALUE		TOLERANCE		SOURCE
	T = -.3	T = 0	T = -.3	T = 0	
Total Transmitter Power	46.1	46.1	-1.	-1.	40.9 watts
Transmitting Circuit Loss	-.3	-.3	-.1	-.1	Assumed
Transmitting Antenna Gain	-8.9	7.1	-.5	-.5	Centerfed microstrip
Space Loss (1.05 GHz)	-204.5	-204.2	0	0	6 radii trajectory
Ionospheric Loss	0	0	0	-.1	Theoretical
Polarization Loss	-3.	-3.	-.5	-.5	Assumed
Receiving Antenna Gain	17.7	17.1	-.5	-.5	Optimal antenna
Receiving Circuit Loss	-.5	-.5	-.1	-.1	Assumed
Total Received Power	-153.4	-151.9	-2.7	-2.8	Subtotal
Receiver Noise Spectral Density	-167.9	-168.1	1.5	1.4	6 radii trajectory
Received Data Power	14.5	16.2	-4.2	-4.3	Subtotal
Bit Rate (2.88 BPS)	4.6	4.6	0	0	Calculated
Required Data Signal/N_0	4.5	4.5	0	0	PSK Rate 1/2
Receiver Loss	1.0	1.0	-.2	-.2	Assumed
Threshold Data Power	4.4	6.1	-4.4	-4.5	Subtotal
Performance Margin	0	1.6			Total

TABLE 29
PREENTRY SIX RADII 1.8 METER PARABOLA

PARAMETER	VALUE		TOLERANCE		SOURCE
	T = -.3	T = 0	T = -.3	T = 0	
Total Transmitter Power	46.1	46.1	-1.	-1.	40.9 watts
Transmitting Circuit Loss	-.3	-.3	-.1	-.1	Assumed
Transmitting Antenna Gain	-8.9	-7.1	-.5	-.5	Centerfed microstrip
Space Loss (1.05 GHz)	-204.5	-204.2	0	0	6 radii trajectory
Ionospheric Loss	0	0	0	-.1	Theoretical
Polarization Loss	-3.	-3.	-.5	-.5	Assumed
Receiving Antenna Gain	23.7	21.5	-.5	-.5	Optimal Antenna
Receiving Circuit Loss	-.5	-.5	-.1	-.1	Assumed
Total Received Power	-147.4	-147.5	-2.7	-2.8	Subtotal
Receiver Noise Spectral Density	-167.9	-168.2	1.5	1.4	6 radii trajectory
Received Data Power	20.5	20.7	-4.2	-4.2	Subtotal
Bit Rate (11.48 BPS)	10.6	10.6	0	0	Calculated
Required Data Signal/N_0	4.5	4.5	0	0	PSK Rate 1/2
Receiver Loss	1.0	1.0	-.2	-.2	Assumed
Threshold Data Power	4.4	4.6	-4.4	-4.4	Subtotal
Performance Margin	0	.2			Total

The link cannot support the target 83-1/3 to 166-2/3 BPS. In addition to the greater transmission range, this is primarily due to the nearly normal probe view angles which are outside the center fed microstrip beamwidth. The alternative is to replace the center fed microstrip. Alternatives include a half wave dipole, a 200° beamwidth 1/4 turn quadrafilar, a 3/4 turn quadrafilar (85° beamwidth, 42.5° beamcenter) and a Loop Vee (50° beamwidth, 65° beamcenter). Table 30 summarizes the relative advantages of the candidates. The dipole, although linearly polarized, is the best link choice. The other circularly polarized transmission antennas are however almost as good. The dipole transmission antenna with a 1.8 meter parabolic reception antenna just exceeds the minimum target data rate requirements. The antenna might be fabricated as a self-erectable whip 42.85 cm long to include a wavelength for isolation.

TABLE 30

ALTERNATE PREENTRY TRANSMISSION ANTENNAS FOR A SIX RADII PERIAPSIS MISSION

Antenna	Relative Magnitude (dB)		Data Rate (BPS)	
	T = -.3 Hr	T = 0- Hr	.9m Dish	1.8m Dish
Reference, Gain	-8.9	-7.1	2.88	11.48
Dipole, Advantage	11.	9.2	36.26	95.49
1/4 T-QF, Advantage	10.2	8.6	30.16	83.17
3/4 T-QF, Advantage	9.3	8.2	24.51	75.85
LV, Advantage	9.5	8.9	25.67	89.11

Direct to Earth Links

An interesting alternative to pre-entry relay communications is to communicate directly to Earth. Herein the probe would be positioned at spacecraft release to be on Earth line at entry. As seen in the previous section this does not result in an unacceptable entry angle-of-attack.

Table 31 is an abbreviated link table to define the allowable data power. Briefly a 2.3 GHz wave is launched from a .9 meter parabola, assumed to be mounted aft of the probe, to a standard 64 m dish Deep Space Network station. The transmitter power is a variable, as is the form of the transmission, that is with or without a Doppler measurement. The double sided carrier tracking loop bandwidth would be 41.62 Hz if loop aiding were not used in order to track the maximum Doppler rate defined in Reference 16, of 16 meters per second squared. Using loop aiding, a 12 Hertz loop offers a 5.4 dB advantage.

There are fundamentally three forms of transmission: a tone only to derive Doppler, a tone plus data, and data only. Note that in the data only mode, no carrier power is available, that is a Costas loop is required to demodulate the data. As the Deep Space Network does not have Costas capability, the data would be predetection recorded and demodulated off line. Table 32 summarizes the data return plus the estimated transmitter characteristics.

TABLE 31
DIRECT TO EARTH PREENTRY TRANSMISSION

Parameter	Value	Tolerance	Comments
Total Transmitter Power	XP	-1.	To be determined
Transmit Circuit Loss	-.3	-.1	Assumed
Transmit Antenna Gain	24.5	-3.	.9 m 55% parabola
Space Loss (2.3 GHz)	-277.5	-.8	$5.2 \pm .5$ AU
Receive Antenna Gain	61.4	-.5	64 m dish
Polarization Loss	-.2	-.1	Assumed
Receive Circuit Loss	0.	0.	Preamp at antenna
Total Received Power	XP-192.2	-5.5	Subtotal
Receiver N.S.D.	-183.4	+.5	25° Elevation Angle
Carrier Modulation Loss	CML	CMLT	To be determined
Noise Bandwidth	10.8	0.	$2 B_L = 12$ Hz
Threshold SNR in $2 B_{L_0}$**	TL	0.	Requirement
Threshold Carrier Pwr	TCP	-6.-CMLT	Subtotal
Data Modulation Loss	DML	DMLT	To be determined
Data Rate	$10 \log_{10} B$	0.	To be determined
Receiver Loss*	RL	-.2	Assumed
Required Data Signal/N_0	4.5	0.	PSK Rate 1/2, Q=8
Threshold Data Power	TDP	-62.-DMLT	Subtotal

*RL = 1.0 with a carrier channel, = 2.0 without a carrier channel.
**TL = 10. with tone only; = 11. with $P_e = 10^{-3}$ and $E_B/N_0 = 4.5$.

TABLE 32
DIRECT TO EARTH DATA FORMATS

Format	Transmitter Power (w)	Data Rate (BPS)	Weight (kg)	Power (w)
1. Tone Only	3.63	N/A	2.4	23
2. Tone Plus Data	20	121.3	3.8	126
3. Tone Plus Data	15	81.3	3.4	95
4. Tone Plus Data	10	32.5	2.9	63
5. Data Only	20	141.3	3.8	126
6. Data Only	15	107.2	3.4	95
7. Data Only	10	70.8	2.9	63

It is apparent that with a moderate sized transmitter a fair amount of data can be returned directly to Earth.

Summary

A number of communications links have been described. First the basic preentry data links, both with a spun an⁻ a despun spacecraft antenna, were defined. These links support the assume ,ata rate requirements. Next, four pre-entry links were defined when a dual requency Doppler experiment is incorporated: the tone only link and the tone plus data link, each with both a spun and a despun spacecraft antenna. Link margin histories show that the margin during the ⌐ansmission is equal to or greater than that of the end points.

Various antennas were compared to the "baseline" antennas: two preentry transmission, and four preentry reception antennas. Considering both the link viewpoint and their physical impact, the baseline antennas are preferable.

High periapsis cases were also considered with a .9 and a 1.8 meter reception parabolic dish. The available preentry data rates are not acceptable. Four alternate preentry antennas were explored, all of which nearly meet the required pre-entry data rate.

Finally seven variants of a direct to Earth link were explored with Doppler only, Doppler plus data and data only. It was seen that a direct to Earth link is a viable alternative to a relay link for pre-entry communications.

PRE-ENTRY COMMUNICATIONS IMPACT ASSESSMENT

The previous sections have addressed pre-entry communications from the mission or trajectory viewpoint, and from the electronics viewpoint. A complete assessment of the impact of the incorporation of pre-entry communications into a basically post entry communications probe requires thermodynamic, power systems, and design layout analyses.

The outer planets entry probe defined in References 1 and 2 is designed specifically to gather information after the entry into the planetary atmosphere. The probe is encapsulated in multilayer radio opaque insulation prior to entry to provide thermal control prior to entry. The probe has a favorable ratio of roll to pitch inertias to maintain entry altitude during the long coast period from spacecraft separation. Finally, the probe has a forward center of gravity to maintain stability throughout the post entry period. The incorporation of pre-entry communications into this design must not seriously constrain any of the foregoing design elements.

Thermal Requirements

While attached to the spacecraft, the thermal control of the probe is provided by the spacecraft. After entry, heat is provided by the operation of the internal equipments. In the free flight phase, when pre-entry communications would occur, thermal control is provided by the multilayer insulation and radioactive thermal isotope heaters. Either some of the radio opaque insulation must be "removed" for pre-entry communications, or the antenna must be outside the multilayer insulation.

An 82 node SPCM thermal model was used to assess the impact of pre-entry communications on the probe thermal control system. A schematic of the model is shown in Figure 23. In the analysis the multilayer insulation (MLI) was assumed to have a conductivity of 8.65×10^{-7} w/cm/°K, and external polyurethane foam, where used, was assumed to have a conductivity of 1.21×10^{-4} w/cm/°K in a vacuum. All analysis included the effects of solar input at Jupiter. For a "nominal" sun the flux at 5.2 AU is $\dot{Q}_s = 4.95 \times 10^{-3}$ w/cm². The absorbed flux on any portion of the aft dome was calculated as:

$$\dot{Q}_{ABS} = 2\pi R^2 \, \alpha_s \, \dot{Q}_s \int_{\theta_1}^{\theta_2} \sin \theta \cos \theta \, d\theta$$

where

R = Radius of the probe

α_s = Solar absorptivity of the aft dome

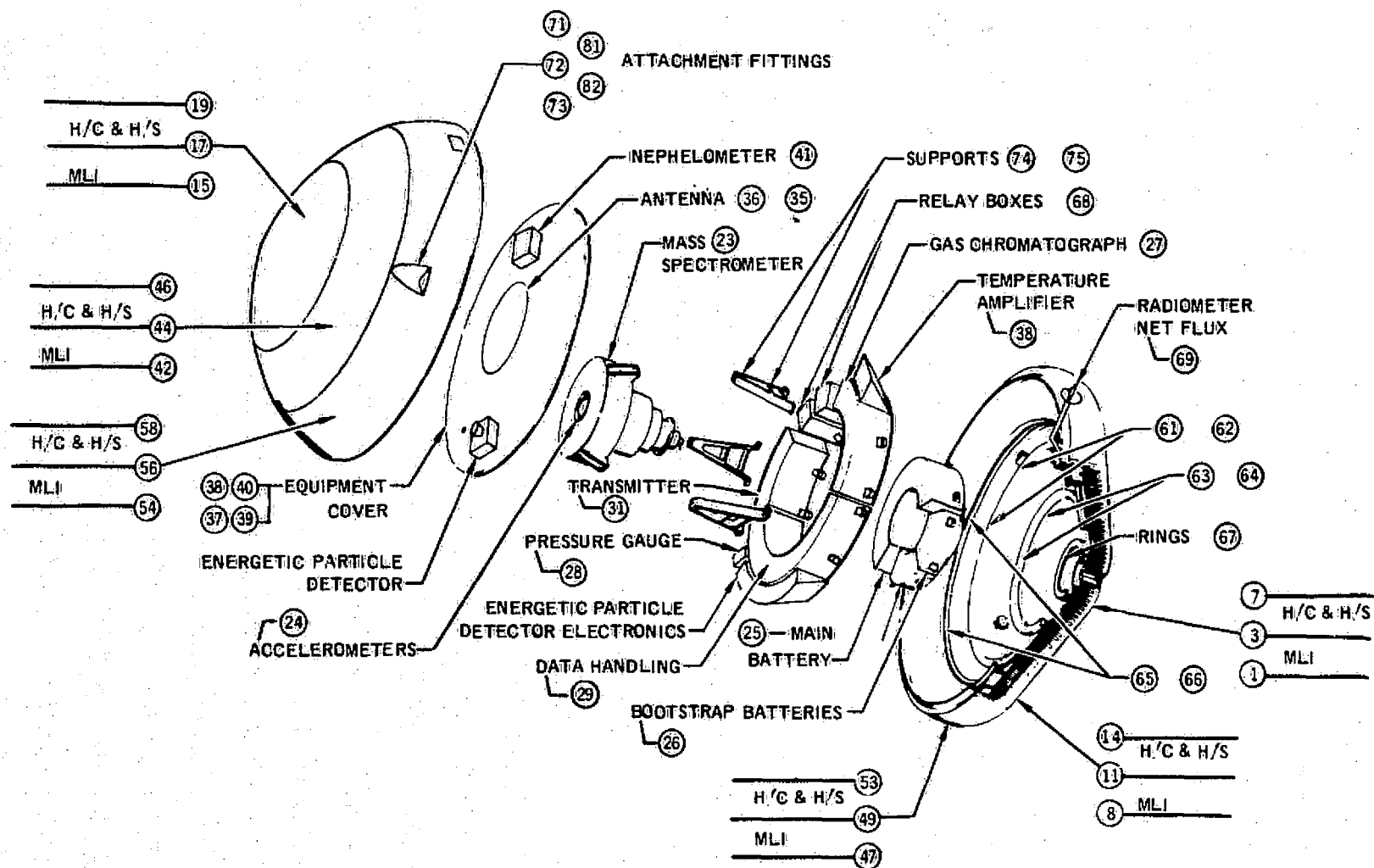θ = Angle measured from the top of the dome

FIGURE 23
THERMAL MODEL

For Configuration 1 of Figure 24 the aft multilayer insulation blanket is left unchanged, and the antenna platform is suspended from the attachment fittings. The additional heat leak for this configuration is negligible. This configuration would perform the same as the baseline system without pre-entry communications.
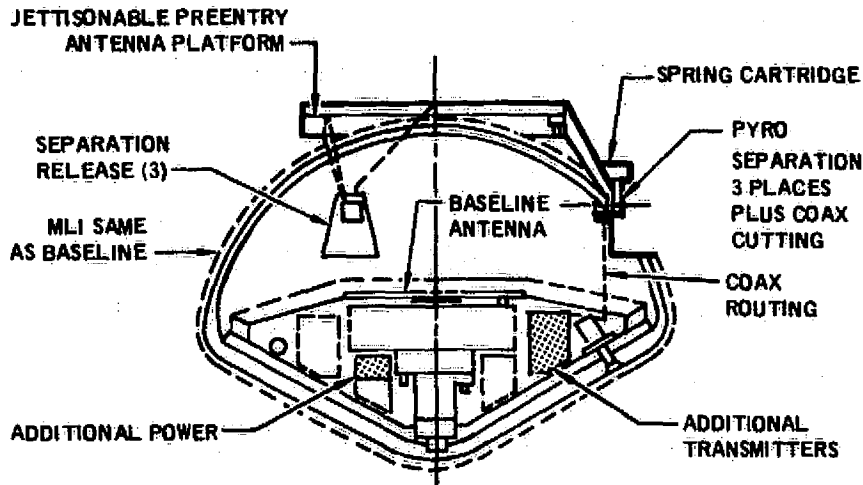

FIGURE 24

THERMAL CONFIGURATION 1

In Configuration 2, Figure 25, one inch thick foam was assumed to cover the aft 30° of the dome to provide support for the pre-entry antenna. The results of this analysis indicate that only two additional (seven total) RHU's (radioisotope heater units) would be necessary. Thermal effects on the external antennas were not considered in this study.
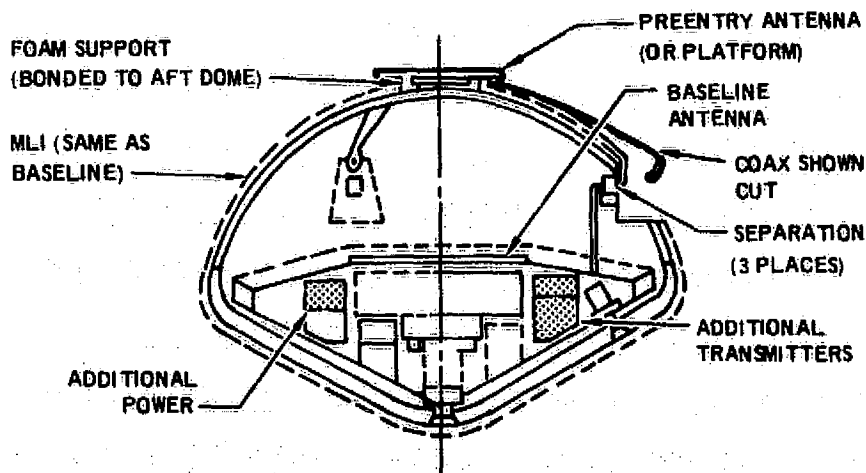

FIGURE 25

THERMAL CONFIGURATION 2

Configuration 3, Figure 26, assumed that the MLI over the aft dome was replaced with one inch thick, RF transparent polyurethane foam ($\alpha_s = \epsilon = .9$). The results indicate that 35 RHU's would be necessary to maintain a 40°F internal temperature.
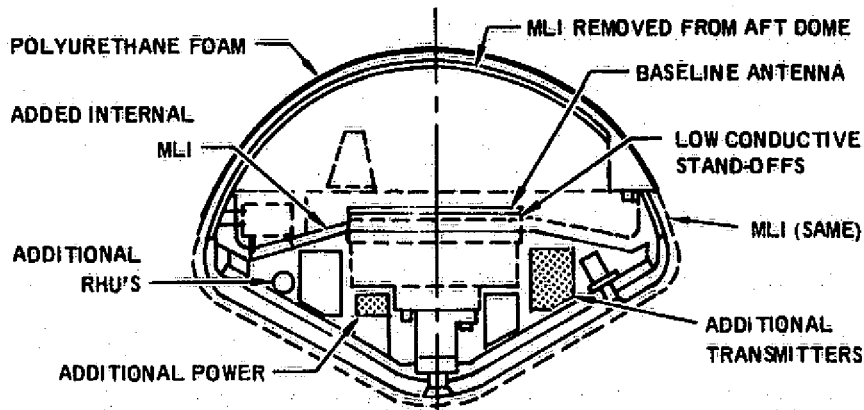

FIGURE 26

THERMAL CONFIGURATION 3

Configuration 4, Figure 27, has basically the same insulation properties as the baseline case. Because of the large time constant of the outer planet probe, jettisoning the aft blanket even up to 2 hours before entry would have only a small effect on the equipment temperature. The cold soaking of the aft heat shield, though, could produce potential problems during entry. The transient effects are shown in Figure 28. For this reason, it is not recommended that this configuration be considered for pre-entry communications.
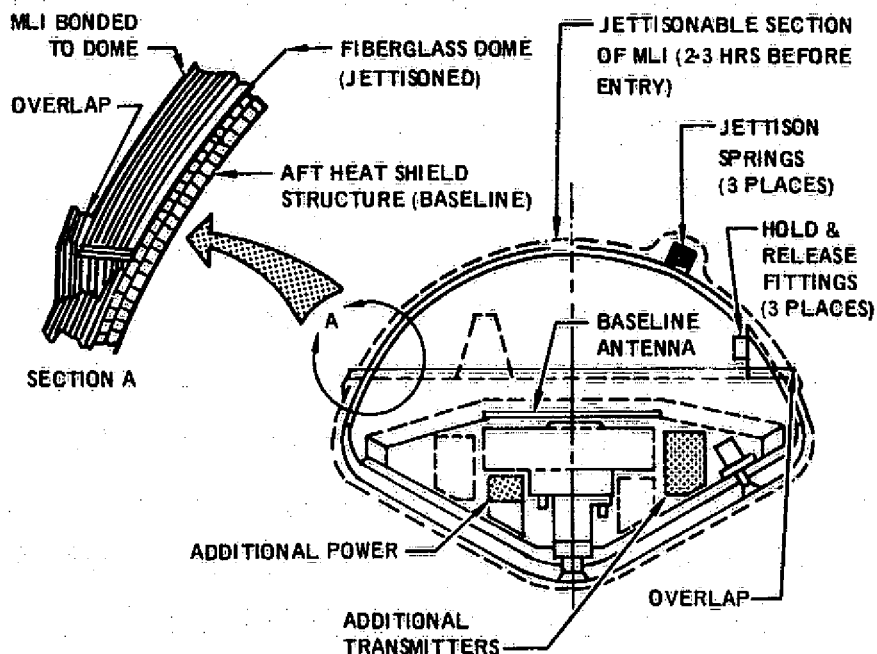

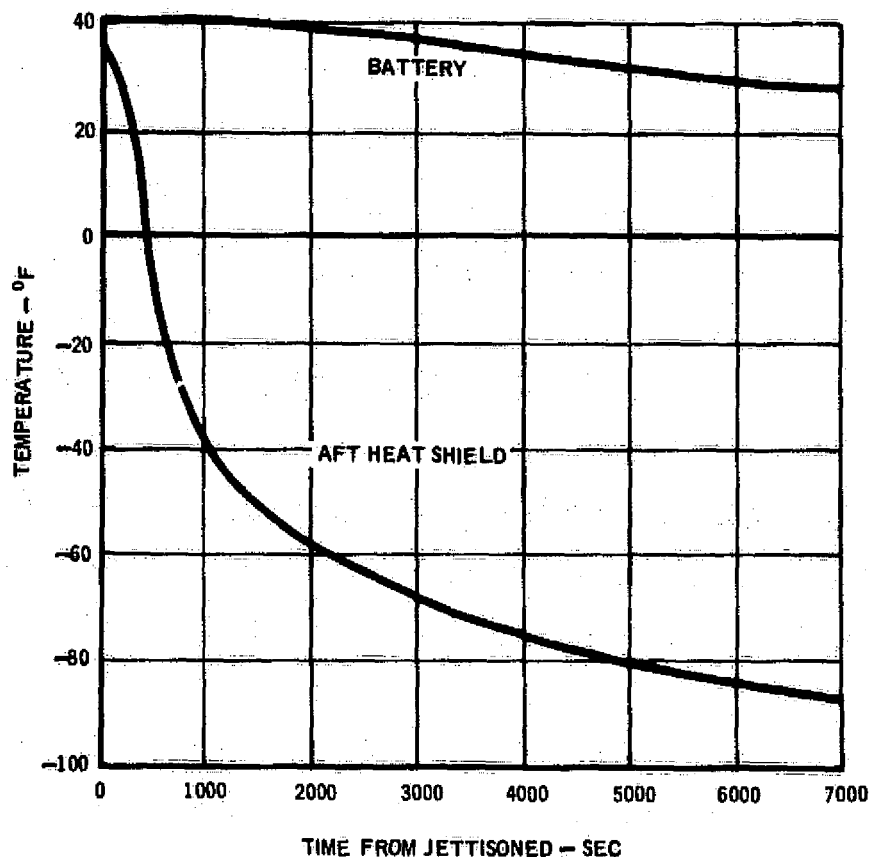FIGURE 27

THERMAL CONFIGURATION 4

FIGURE 28

TRANSIENT CHARACTERISTICS OF CONFIGURATION 4

Neither thermal control system Configurations 1, 2, or 4 would have any effect on the atmospheric descent thermal control system. Although Configuration 3 would have an impact, it was not analyzed since it was not considered a realistic approach for the autonomous portions of the flight.

The results of the thermal analysis of these configurations are summarized in Figure 29. Both of the external antenna concepts, Configurations 1 and 2, are acceptable. Configuration 1 required no additional RHU's and Configuration 2 required only two additional RHU's. The configurations using the existing post entry antenna location, Configurations 3 and 4, are unacceptable. Configuration 3 would require 35 RHU's, where as Configuration 4 would result in unacceptably cold pre-entry aft heat shield temperatures. From the thermal control viewpoint, the only approach to pre-entry communications would be to mount the pre-entry antenna external to the multilayer insulation.
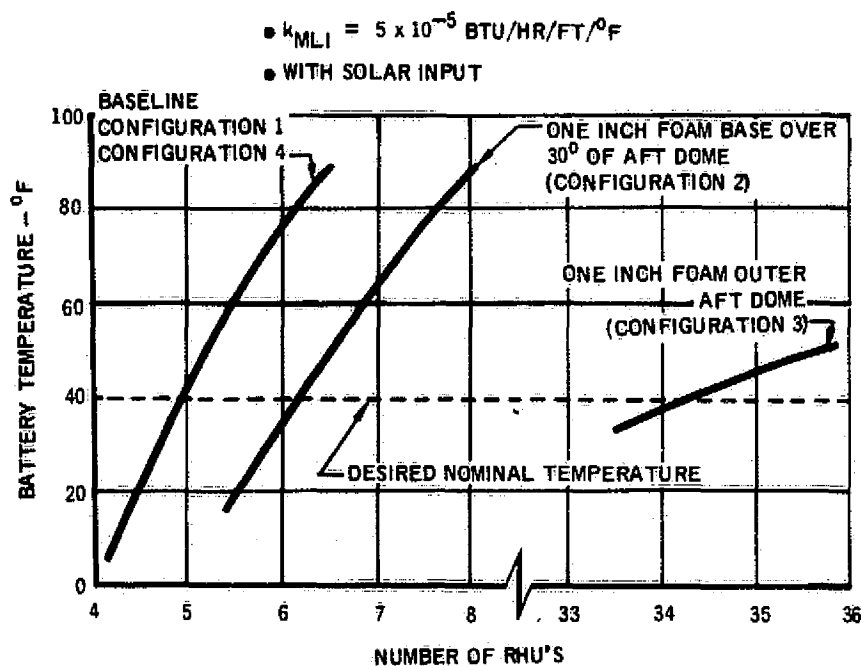
FIGURE 29

RHU REQUIREMENTS

Power Requirements

The next step is to assess the power supply requirements. Table 33 and Figure 30 show the power/energy requirements and power profile, respectively. The energy requirement is 207.97 watt-hours for a Jupiter mission compared to 125.71 watt-hours in a 1.18 kg weight increase. The battery baseline design common for missions to Jupiter, Saturn, and Uranus has a capacity of 235 watt-hours at a current discharge rate of 6.25 amperes. Although the maximum discharge current is slightly larger, the common baseline designed battery is satisfactory for the Jupiter mission with pre-entry communications.

The baseline battery design is based on the probe temperature profile, Figure 31. The baseline allocates 15 watt-hours (30 watts for 30 minutes) of energy to heat the battery so that regulation is maintained at the time the transmitter is activated. Evaluation of the new power profile indicates the energy allocated for battery heat and the inherent internal heating is satisfactory to provide adequate regulation when the pre-entry power amplifiers are activated.

Since the common baseline designed battery can adequately meet the probe power/energy requirements with the added pre-entry communications, there would be no identifiable impact to the probe electrical power subsystem, if all of the pre-entry equipments can be internally mounted.

64

TABLE 33
EQUIPMENT POWER/ENERGY REQUIREMENTS

| EQUIPMENT	UNIT POWER (WATTS)	TIME (MIN)	ENERGY (W-H)
ENTRY DETECTION			
X-DAY CLOCK (2)	140×10^{-6}	82,080	0.38
G-SWITCH	0.2	60	0.20
DATA HANDLING SUBSYSTEM (POST ENTRY)	10.0	90	15.00
TRANSMITTER (POST ENTRY)			
OSC MOD	1.0	90	1.50
POWER AMPLIFIER	151.3	30	75.65
SCIENCE (POST ENTRY)			
MASS SPECTROMETER	11.0	40	7.33
GETTER PUMP HEATER	30.0	10	5.00
GAS CHROMATOGRAPH	9.7	30	4.85
ACCELEROMETER	1.5	90	2.25
PRESSURE GAGE	1.2	90	1.80
TEMPERATURE GAGE	1.0	30	0.50
NEPHELOMETER	1.0	30	0.50
NET FLUX RADIOMETER	3.0	30	1.50
DATA HANDLING SUBSYSTEM (PRE-ENTRY)	2.0	60	2.00
TRANSMITTERS (PRE-ENTRY)			
OSC MOD	1.0	60	1.00
POWER AMPLIFIER	162.7	20	54.23
DOPPLER	8.2	20	2.73
SCIENCE (PRE-ENTRY)			
MAGNETOMETER	1.0	60	1.00
ENERGETIC CHARGED PARTICLE DETECTOR	1.0	60	1.00
RETARDING POTENTIAL ANALYZER	1.0	60	1.00
RADIO EMISSION SPECTRUM ANALYZER	1.0	60	1.00
LANGMUIR PROBE	1.0	20	0.33
NEUTRAL MASS SPECTROMETER	5.0	20	1.66
ION MASS SPECTROMETER	2.0	20	0.66
ORDNANCE RELAYS	3.0	0.001	NEG
BATTERY HEATER	30.0	30	<u>15.00</u>
EQUIPMENT ENERGY			198.07
DISTRIBUTION LOSSES			9.90
TOTAL ENERGY REQUIRED			207.97
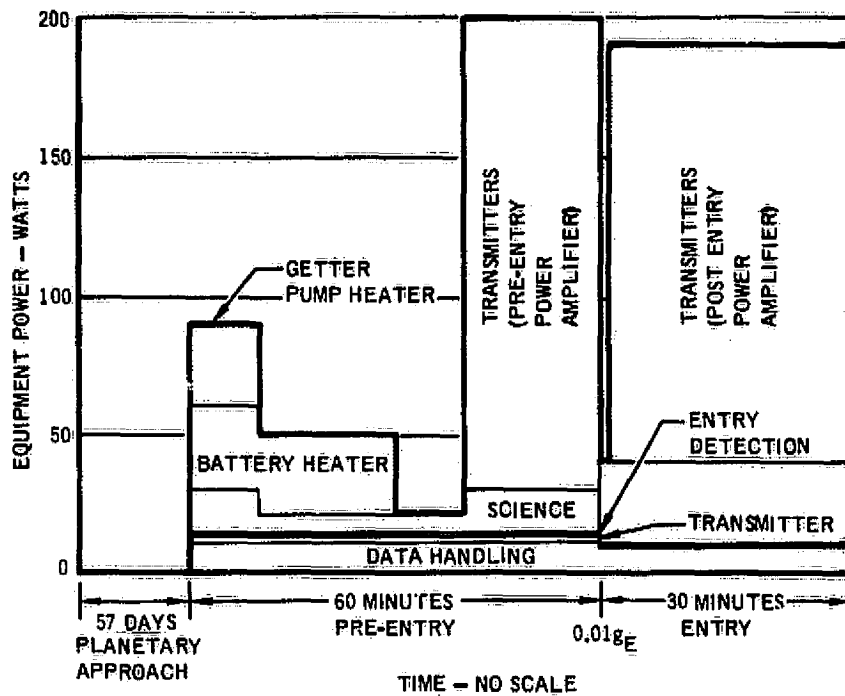
FIGURE 30

ELECTRICAL POWER PROFILE
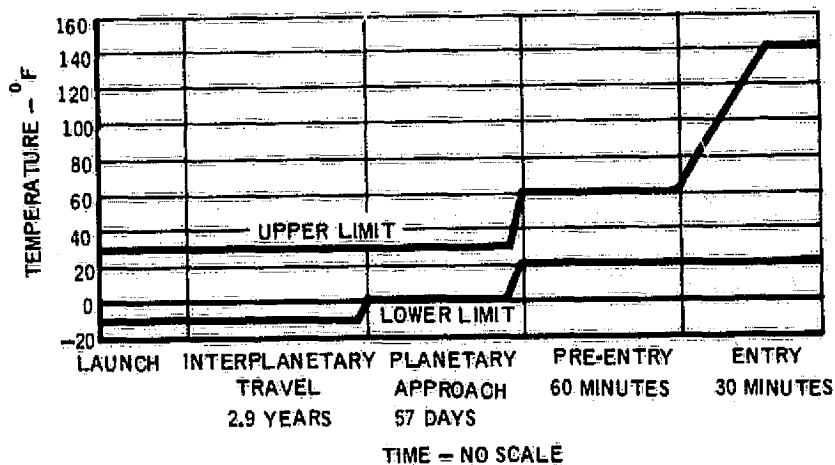
FIGURE 31

PROBE TEMPERATURE PROFILE

Mass Properties Requirements

The final step is to configure the probe with the required pre-entry equipments. It was seen from the thermal control system analysis that it was unacceptable to break the multilayer insulation to allow a radio frequency transparent area, thus the pre-entry transmission antenna must be outside the blanket. Preliminary design layout shows that the pre-entry instruments of Reference 13 cannot be accommodated within the baseline probe size of References 1 and 2 without an unacceptable center of gravity. Hence the only jointly acceptable thermal control and design layout concept is to place the pre-entry equipment outside of the probe. A typical layout is shown in Figure 32. Although it was acceptable to the power system to use the post entry battery, an external battery is shown in Figure 33. This design retains all of the desirable post entry design elements as the pre-entry equipments are all contained on a structure which is jettisoned prior to entry.

There may be a potential hazard to the post entry mission by attempting to retain the pre-entry package too far into the mission. The timing of the release, and the dynamics of the two bodies is critical. Entering the nominal Jovian atmosphere the shock forms +1.28 seconds of the peak ionospheric electron density at 250 kilometers, and viscous heating begins between 2.57 and 4.49 seconds later. Alternatively the pre-entry package might be jettisoned "much" earlier, for example prior to the three Jovian radii point. Of course with a very early jettison, the ionospheric data could not be also stored in the probe for transmission after entry.

Figure 34 is a conceptual layout of a direct to Earth pre-entry communications package. The pre-entry antenna is a .9 meter parabolic dish with an erectable feed. As noted in the trajectory selection section, the orientation of the probe to Earth line at the time of entry does not impose an unacceptable entry angle of attack. Also as noted in the link section, a direct to Earth link can support a reasonable data rate. It should also be noted that such a link would remove the pre-entry constraints on the relative trajectories, and possibly increase the post entry data return.

The mass properties of the pre-entry communications configuration are given in Table 34. The mass properties of the pre-entry science payload are from Reference 13, while those of the basic Jupiter probe are from Reference 17. The ratio of roll to pitch inertias for the design is 1.76, or it is quite stable. Note that this excludes the pre-entry transmission antenna. Figure 35 illustrates the tolerance of the design to additional weight aft of the probe, and still maintain an acceptable ratio of roll to pitch inertias. A microstrip, a dipole or a moderate sized parabolic dish could be placed aft of the probe with negligible mass properties effect.

A spin stabilized spacecraft would impose an additional constraint on the pre-entry antenna design if that design were physically large. The distance from the probe and pre-entry science package center of gravity to the spacecraft center of gravity should be minimized in order to maintain the spacecraft roll inertia higher than the larger of the pitch or yaw inertias during captive flight. For this reason, if a parabolic dish larger than .9 meters is required to support the mission, a furlable design should be considered.
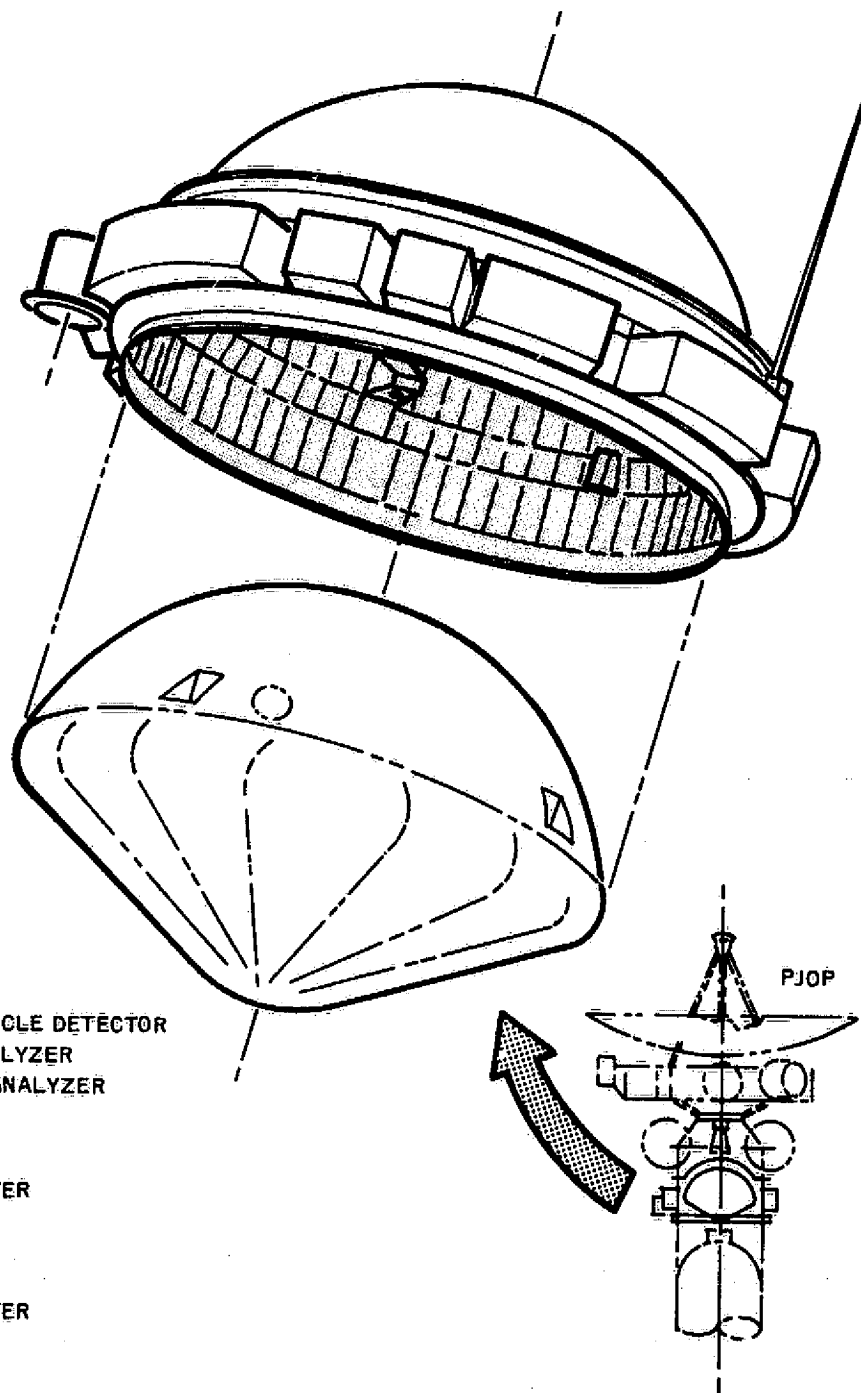
PRE-ENTRY SCIENCE

MAGNETOSPHERE
- MAGNETOMETER
- ENERGETIC CHARGED PARTICLE DETECTOR
- RETARDING POTENTIAL ANALYZER
- RADIO EMISSION SPECTRUM ANALYZER

IONOSPHERIC
- LANGMUIR PROBE
- NEUTRAL MASS SPECTROMETER
- ION MASS SPECTROMETER

ATMOSPHERIC SCIENCE
- NEUTRAL MASS SPECTROMETER
- GAS CHROMATOGRAPH
- ACCELEROMETERS
- TOTAL PRESSURE SENSOR
- TEMPERATURE SENSOR
- NET FLUX RADIOMETER
- NEPHELOMETER
- ENERGETIC PARTICLE DETECTOR
- ENGINEERING MEASUREMENTS
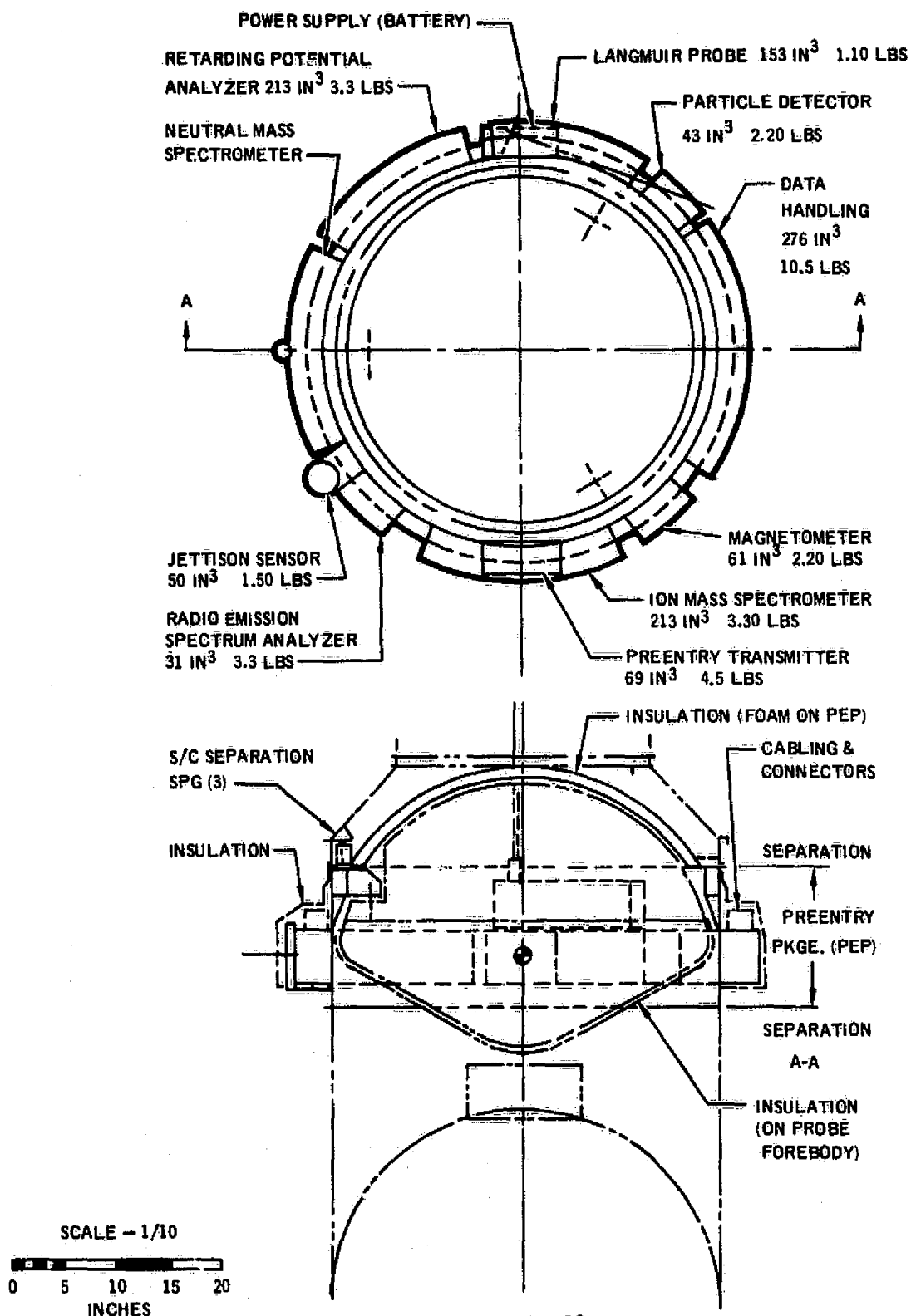
PJOP

FIGURE 32

PREENTRY COMMUNICATIONS CONCEPTUAL DESIGN

68

POWER SUPPLY (BATTERY)

RETARDING POTENTIAL
ANALYZER 213 IN^3 3.3 LBS

NEUTRAL MASS
SPECTROMETER

LANGMUIR PROBE 153 IN^3 1.10 LBS

PARTICLE DETECTOR
43 IN^3 2.20 LBS

DATA
HANDLING
276 IN^3
10.5 LBS

A ← → A

JETTISON SENSOR
50 IN^3 1.50 LBS

RADIO EMISSION
SPECTRUM ANALYZER
31 IN^3 3.3 LBS

MAGNETOMETER
61 IN^3 2.20 LBS

ION MASS SPECTROMETER
213 IN^3 3.30 LBS

PREENTRY TRANSMITTER
69 IN^3 4.5 LBS

INSULATION (FOAM ON PEP)

S/C SEPARATION
SPG (3)

INSULATION

CABLING &
CONNECTORS

SEPARATION

PREENTRY
PKGE. (PEP)

SEPARATION
A-A

INSULATION
(ON PROBE
FOREBODY)

SCALE — 1/10

0   5   10   15   20
        INCHES

FIGURE 33

PRE-ENTRY COMMUNICATIONS CONCEPTUAL LAYOUT

69

PRE-ENTRY SCIENCE AND
COMMUNICATIONS MODULE

DIRECT EARTH LINK

PARABOLIC REFLECTOR
(GRAPHITE EPOXY)
$f = 16''$ $35''$ DIAMETER
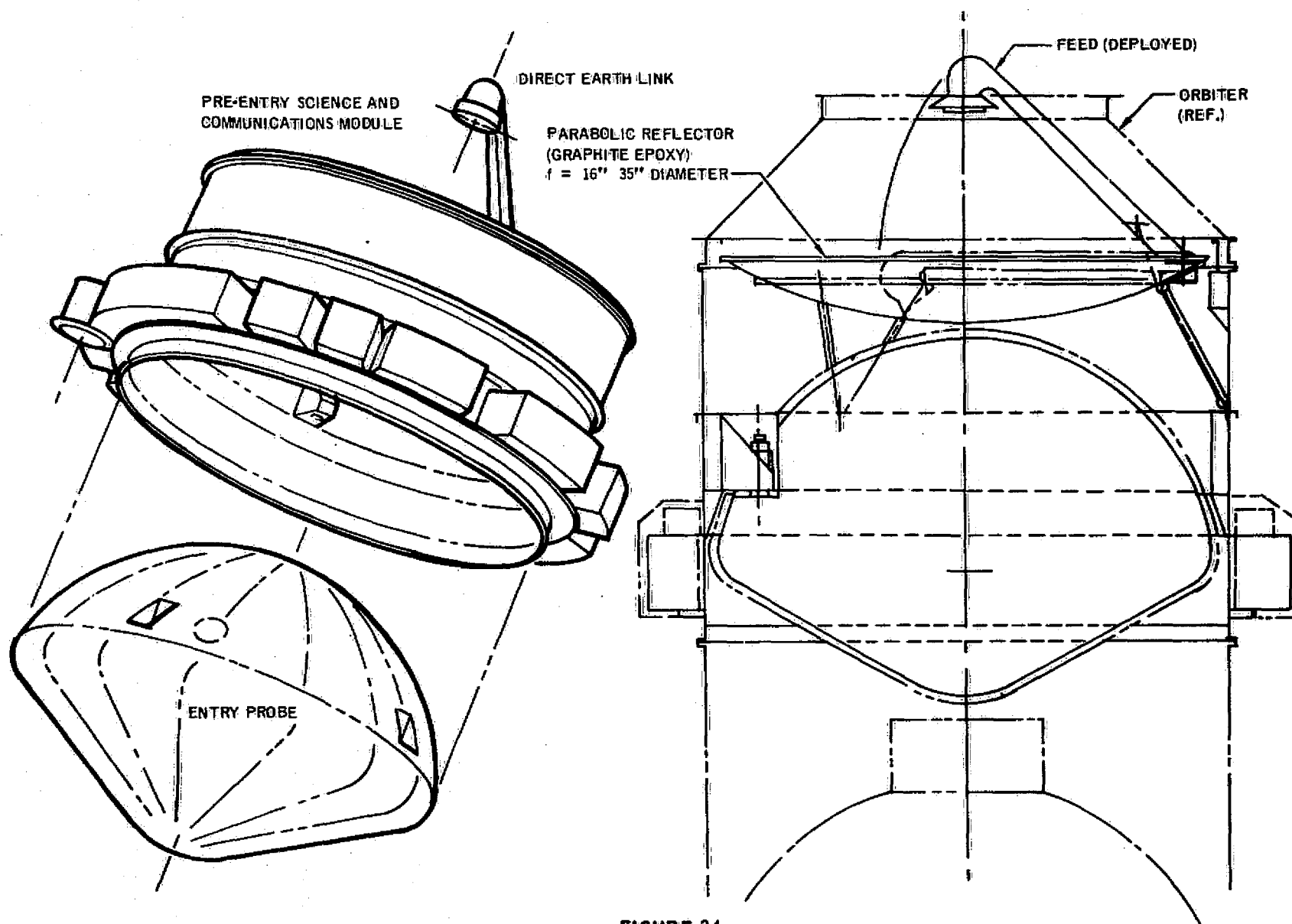
FEED (DEPLOYED)

ORBITER
(REF.)

ENTRY PROBE

70

FIGURE 34

DIRECT TO EARTH PROBE LAYOUT

TABLE 34

MASS PROPERTIES SUMMARY

		CENTER OF GRAVITY (CM)			RADIUS OF GYRATION (CM)		
	WT (KG)	X	Y	Z	K_X	K_Y	K_Z
PROBE WEIGHT (LAUNCH COND)	150.00	20.62	.08	.05	29.39	22.33	22.66
NEUTRAL MASS SPEC	3.99	23.57	0.0	-49.99	14.68	5.72	14.68
RETARDING POTENTIAL ANAL	1.50	23.57	-40.49	-30.25	11.73	10.57	8.43
BATTERY	2.27	23.57	-51.77	0.0	5.87	6.32	4.39
LANGMUIR PROBE	0.50	38.10	-40.87	30.25	11.38	11.23	4.70
PARTICLE DETECTOR	1.00	23.57	-35.94	37.24	5.87	5.74	5.74
DATA HANDLING	4.76	23.57	0.0	48.82	18.36	6.32	18.72
MAGNETOMETER	1.00	23.57	39.65	33.27	5.87	5.74	5.74
ION MASS SPEC	1.50	23.57	50.17	0.0	14.73	14.73	5.74
PRE-ENTRY X-MTR	2.04	38.10	51.74	0.0	5.87	6.32	4.39
RF EMISSION SPECTRUM ANAL	1.50	23.57	37.24	-35.94	5.87	5.74	5.74
JETTISON SENSOR	0.68	23.57	29.90	-43.66	5.08	5.08	5.08
STRUCTURE AND CABLE	27.22	29.41	0.0	0.0	46.99	34.77	34.77
TOTAL	197.94	22.33	0.37	-.01	35.26 I_X=13.39 KG-m^2	26.62 I_Y=7.63 KG-m^2	26.54 I_Z=7.59 KG-m^2
ECCENTRICITY BALLAST	1.50	23.57	-48.23	+1.68	1.91	6.35	6.35
TOTAL	199.44	22.33	0	0	35.38 I_X=13.59 KG-m^2	26.52 I_Y=7.63 KG-m^2	26.52 I_Z=7.77 KG-m^2
LESS: ADAPTER INCREMENT*	-14.68						
LESS: PROBE	-150.00						
PRE-ENTRY PACKAGE ΔWT (LESS: ANTENNA)	34.77						

* THIS IS THE AMOUNT OF ADAPTER STRUCTURE (NEEDED WITHOUT THE PRE-ENTRY SCIENCE PACKAGE) USED FOR THIS ADDITIONAL FUNCTION.

- ANTENNA C.G. IS ASSUMED TO LIE ON ON THE SPIN AXIS.
- ANTENNA IS CONSERVATIVELY TREATED AS A POINT MASS.
- $I_{ROLL}/I_{PITCH} = 1.1$ IS MAINTAINED WITH THE ANTENNA MASSES AND C.G. LOCATIONS DEPICTED
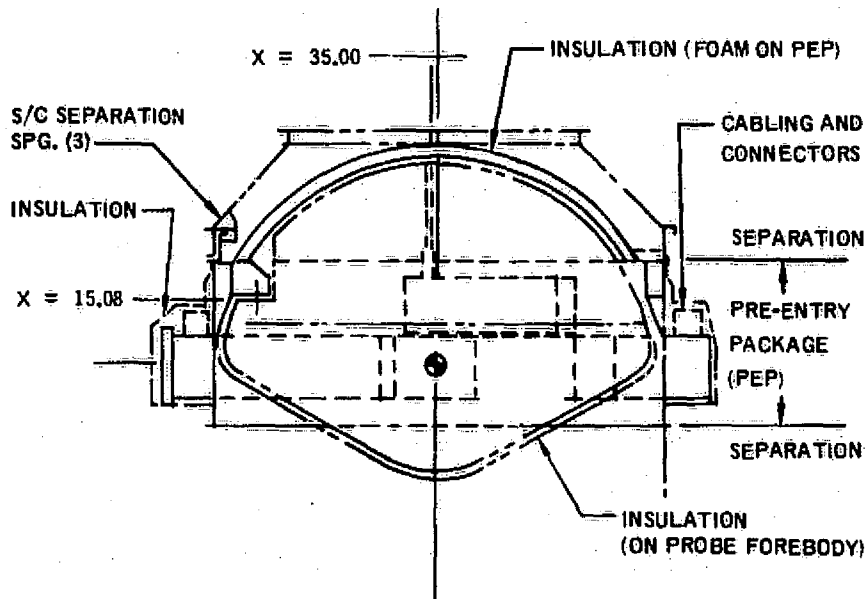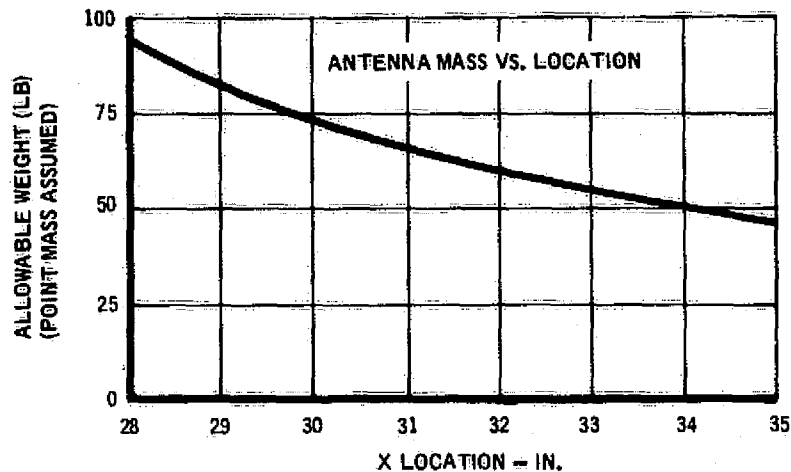- $I_{ROLL}/I_{PITCH} = 1.75$ WITHOUT THE ADDITION OF AN ANTENNA

FIGURE 35
CONFIGURATION CAPABILITY TO TOLERATE ANTENNA MASS

Summary

Because of the dramatic effect of removing a portion of the multilayer insulation, and because of the stringent post entry center of gravity requirements, the pre-entry packages are placed outside of the probe. Thus, the pre-entry requirements do not effect the probe per se. It was further seen that sufficient weight could be added to accommodate a fairly large pre-entry antenna, and still maintain acceptable mass properties.

Except for storage, if required, the impact on the spacecraft would be minimal. The reception antenna is estimated at .91 kg and the receiver and bit synchronizer at 1.91 kg. If the data is stored onboard, a store of 108.18 bits per second for 0.3 hours at rate 1/2, or 233,669 bits is required. Coupled with a post entry store of 44 bits per second for 0.5 hours at rate 1/3 with 8 FSK, or 79,200 bits, the total storage capacity required is 312,869 bits.

ELECTRONICALLY DESPUN ANTENNA

An electronically despun antenna (EDA) has a significant advantage over
a spun antenna because of the increase in gain that can be obtained. However,
there is a price to be paid in added complexity because of an increase in num-
ber of radiating elements, switches, switching logic, and pointing commands
generation. The basic performance design constraints for this study are:

Frequency: 400 MHz
Gain: 7 dB minimum
Conical Beamwidth: 50° minimum

A literature review (References 18 through 21) was made to provide a
basis for a sound conceptual design approach. Much of the literature deals
with spin stabilized communications satellites in a synchronous orbit where
the gain requirements are considerably higher than the 7 dB gain design con-
straint of this study. The general approach is based on a cylindrical array
of columns of radiating elements. The number of elements in each column is a
function of the axial beamwidth. The number of columns excited in the active
array depends on the gain and transverse beamwidth requirements. The active
array size is also limited by the element radiation pattern since, as the
cylinder is traversed the peak of the element pattern is directed more and
more away from the direction of the required array beam direction. If more
than two columns are used in the active array, the columns must have additional
phase control capability to compensate for the physical deployment of the
radiating elements on the cylindrical surface. This may be implemented by a
3 or 4-bit digital phase shifter in the RF section of a transmitter or receiver
(Reference 18). The beam rotation is normally achieved by sequentially
switching one column in and one column out at a rate determined by the spin
rate of the spacecraft. Switching is normally achieved by either activating
or deactivating the transmitter or front end receiver modules feeding each
column of radiators by means of a diode power supply switch or mechanically
switching the RF feed cable to the radiating element columns. The latter is
less reliable, requires longer switching time, and could result in switching
transients detrimental to the RF phase stability. However, with the present
solid state circuitry, transmitter modules or receiver front ends for each
radiating column does not pose a significant weight penalty.

There are other EDA configurations which can be employed if there is
complete access to the center of the array. For example, a biconical horn
with probe feeds (Reference 19) can be designed where digital switching is
eliminated and continuous beam rotation obtained. However, EDA configurations
like this are not adaptable to this study because of the physical configura-
tion of the Pioneer spacecraft and the low design frequency.

Conceptual EDA Design

The EDA design resulting from this study is shown in Figure 36. It con-
sists of 16 panels of two elements each. These panels surround the probe

JUPITER ORBITER
SPACECRAFT
(REF.)

ANTENNA
SUPPORT TRUSS

ANTENNA
16 PANEL – DUAL
MICROSTRIP
ELEMENTS

JUPITER ENTRY PROBE
(REF.)

MICROSTRIP
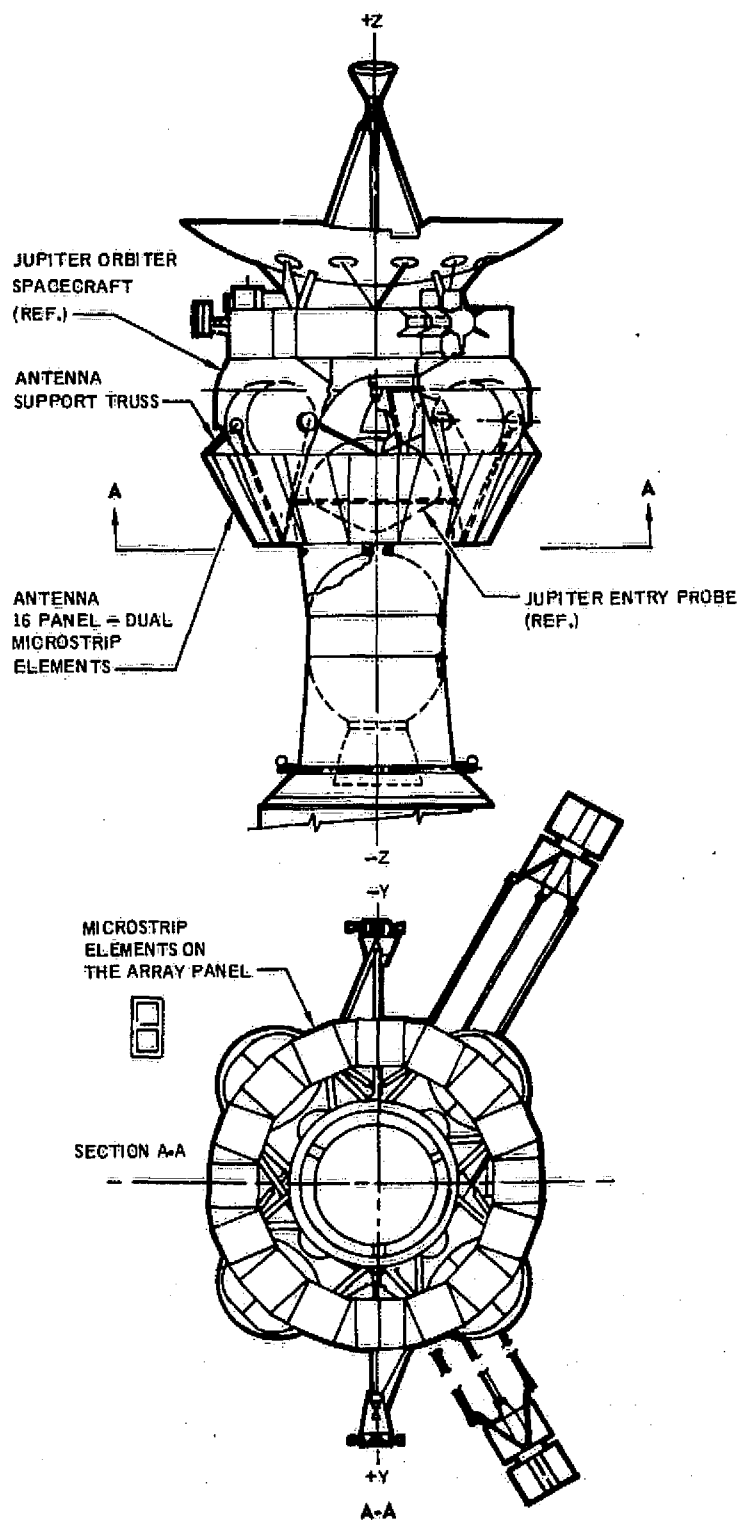ELEMENTS ON
THE ARRAY PANEL

SECTION A-A

A-A

FIGURE 36
EDA CONFIGURATION

adapter and are supported on the Pioneer spacecraft as shown in Figure 37.
The array is 1.71 m in diameter at the top, 2.39 m at the base and 59.38 cm
in length. The phase centers of the adjacent panel are spaced (.521 wavelengths
(λ)) at 400 MHz. A cylindrical array was considered with the two elements in
each panel phased for a beam tilt 30° from the panel normal. However, these
patterns resulted in a high side lobe, as will be shown later, which would
reduce the directivity of each array panel. The array diameter can be reduced
to 1.28 m at the top by reducing the number of panels or radiating element
columns to 12. However, this will result in less overlap of adjacent beam
positions and a smaller angular beamwidth and a gain of 7 dB or greater as
will be discussed later. Two adjacent panels are fed in phase to form a beam-
width of 50 x 50 degrees and the remaining 14 panels are switched off. The
beam is rotated by simultaneously switching on and off adjacent panels in the
proper sequence. The direction of beam rotation is dependent upon the switch-
ing sequence. A typical switching sequence (Reference 20) is shown in Figure
38. As the spacecraft rotates, a beam formed by 1 and 2 is switched to a
beam formed by 2 and 3 by switching the SP4T (single pole four throw) switch
on the left from position 1 to position 2. A brief study of Figure 38 will
show that only one switch operation is required to change the beam position.
This switching scheme can easily be adapted to 12 elements by replacing the
SP4T switches with SP3T switches. This switching scheme can also be adapted
to feed more elements simultaneously by using an n-way summer (Reference 20)
where n is the number of elements being summed. A typical EDA system electron-
ics diagram is shown in Figure 39. Alternatively, switching could be achieved
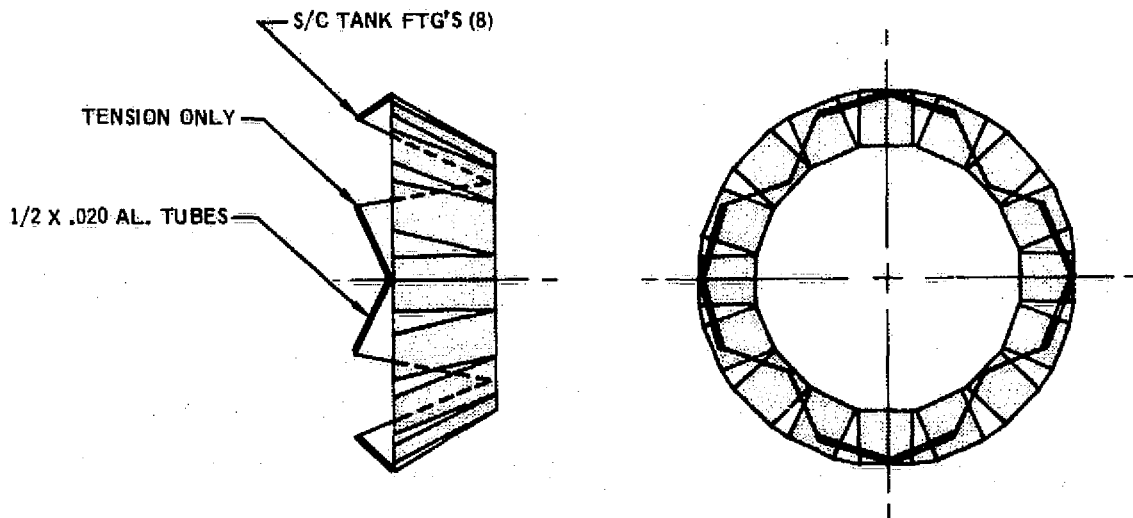by turning the receivers on and off and providing a 16-way summer.

FIGURE 37

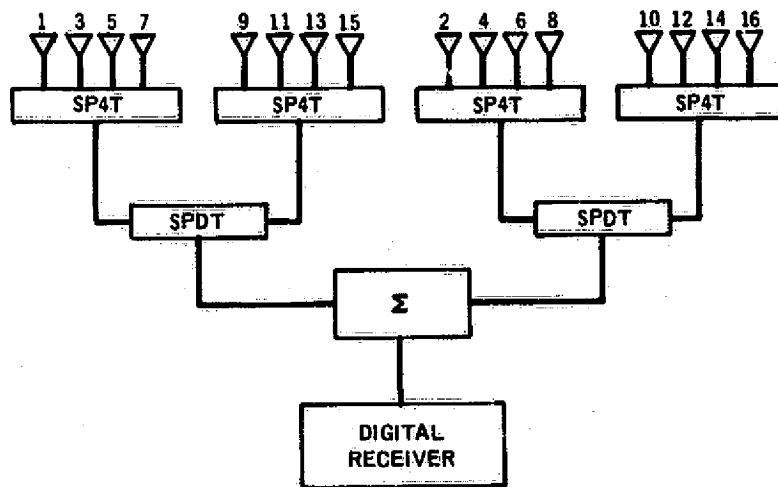**EDA SPACECRAFT STRUCTURAL SUPPORT**

FIGURE 38
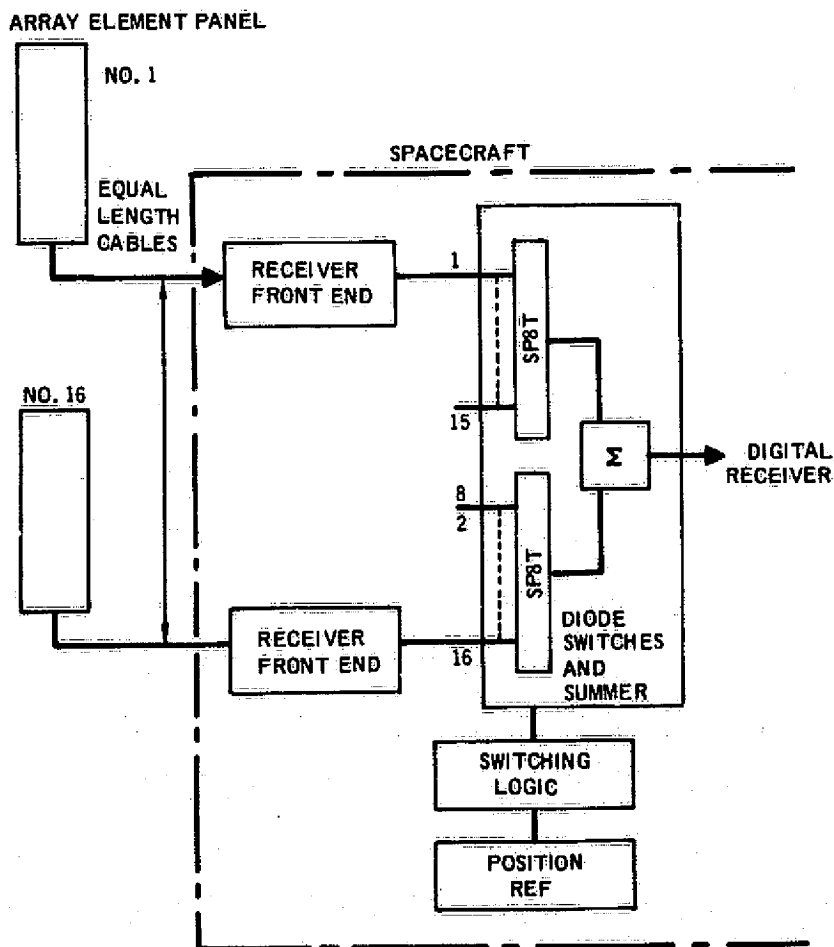
EDA ARRAY SWITCHING SCHEME

FIGURE 39

EDA SYSTEM ELECTRONICS

Radiating Element Design

For maximum signal reception a circularly polarized radiating element is required. The element must have good axial ratio characteristics and be light weight because of the number required.

At 400 MHz, the choice of light weight elements is limited. Two candidate radiating elements include crossed-dipole and microstrip antennas. Both have symmetrical broad beam patterns suitable for elements in an array. However, the microstrip antenna is the most compact and is ideally configured for launch shock and vibration. The axial ratio of the microstrip is also generally lower over broader beamwidths than has been observed for crossed-dipole patterns. Therefore, the microstrip element has been selected for the EDA array element.

The array panel design is shown in Figure 40. Two microstrip radiating elements are included on each panel to make up one column of the EDA array. To minimize the weight, microstrip elements can be constructed on a fiberglass-phenolic honeycomb panel (Reference 22, Ball Brothers Research patent pending) where the effective dielectric constant is about 1.1. By filling the honey-comb core with an artificial dielectric to make the effective dielectric constant equal to 2, the microstrip radiator size can be reduced significantly and the beamwidth increased (Reference 23). This technique is required to obtain the required pattern beamwidth and an acceptable EDA size and weight. The ground plane side of the microstrip element is 2.5 mm thick sheet of aluminum. This eliminates one of the fiberglass face sheets and reduces the panel weight. With this approach the panel weight is about 0.608 kg. Table 35 gives the weight of the EDA components. The two microstrip elements on each panel are fed in phase to form a beam center normal to the panel. The panels are tilted 30° to obtain a beam center 30° above the equatorial plane of the spacecraft. The beamwidth of the microstrip element can be obtained from

$$E = A \cos (63.44° \sin \theta) \qquad (1)$$

where A is the maximum amplitude, θ is the angular displacement from a direction normal to the plane of the element and 63.44° is the electrical length of the microstrip elements for a substrate dielectric constant of 2. The patterns are symmetrical about the normal, and are best characterized by

$$E = A(.316 + .684 \cos^{1.614} \theta), \ - 90 < \theta < 90 \qquad (2)$$

based on the techniques given in Reference 21. Figure 41 shows a plot of Equation 2. The element spacing on the panels is 37.49 cm or .500λ at 400 MHz. The array pattern for a two element array referred to mid point between the radiating elements is given by (Reference 24).

$$E = 2E(\theta) \cos \left(\frac{\frac{2\pi d}{\lambda} \sin \theta + \delta}{2} \right) \qquad (3)$$

where E(θ) is the element pattern, d is the spacing between radial elements,

16 ELEMENT
ANTENNA ARRAY

MOLDED PANEL
CLOSURE WITH
INTEGRAL ATTACH
FITTINGS

A

A

B

C

.010 ALUMINUM
FACESHEET

13.00

10.44

.012 FIBERGLASS
FACE SHEET

10.64

DIELECTRIC FILLER
3.0 LB/FT^3

HIRP 3/8-2.2
HEXCELL CORE

27.00

14.76

COPPER
MICROSTRIP
.0014 THICK

.25 THICK (REF.)

B-B

DETAIL C
2 x SIZE

B

1/8 SIZE

.25

A-A VIEW OF ANTENNA ELEMENT
(16 REQUIRED)

FIGURE 40
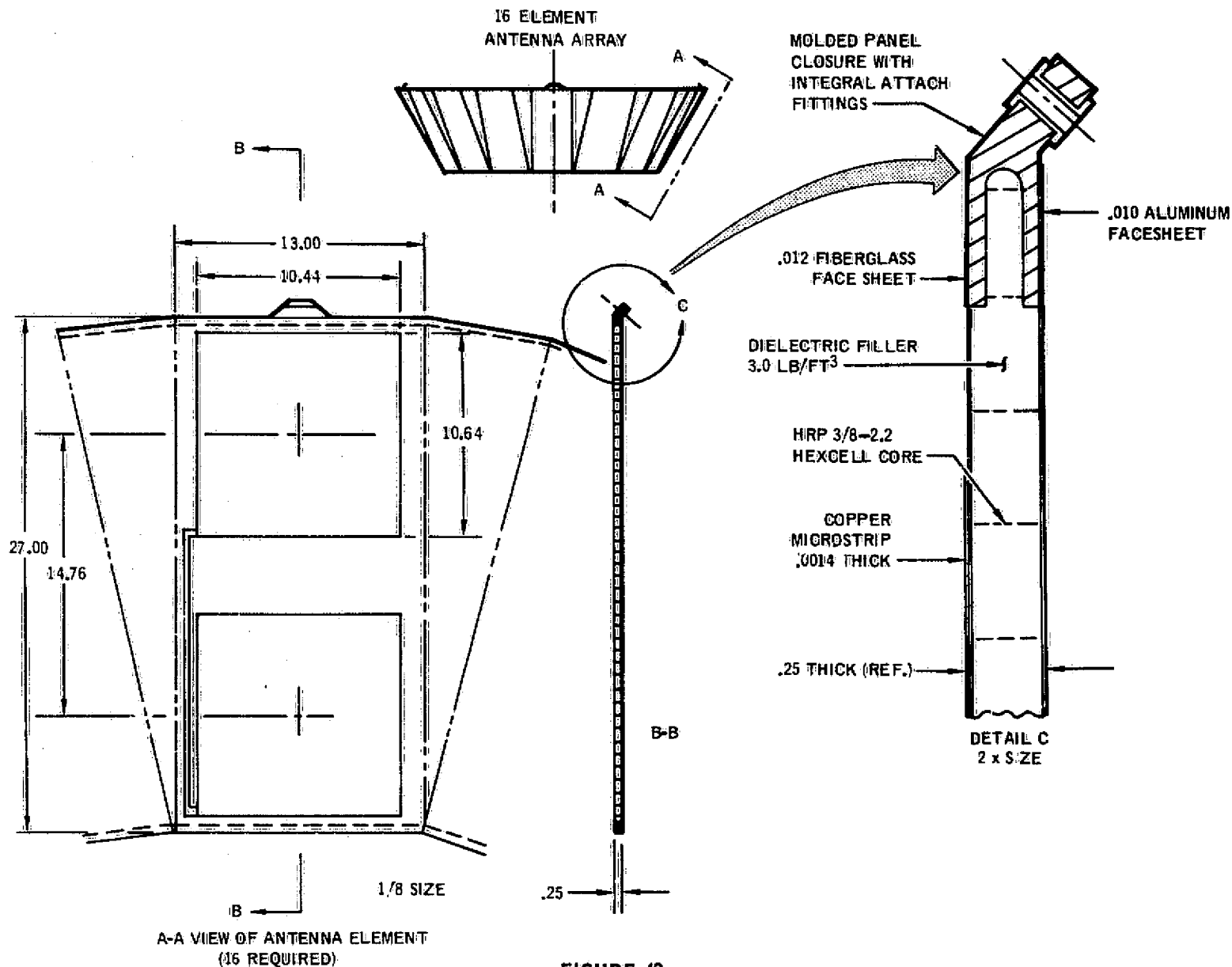
EDA ARRAY PANEL

TABLE 35

EDA ARRAY PANEL WEIGHT

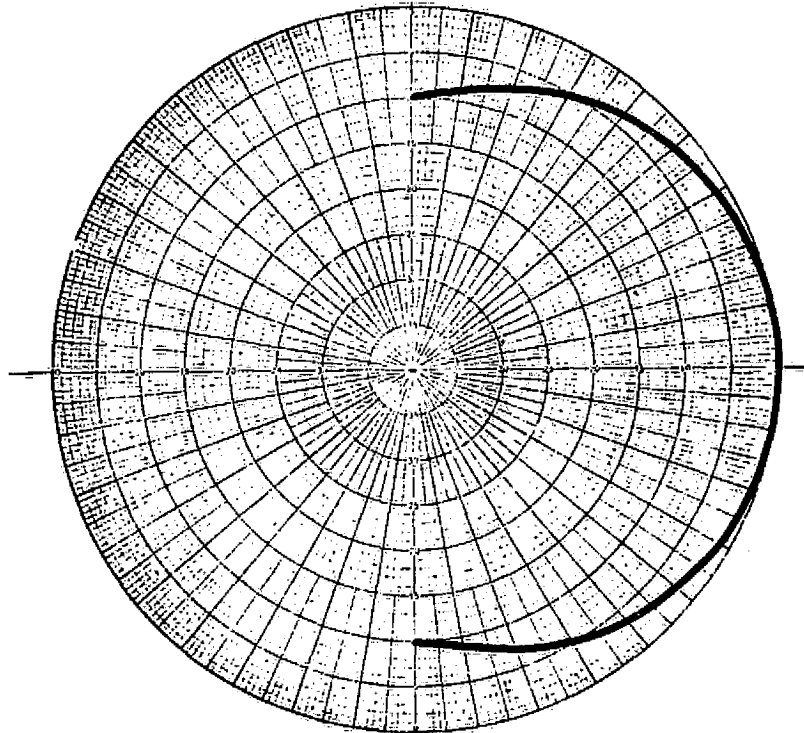| ITEM	UNIT (KG)	TOTAL (KG)
MICROSTRIP ELEMENT PANEL	0.61	9.73
RF CABLING	0.15	2.46
RF CIRCUITRY	0.23	3.63
SUPPORT FRAME	0.15	2.38
TOTAL		18.20

FIGURE 41

MICROSTRIP ELEMENT PATTERN

δ is the phase difference of the element excitation and θ is the angle rela-
tive to the array normal. Figure 42 shows a plot of Equation 3 for the two
elements in phase. This is the pattern of the EDA array in the elevation
planes (that is the planes which contain the spacecraft roll axis). For a
cylindrical EDA array the microstrip elements must be phased to obtain the
desired beam tilt. The phase difference (δ) required to form a beam center
30° from the normal is given by

$$\delta = -\frac{2\pi d}{\lambda} \sin \theta$$

$$= -2\lambda(.500)(.5) \tag{4}$$

$$= -1.57 \text{ rad } (90°)$$

Combining Equations 2 and 3 and inducing the above phase difference the normalized field pattern is

$$E = (3.16 + .684 \cos^{1.614} \theta) \underbrace{\cos (90 \sin \theta - 45)}, -90 < \theta < 90 \tag{5}$$

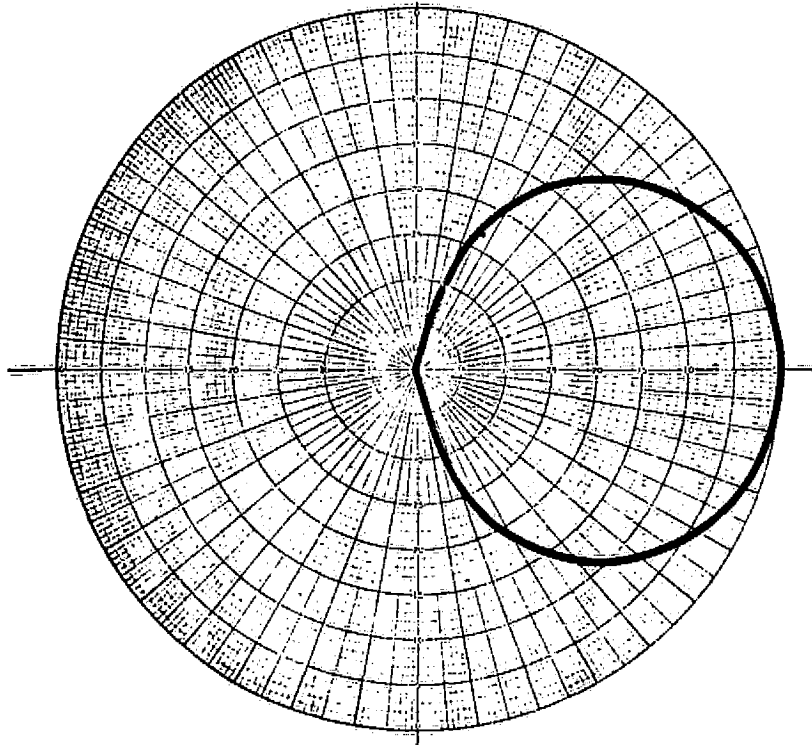<u>element pattern</u>   <u>array factor</u>

FIGURE 42

EDA ARRAY PANEL PATTERN IN THE ELEVATION PLANE

A plot of Equation 5 is shown in Figure 43 for phase differences of 90° and 120° which correspond to array factor beam tilts of 30° and 41.8°. Both patterns have a high side lobe and do not form symmetrical 50° beams 30° off the panel normal. Therefore, the cylindrical EDA array is not considered an acceptable approach for this study. The EDA array pattern in the conic plane 30° above the equatorial plane cannot be calculated simply by multiplying the element pattern by the array factor as is the case for the above, because the element patterns are dissimilar due to the rotation of one relative to the

other. Thus, the energy from each array element (i.e., two element panel) must be added vectorially to obtain the total array pattern (Reference 24). The expression for the array patterns of two adjacent panels is

$$E(\phi) = E_1(\phi) + E_2(22.5 - \phi)e^{j(\frac{2\pi d}{\lambda} + \delta)} \tag{6}$$

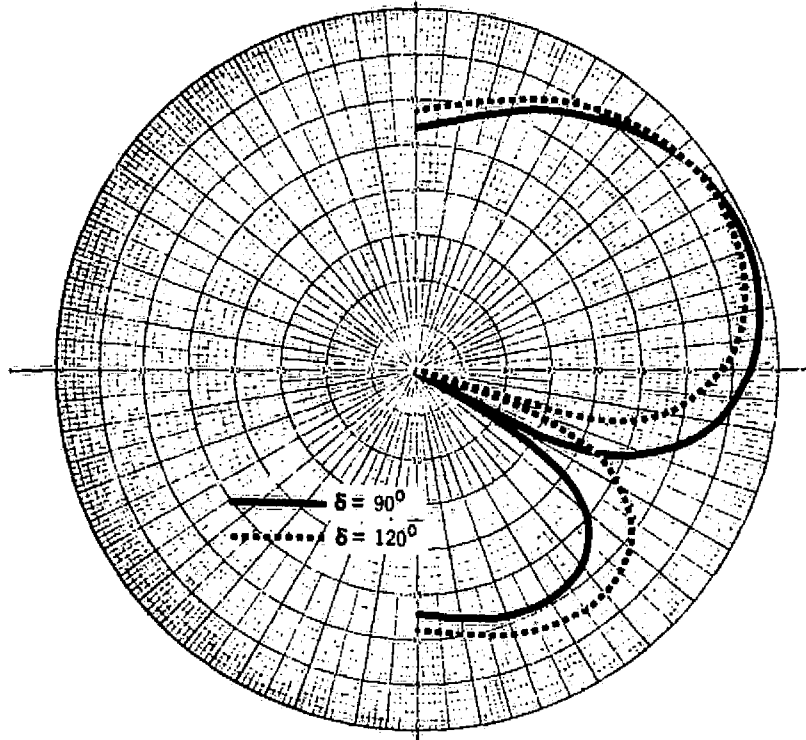where $E_1(\phi)$ and $E_2(22.5 - \phi)$ are the element patterns

FIGURE 43

EDA PANEL PATTERN WITH SCANNED BEAMS

Since the principal EDA plane of interest is a conic plane 30° (θ = 60° standard coordinate system) above the equatorial plane, the pattern of the array panel must be considered in that plane. This pattern was derived by considering the array panel pattern with the appropriate coordinate transformations in a spherical coordinate system. Figure 44 shows the EDA array element pattern in the θ = 60° plane with the EDA panel tilted 30°. The expression for this pattern is

$$E_1(\phi) = A(.26 + .74 \cos^{1.158}\phi), \quad -90 \le \phi \le 90 \tag{7}$$

where ϕ is the clock angle around the spacecraft. This expression gives a pattern within .1 dB of the pattern derived from the array panel principal plane patterns.
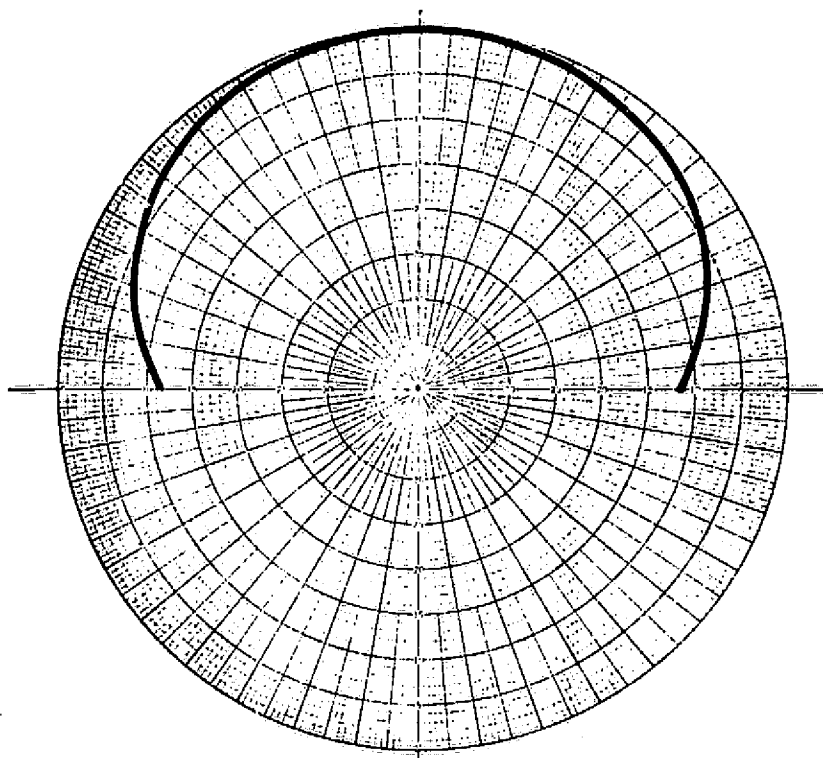
FIGURE 44

EDA PANEL PATTERN WITH PANEL TILTED 30°

Figure 45 shows a plot of the EDA array pattern in the conic plane at 30° above the equatorial plane. The beamwidth of this pattern is 50°. Using this pattern beamwidth and that shown in Figure 42 the conic beam shape can be constructured. Figure 46 shows a construction of the adjacent beams. As can be seen, significant overlap is necessary to ensure a continuous angular band of coverage. A large angular displacement between adjacent beams will result in a narrower angular band where the gain is 7 dB or greater.

Phase Variation Considerations

The array element panels form a conical array as shown in Figure 36. Since the rotation is about the spin axis of the spacecraft instead of the respective two panels array phase centers, the phase variation in the main beam is not zero as a function of the rotation angle (Reference 24). Since the microstrip antennas have a uniform cylindrical phase front over essentially the entire hemisphere they can be essentially considered as isotropic radiators over the small angles in which they are active. Figure 47 shows a diagram of three isotropic elements on a circle. If switching occurs when the direction of the received signal is in the direction of the center element, the element to be switched off lags the center element by the same amount, and thus, no phase variation at switching. At any other angle there is a

phase discontinuity. However, since there is some uncertainty as to where the probe is relative to the spacecraft at switching time the magnitude of this error must be considered.
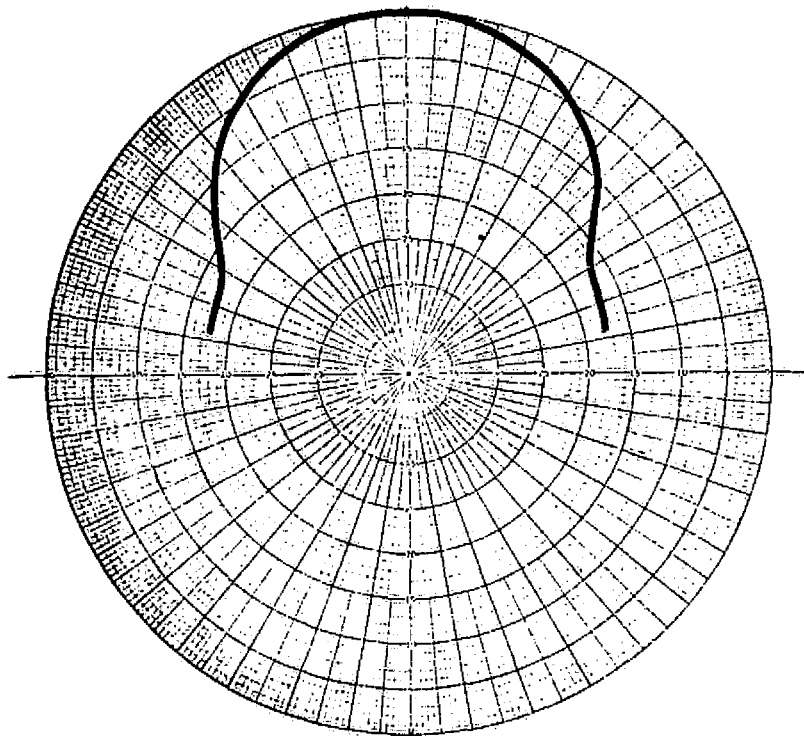

FIGURE 45

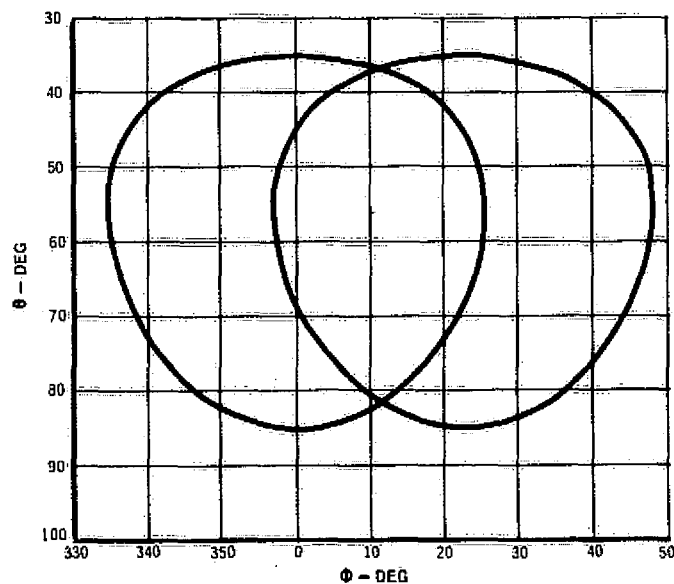**ARRAY PATTERN — CONE AZIMUTH PLANE (θ = 60°)**

FIGURE 46

CONIC BEAM COVERAGE OVERLAP

From Figure 47 the phase error can be constructed and calculated as a function of the angle from the direction of the center element. The expression for the phase error is

$$\Delta\psi = 2 \ [\frac{R}{\lambda} (\cos \phi - \cos (22.5 + \phi)) - \frac{d}{\lambda} \sin (11.2 - \phi)] \qquad (8)$$

where R is the array radius, d is the element spacing and ϕ is the angular displacement from the direction of the center element. Figure 48 shows a plot of the phase error. The error increases rapidly with an increase in the displacement angle. Therefore, rather large phase discontinuities can exist at the time of switching because of the uncertainty in the determination of when to switch.
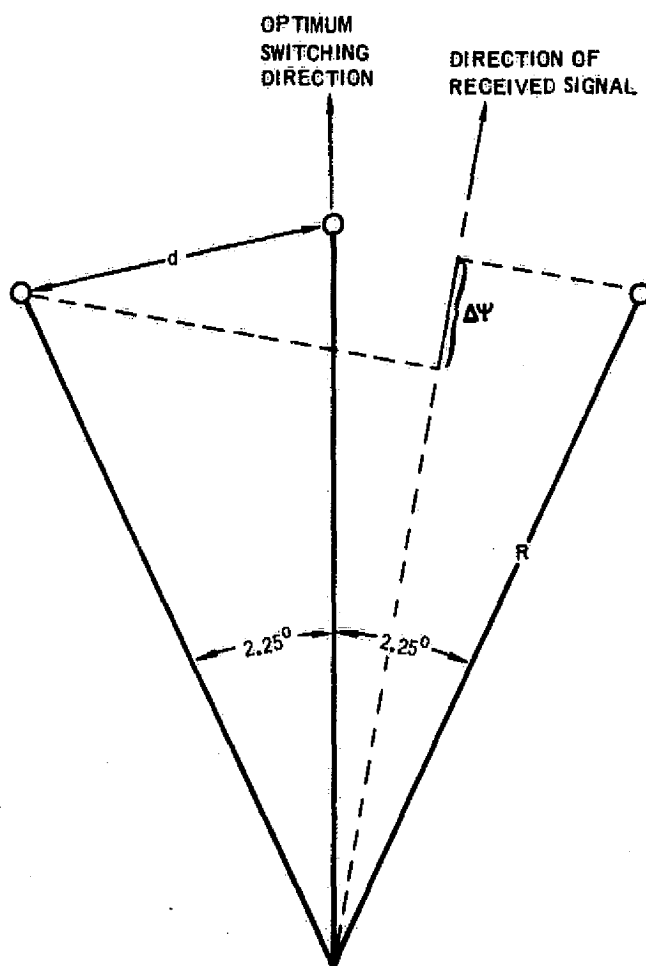

FIGURE 47

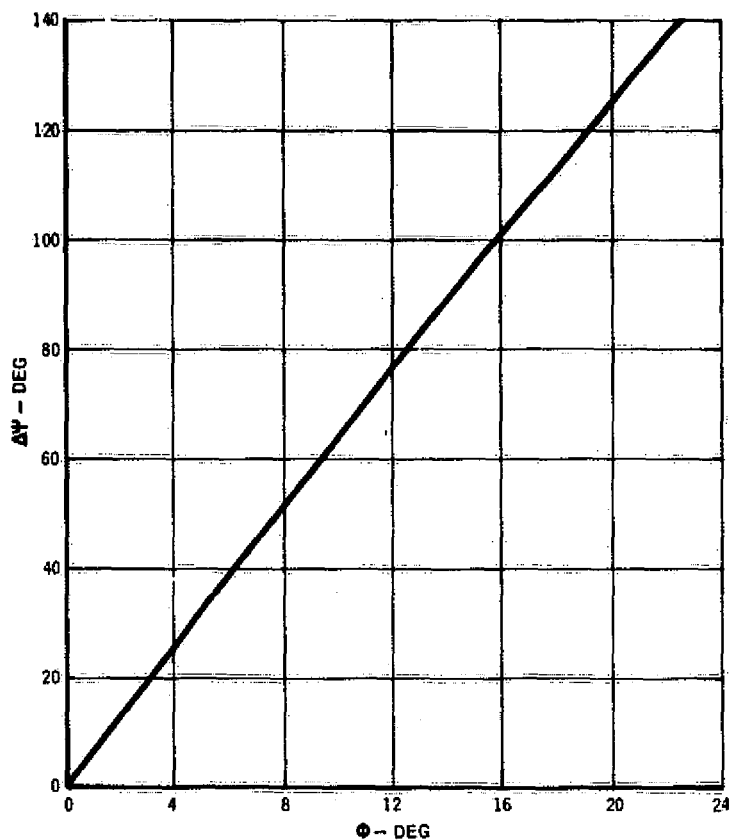**EDA ARRAY ELEMENT PHASE RELATIONSHIP**

FIGURE 48

PHASE ERROR DUE TO SWITCHING UNCERTAINTY

A phase discontinuity in the received wave may have a significant impact on the operation of the Modem. Abrupt phase discontinuities are a form of phase modulation of the wave. Herein, typically the rate is 5 revolutions per minute times 16 (typical switchings) divided by 60 second per minute, or 1-1/3 Hertz, equivalent to 2-2/3 bits per second. This constitutes spectrum "splatter" over the desired modulation. Whether the Modem is coherent or noncoherent, this spectrum splatter is a form of colored noise which cannot be circumvented by increasing carrier power. Further, if the receiver contains a phase locked loop, the discontinuities increase the probability of a loss of lock thereby inferring burst error patterns.

Summary

The design shown in Figure 36 using microstrip radiating elements yields a conical beam width of 50° with 16 beam positions. The peak gain for a 50° conical beamwidth is 10.2 dB assuming an efficiency of 65%. Therefore the overlap gives a band of coverage 7 dB or greater from $\theta = 37°$ to $\theta = 81°$ for any spacecraft clock angle. The weight of this design adds about 18.20 kg to the spacecraft weight.

87

CONCLUSION

The impact of the addition of pre-entry communications to a basic post entry mission probe has been examined for a candidate mission and pre-entry science set. The analysis began with a review of the Jovian propagation channel. Although there are considerable uncertainties in the channel definitions, enough information exists to bound the performance of a communications link, and to postulate optimal carrier frequencies.

The next step in the analysis was to define optimal joint probe and spacecraft trajectories which maximize the total available data power in the receiver. In addition to defining such optimal trajectories, the analysis defined the optimal spacecraft reception antenna pattern for each candidate joint trajectory. It was found that the joint trajectory selection was a critical design element of a mission with relay communications.

The communications link analysis combined the propagation analysis and the trajectory analysis, and defined the maximal data transfer. It was found that a despun spacecraft antenna provided approximately eight decibels additional data over a spun spacecraft antenna. The probe "penalty" of incorporating a dual frequency Doppler experiment is 1.4 or 2.73 kilographs and .8 or 2.5 decibels of data for the despun and spun cases respectively. It was also found that a parabolic dish the size of the probe could transfer a reasonable amount of data direct to Earth prior to entry.

Following this, the "impact" of incorporating pre-entry communications was assessed. Due to the fundamental design characteristics of the probe, it was found to be impracticable to incorporate the necessary pre-entry equipments inside the probe. An external configuration was thus designed which is quite stable, and has the capability to carry sufficient weight on the aft center-line for a wide variety of antennas.

Finally, a conceptual design of an electronically despun reception antenna for a Pioneer class of spacecraft was made. The design features sixteen microstrip reception elements on a truncated conical section. The despun beamwidth is 50 degrees, which corresponds to a 7 decibel gain at beamedge with a 65% efficiency. The estimated weight of the array and cabling is 18.2 kg.

REFERENCES

1. "Saturn/Uranus Atmospheric Entry Probe," MDC Report E0870, July 18, 1973.

2. "Pioneer Jupiter Orbiter Probe," NASA CR-137591, November 8, 1974.

3. "The Planet Jupiter," NASA SP-8069, December 1971.

4. "Jupiter Antenna Noise Distribution Program," D. A. Rasmussen, T. L. Grant and S. C. Noble, August 1975.

5. C. A. Hinrichs' Memo No. OPP-59, "Outer Planet Absorption," 28 May 1975.

6. B. T. Miller's Memo No. OPP-65, "Orten-Hunten Jupiter Atmosphere-Model I," 8 July 1975.

7. C. A. Hinrichs' Memo No. SAEP-E412-25, "Outer Planet Ionospheric Effects," 19 February 1973.

8. R. Woo and F. Yang, "Measurements of Electron Density Irregularities in the Ionosphere of Jupiter by Pioneer 10," 18 May 1975.

9. C. A. Hinrichs' Memo No. OPP-53, "Jovian Atmospheric and Ionospheric Turbulence," 6 May 1975.

10. C. A. Hinrichs' Memo No. OPP-106, "Ionospheric Scintillation Revisited," 9 March 1976.

11. J. K. Cline's Memo No. OPP-103, "Conversion Algorithm from MDAC Phasing Time to ARC Lead Time," 9 February 1976.

12. C. A. Hinrichs' Memo No. OPP-94, "Trajectory and Spacecraft Antenna Selection," 6 January 1976.

13. R. R. Nunamaker's Letter No. 229-8: SM-5 223, "NASA2-9027, Constraints and Assumptions for the Pre-entry Telecommunications Task", 5 November 1975.

14. "Outer Planet Atmospheric Entry Probe," (COMPLEX) July 1975 by NASA Ames Research Center.

15. Pre-entry Communications Statement of Work, NASA Ames Research Center, March 1975.

16. J. K. Cline's Memo No. OPP-104, "Pre-entry Probe to Earth Doppler and Doppler Rate," 16 Feburary 1976.

17. W. H. Gustin's Memo No. OPP-100, "Jupiter Probe Mass Properties and Configuration Study," 28 January 1976.

18. Meeks, R. D., Jones, A. S. and Nix, J. L.; Texas Instruments Incorporated, "An Electronically Phased Modular Array Antenna for Pioneer Venus Communications," Contract No. NAS2-7154, 22 Nov. 1972.

19. Andre, S. N. and Leonard, D. J., "Gain Limits of Electronically Despun Satellite Antenna System," AIAA Paper 66-325, Communications Satellite Systems Conference, Washington, .D.C, May 1966.

20. Gregorwich, W. S., "An Electronically Despun Array Flush Mounted on a Cylindrical Spacecraft," IEEE Trans. Antennas and Propagation (Communications), Volume AP-22, pp. 71-74, January 1974.

21. King, H. E. and Wong, J. L., "225-400 MHz Antenna System for Spin-Stabilized Synchronous Satellites," Air Force Report No. SAMSO-TR-72-77, 15 March 1972.

22. Munson, R. E., Ball Brothers Research, Private Communication.

23. Kuhlman, E. A., McDonnell Douglas Astronautics Company-East, "Microstrip Antenna Study for Pioneer Saturn/Uranus Atmospheric Entry Probe," NASA CR-137513, May 1974.

24. Kraus, J. D., "Antennas," McGraw Hill Book Company, (New York), 19750.